

## Supporting Information

### 3,5,7-Substituted Pyrazolo[4,3-*d*]pyrimidine Inhibitors of Cyclin-Dependent Kinases and Their Evaluation in Lymphoma Models

Radek Jorda<sup>a,#</sup>, Libor Havlíček<sup>b,#</sup>, Antonín Šturc<sup>b</sup>, Diana Tušková<sup>c</sup>, Lenka Daumová<sup>c</sup>, Mahmudul Alam<sup>c</sup>, Jana Škerlová<sup>d,e</sup>, Michaela Nekardová<sup>d,f</sup>, Miroslav Peřina<sup>a</sup>, Tomáš Pospíšil<sup>a</sup>, Jitka Široká<sup>a</sup>, Lubor Urbánek<sup>a</sup>, Petr Páchl<sup>d</sup>, Pavlína Řezáčová<sup>d,e</sup>, Miroslav Strnad<sup>a</sup>, Pavel Klener<sup>c</sup>, Vladimír Kryštof<sup>a\*</sup>

<sup>a</sup> Laboratory of Growth Regulators, Palacký University and Institute of Experimental Botany, The Czech Academy of Sciences, Šlechtitelů 27, 783 71 Olomouc, Czech Republic

<sup>b</sup> Isotope Laboratory, Institute of Experimental Botany, The Czech Academy of Sciences, Vídeňská 1083, 14220 Prague, Czech Republic

<sup>c</sup> Institute of Pathological Physiology, First Faculty of Medicine, Charles University, Prague, Czech Republic

<sup>d</sup> Institute of Organic Chemistry and Biochemistry, The Czech Academy of Sciences, Flemingovo nám. 2, 166 10 Prague 6, Czech Republic

<sup>e</sup> Institute of Molecular Genetics, The Czech Academy of Sciences, Vídeňská 1083, 14220 Prague, Czech Republic

<sup>f</sup> Faculty of Mathematics and Physics, Charles University in Prague, Ke Karlovu 3, Prague 2, 121 16, Czech Republic

## **Content**

### **1. Computational Analysis**

Supplementary Figure S1.

Supplementary Table 1.

Supplementary Figure S2.

Supplementary Figure S3.

Supplementary Figure S4.

Supplementary Figure S5.

### **2. Crystal parameters, data collection and refinement statistics**

Supplementary Table 2.

### **3. Kinase selectivity profile**

Supplementary Table 3.

### **4. Further in vitro data**

Supplementary Table 4.

Supplementary Figure S6.

Supplementary Figure S7.

Supplementary Figure S8.

### **5. Physicochemical and pharmacological properties of 4.35**

Pharmacokinetic analysis in mice

Supplementary Figure S9.

### **6. Further in vivo data**

Supplementary Figure S10.

Supplementary Figure S11.

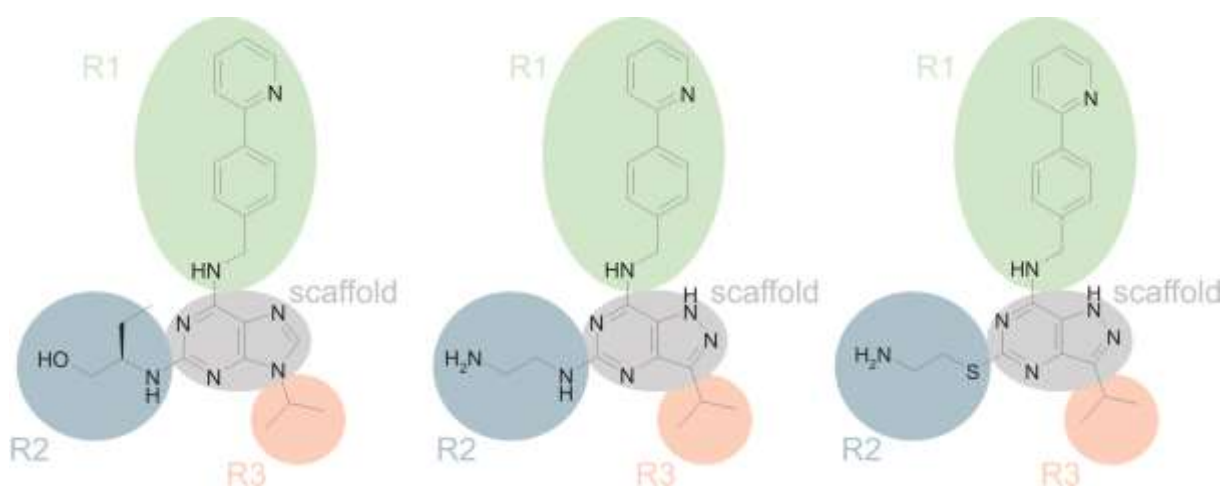
### **7. Additional Methods**

### **8. NMR Spectra of Prepared Compounds**

### **9. References**

## 1. Computational Analysis

The theoretical study analyses the binding mode of compound **4.35** described in this work, and its nitrogen-containing pyrazolo[4,3-*d*]pyrimidine analog **5i** which was described previously.<sup>1</sup> We computationally investigated two conformers of each inhibitor. The conformers **4.35**<sub>calc1</sub> and **5i**<sub>calc1</sub> were identified by the computational procedure<sup>2</sup> as the most stable geometries. For this purpose, we utilized the **CR8** (PDB ID: 3DDP)<sup>3</sup> molecule as the template. The **4.35**<sub>calc2</sub> conformer is identical to the **4.35** geometry published here and **5i**<sub>calc2</sub> was designed according to this conformation. As CDK2 model, we used the crystal structure 3DDQ which was computationally adjusted in our previously study<sup>2</sup>.



**Supplementary Figure S1.** Structures of CR8 (left), compound **5i** (middle) and **4.35** (right). To assess the  $\Delta G'_{\text{int}}$  contributions of the inhibitor parts, the inhibitors were fragmented into four parts (the scaffold and three substituents).

We used computational methods and methodology validated by a representative dataset of CDK2 inhibitors.<sup>2</sup> The approach is based on the hybrid quantum mechanics/semiempirical quantum mechanics (QM/SQM) method,<sup>4</sup> which employs the DFT method with an empirical dispersion for QM and the PM6 method<sup>5</sup> for SQM part. The solvent effect is described by the continuum solvation model COSMO<sup>6</sup> at the SQM level for the whole system. The protein-inhibitor binding affinities are expressed as the computational interaction “free” energies  $\Delta G'_{\text{int}}$  (in kcal mol<sup>-1</sup>) of the protein-inhibitor complexes. They are fundamental for the description of protein-inhibitor interactions.

The fragmentation of the inhibitors enables the assessment of the  $\Delta G'_{\text{int}}$  contributions of the inhibitor parts (molecular fragments) in the complex with the whole protein. The inhibitors taken from the optimized protein–inhibitor complex were divided into four parts

(the scaffold and three substituents), and the  $\Delta G'_{\text{int}}$  values are described at the QM/SQM level as well.<sup>2</sup>

The computationally optimized protein-inhibitor complexes have the following binding modes. The inhibitors are bound by three hydrogen bonds between the scaffold and the protein hinge region (carbonyl of Leu83, backbone NH of Leu83, carbonyl of Glu81), similar to the binding modes of **CR8**. The compounds also create a hydrogen bond between Lys89 and the 4-(2-pyridyl)benzylamine moiety at position 7. The compounds are stabilized by dispersion interactions between the 3-isopropyl group and Phe80 as well. The inhibitors make other hydrogen bonds between the substituents at position 5 and the residues situated at the edge of the active site. The 2-aminoethylthio moiety of **4.35<sub>calc1</sub>** is bound to carbonyl of Gln131 and the terminal amide of Asn132. The 2-aminoethylamino moiety of **5i<sub>calc1</sub>** forms the hydrogen bonds with the same residues. An analogous 4-hydroxybutylamine group of **CR8** is bound by two hydrogen bonds with the backbone NH and Glu12 carbonyl (**Supplementary Figures S2 and S3**).

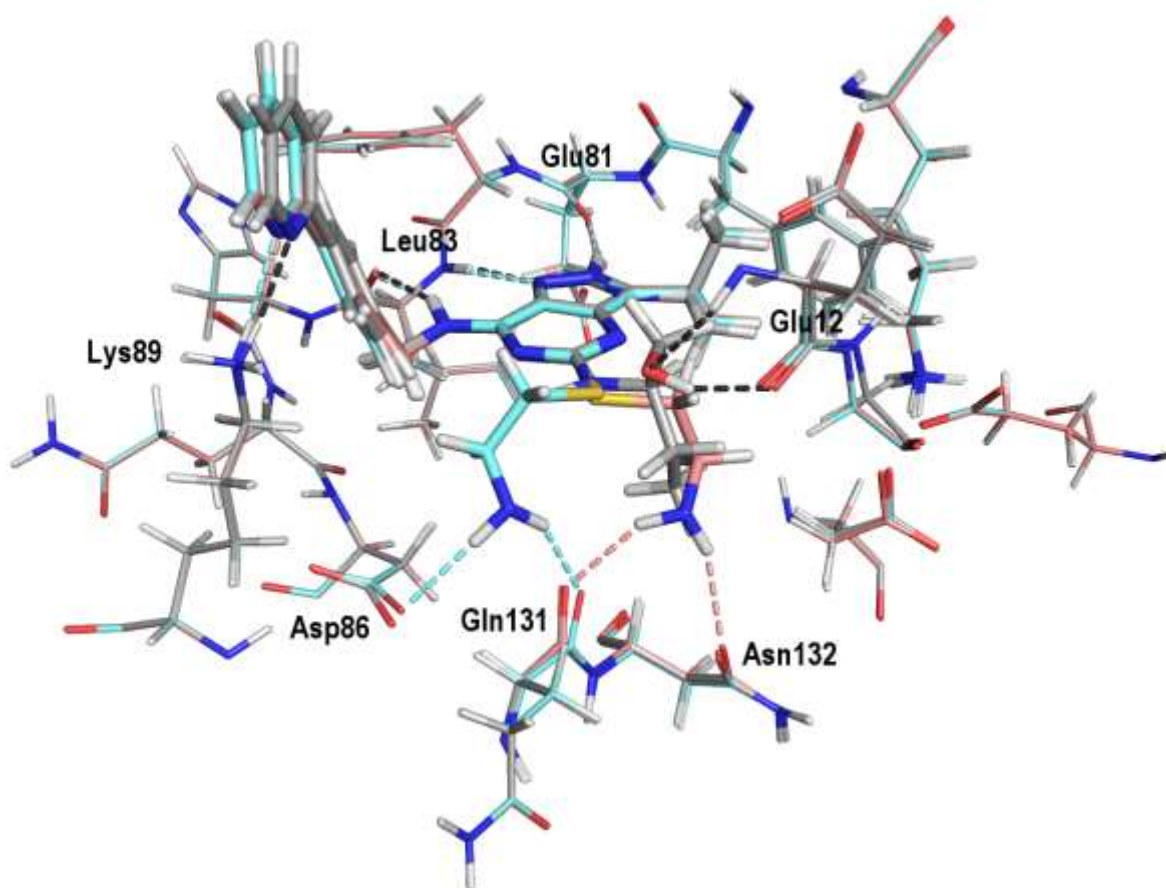
The evaluation of the computational data (**Supplementary Table 1**) shows that the interaction between the protonated amino group of Lys89 and the free electron pair of the pyridine nitrogen substantially contributes to the total  $\Delta G'_{\text{int}}$  values of all the complexes. The  $\Delta G'_{\text{int}}$  of **4.35<sub>calc1</sub>** indicates that this inhibitor is the best. The  $\Delta G'_{\text{int}}$  contributions of the scaffolds denote the larger values of the pyrazolo[4,3-*d*]pyrimidine core (**4.35<sub>calc1</sub>** and **5i<sub>calc1</sub>**) compared with the purine core (**CR8**), in line with our previous report.<sup>2</sup> Importantly, the  $\Delta G'_{\text{int}}$  contribution of the 2-aminoethylthio moiety of **4.35<sub>calc1</sub>** is significantly higher than that of the 2-aminoethylamino of **5i<sub>calc1</sub>**. In addition, the total  $\Delta G'_{\text{int}}$  of **4.35<sub>calc1</sub>** (as well as the sum of the  $\Delta G'_{\text{int}}$  of its fragments) indicates higher binding affinity than **5i<sub>calc1</sub>**. Thus, the computational results indicate that the replacement of the alkylamino group at the 5-position of the heterocycle by the 5-alkylthio group is completely relevant.

It should be noted that the computationally predicted conformer **4.35<sub>calc1</sub>** differs in the geometry of the 2-aminoethylthio moiety at position 5 from the conformer detected in the crystal structure. This substituent in **4.35<sub>calc1</sub>** and **5i<sub>calc1</sub>** is similarly oriented to the analogous moiety of **CR8** at position 5 (**Supplementary Figures S2, S3 and S5**). In contrast, in the crystal structure, the substituent is oriented in the opposite direction. We evaluated the effect of this orientation in the **4.35<sub>calc2</sub>** and **5i<sub>calc2</sub>** conformers. **4.35<sub>calc2</sub>** corresponds to the crystal structure and **5i<sub>calc2</sub>** was modeled similarly. The amino group of the moiety at position 5 of **4.35<sub>calc2</sub>** is bound to the carboxylate of Asp86 and the backbone carbonyl of Gln131, and the

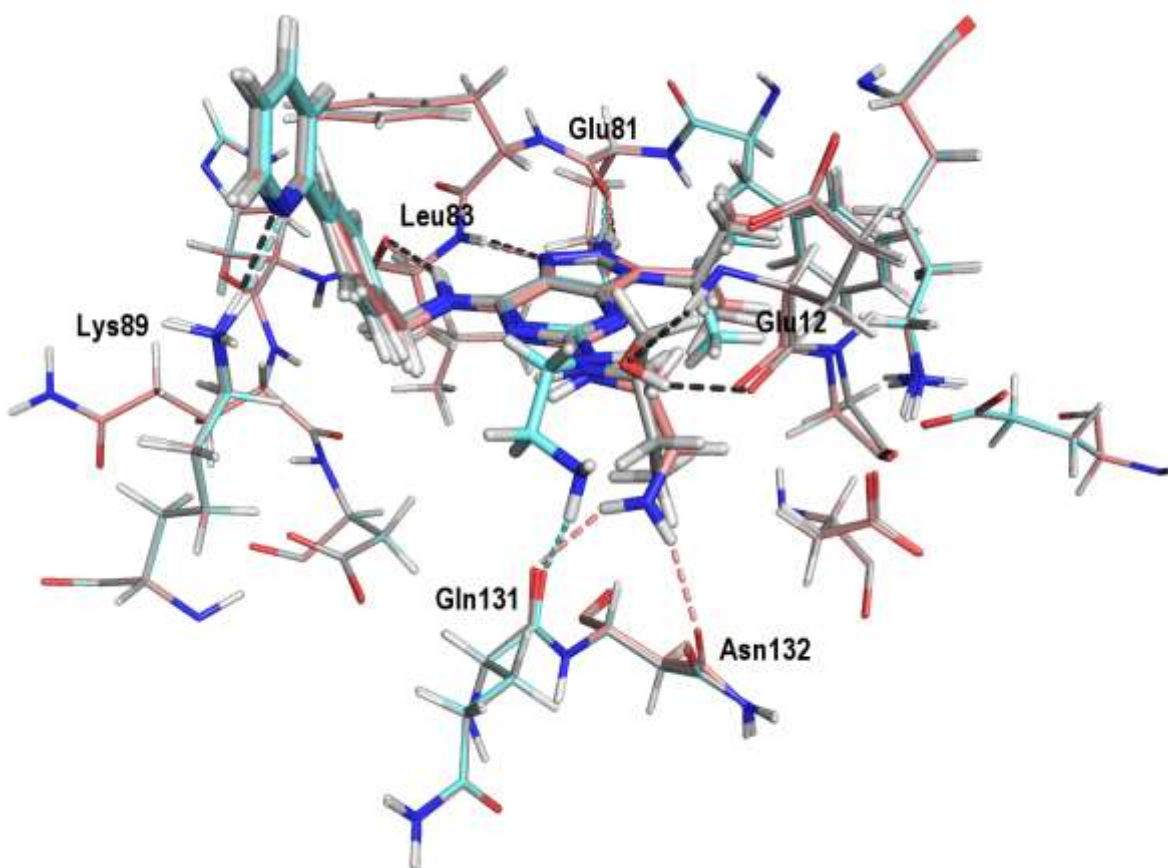
amino group of the moiety at position 5 of **5i**<sub>calc1</sub> forms the hydrogen bond with the backbone carbonyl of Gln131 (**Supplementary Figures S2 and S3**). The comparison of the total  $\Delta G'_{\text{int}}$  values of these conformers shows lower binding affinity than those of **4.35**<sub>calc1</sub> and **5i**<sub>calc1</sub>. The  $\Delta G'_{\text{int}}$  contributions of the moiety at position 5 are also lower than **4.35**<sub>calc1</sub> and **5i**<sub>calc1</sub>; the **5i**<sub>calc2</sub> moiety even results in repulsion (**Supplementary Table 1**). We conclude that although the **4.35**<sub>calc1</sub> conformer is more stable than the **4.35**<sub>calc2</sub> conformer, the **4.35**<sub>calc2</sub> conformer (in complex with the protein) is favorable because the protein-inhibitor complex can be substantially stabilized by two crystal water molecule chains (**Figure 2, Supplementary Figures S4 and S5**).<sup>7</sup>

**Supplementary Table 1.**  $\Delta G'_{\text{int}}$  values of the protein-inhibitor complexes and  $\Delta G'_{\text{int}}$  of the protein-fragment complexes that describe the contributions of the molecular parts (the scaffold and the substituents, see **Supplementary Figure 1**) to the binding affinity.

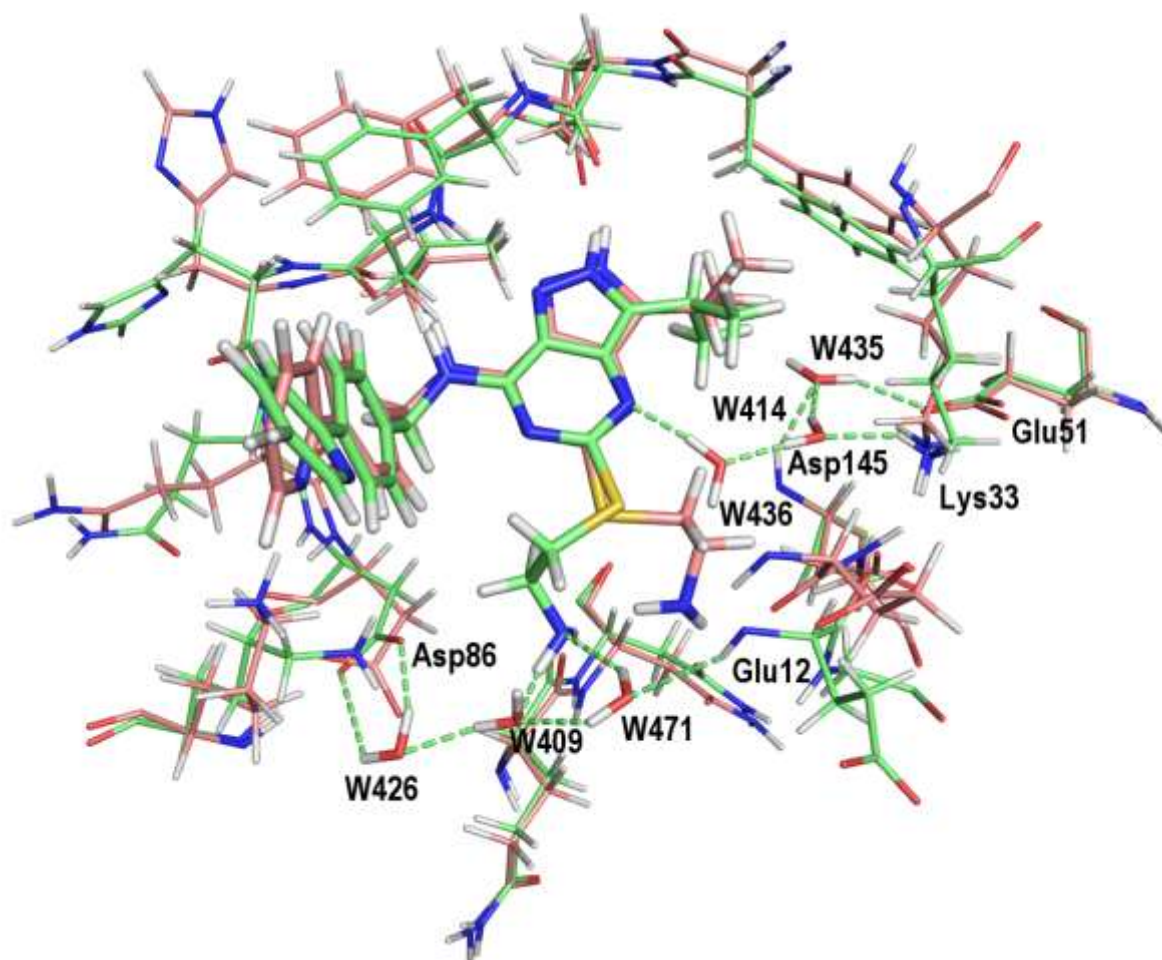
Inhibitor	$\Delta G'_{\text{int}}$ in kcal mol <sup>-1</sup>				Suma of Fragments	CDK2-inhibitor complex
	Fragments of Inhibitors					
	scaffold	R1	R2	R3		
<b>CR8</b>	-11.69	-17.92	-8.24	-3.81	-41.66	-44.37
<b>4.35</b> <sub>calc1</sub>	-15.25	-18.28	-7.41	-3.20	-44.15	-47.15
<b>4.35</b> <sub>calc2</sub>	-13.74	-17.43	-5.34	-3.55	-40.07	-44.19
<b>5i</b> <sub>calc1</sub>	-14.62	-17.99	-4.52	-3.11	-40.24	-44.62
<b>5i</b> <sub>calc2</sub>	-18.40	-17.94	0.20	-4.55	-40.70	-43.57



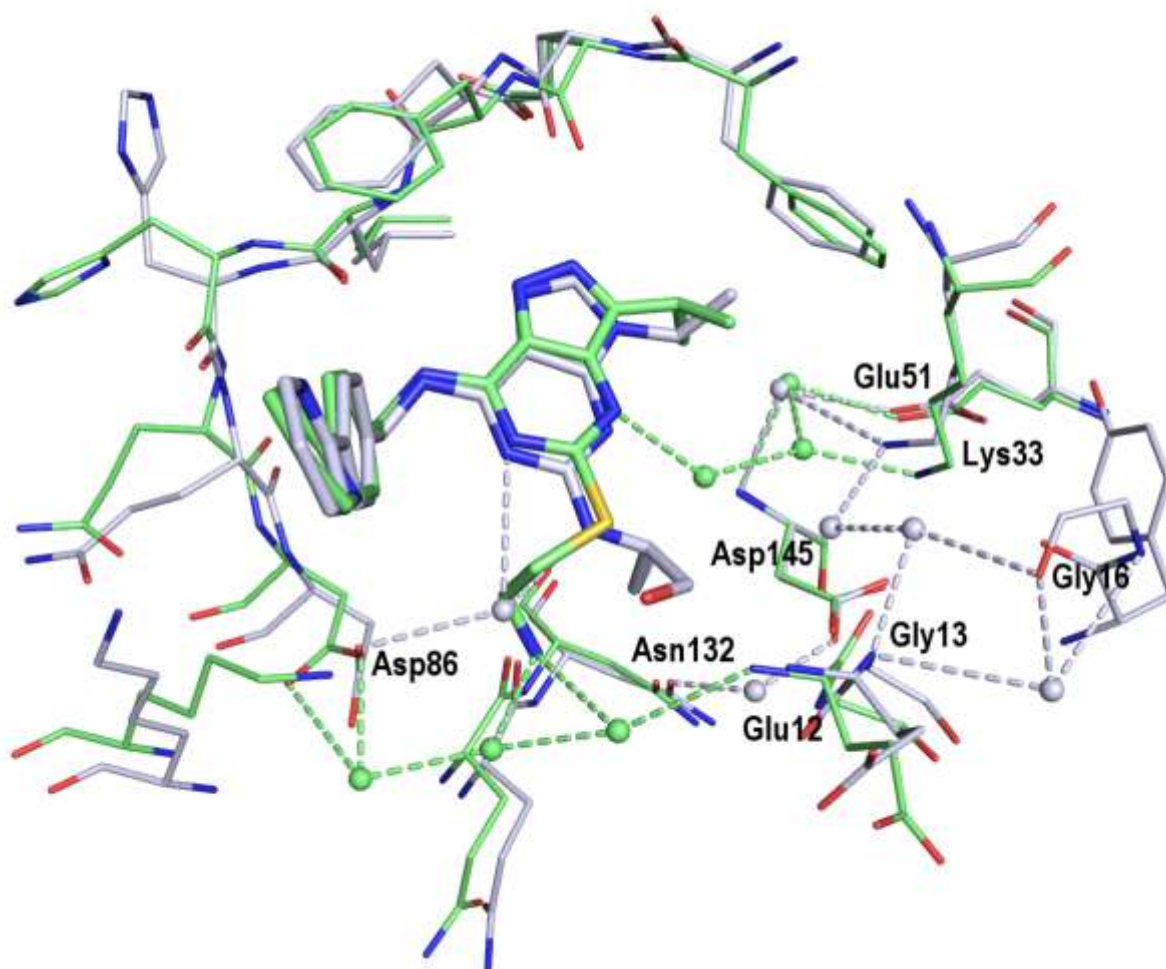
**Supplementary Figure S2.** The computationally optimized complexes of CDK2 with the inhibitors **4.35** and **CR8**. Only the key residues are depicted. The geometries of the **4.35** conformers (**4.35<sub>calc1</sub>** – salmon color, **4.35<sub>calc2</sub>** – aquamarine color;  $IC_{50} = 0.002$ ) in comparison with **CR8** (gray color;  $IC_{50} = 0.062$ ) are illustrated.



**Supplementary Figure S3.** The computationally optimized complexes of CDK2 with the inhibitors **5i** and **CR8**. Only the key residues are depicted. The geometries of the **5i** conformers (**5i**<sub>calc1</sub> – salmon color, **5i**<sub>calc2</sub> – aquamarine color; IC<sub>50</sub> = 0.018) in comparison with **CR8** (gray color; IC<sub>50</sub> = 0.062) are illustrated.



**Supplementary Figure S4.** The nonoptimized complex of CDK2 with **4.35** (lime color) compared with the computed complex of CDK2 with the conformer **4.35<sub>calc1</sub>** (salmon color). Only the key residues are depicted. This demonstrates how the less stable **4.35** conformer is substantially stabilized by the hydrogen bonds with two crystal water chains. The geometry of hydrogens of water molecules was modeled in PyMol.<sup>8</sup>



**Supplementary Figure S5.** The nonoptimized complex of CDK2 with **4.35** (lime color) compared with the nonoptimized complex of CDK2 with **CR8** (blue-white color). Only the key residues are depicted. The inhibitors stabilized by hydrogen bonds with the crystal water chains are shown.

## 2. Crystal parameters

**Supplementary Table 2.** Crystal parameters, data collection and refinement statistics

<b>Data collection statistics</b>	
Space group	$C222_1$
Cell parameters ( $\text{\AA}$ ; $^\circ$ )	$a = 71.0, b = 112.6, c = 159.7; \alpha = \beta = \gamma = 90$
Number of molecules in AU	1
Wavelength ( $\text{\AA}$ )	0.918
Resolution ( $\text{\AA}$ )	48.01–2.15 (2.28–2.15)
Number of unique reflections	34,773 (5,088)
Multiplicity	6.2 (4.3)
Completeness (%)	98.3 (90.3)
$R_{\text{meas}}^a$	21.2 (166.4)
$CC_{(1/2)}$	99.4 (29.8)
Average $I/\sigma(I)$	8.0 (0.9)
Wilson B ( $\text{\AA}^2$ ) <sup>b</sup>	38.4
<b>Refinement statistics</b>	
Resolution range ( $\text{\AA}$ )	48.00–2.15 (2.20–2.15)
No. of reflections in working set	33,033 (2,066)
No. of reflections in test set	1,739 (109)
R value (%) <sup>c</sup>	19.4
$R_{\text{free}}$ value (%) <sup>d</sup>	24.0
RMSD bond length ( $\text{\AA}$ )	0.013
RMSD angle ( $^\circ$ )	1.619
Number of atoms in AU	4,638
Number of protein atoms in AU	4,394
Number of water molecules in AU	160
Mean B value ( $\text{\AA}^2$ )	40.2
<b>Ramachandran plot statistics<sup>e</sup></b>	
Residues in favored regions (%)	97.8
Residues in allowed regions (%)	99.8

<sup>a</sup> $R_{\text{meas}}$  defined in reference.<sup>9</sup> <sup>b</sup>Wilson B by Sfccheck program from CCP4 suite.<sup>10</sup> <sup>c</sup>R-value =  $(|F_o| - |F_c|)/|F_o|$ , where  $F_o$  and  $F_c$  are the observed and calculated structure factors, respectively. <sup>d</sup> $R_{\text{free}}$  is equivalent to the R-value but is calculated for 5% of the reflections chosen at random and omitted from the refinement process.<sup>11</sup> <sup>e</sup>As determined by MolProbity.<sup>12</sup>

### 3. Kinase selectivity profile

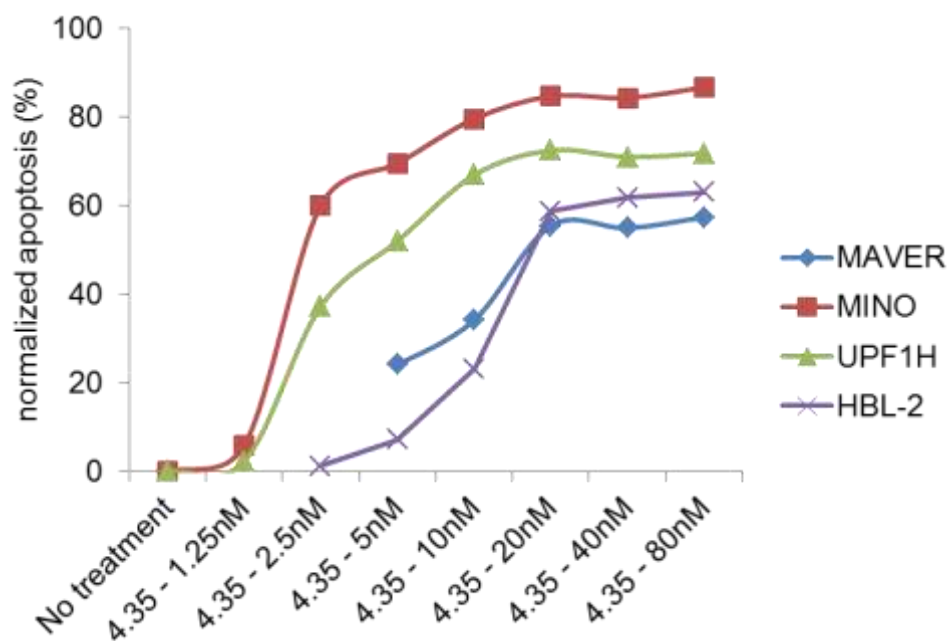
**Supplementary Table 3.** Kinase selectivity profile against a panel of 50 human kinases. The profiling was performed in duplicate at a compound concentration of 1  $\mu$ M.

kinase	Residual activity (%)	kinase	Residual activity (%)
AMPK (hum)	34	NEK6	89
Aurora B	55	p38a MAPK	92
BTK	95	PAK4	33
CAMK1	35	PDK1	106
CAMKKb	58	PIM1	116
CK1 $\delta$	11	PKA	92
CK2	75	PKBa	124
DYRK1A	63	PKCa	80
EF2K	99	PKD1	44
EPH-A2	102	PLK1	94
GSK3b	99	PRK2	106
HER4	100	RIPK2	103
HIPK2	96	ROCK 2	111
CHK2	18	RSK1	35
IGF-1R	116	S6K1	93
IRAK4	131	SGK1	107
JAK2	111	SmMLCK	45
JNK1	94	Src	74
Lck	82	SRPK1	86
LKB1	86	SYK	117
MARK3	32	TAK1	97
MKK1	48	TBK1	98
MLK3	97	TrkA	91
MSK1	78	TTK	78
MST2	96	VEG-FR	114

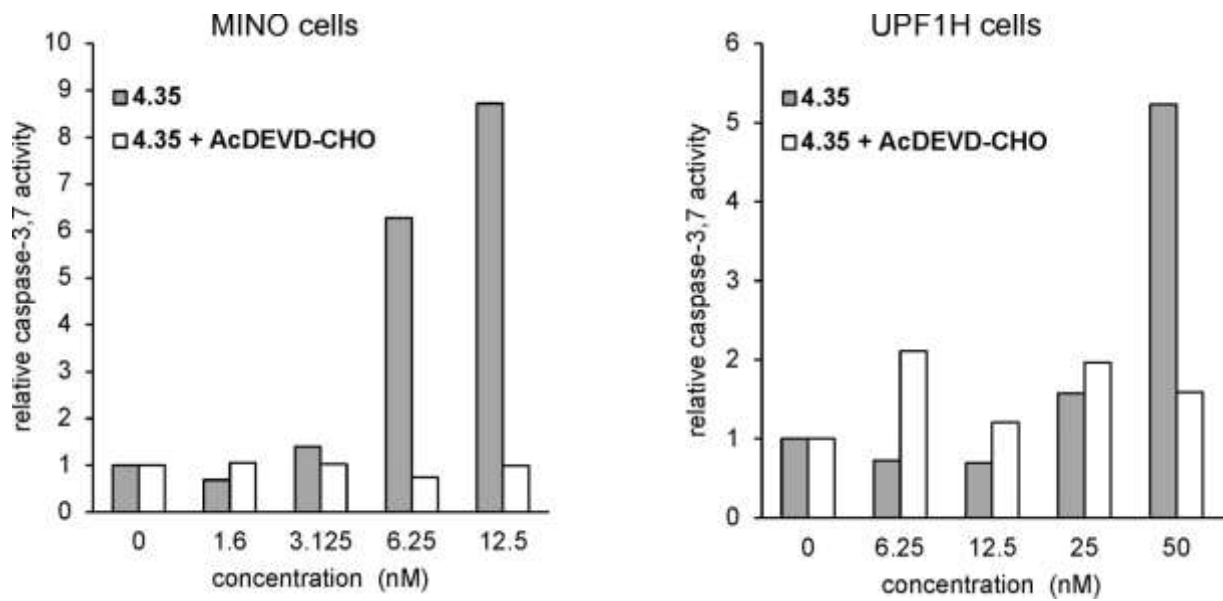
#### 4. Additional in vitro data

**Supplementary Table 4.** In vitro testing of 4.35 on a panel of cancer cell lines (National Cancer Institute Developmental Therapeutics Program).

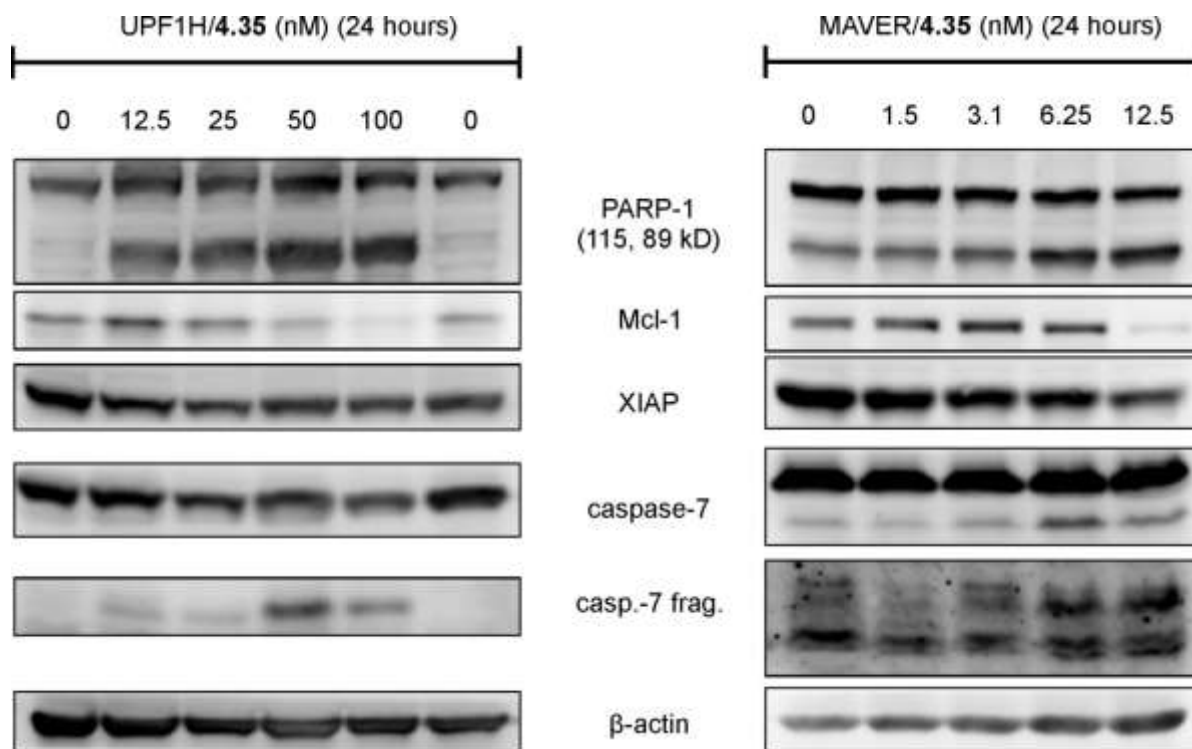
Panel/Cell Line	Time Zero	Log10 Concentration										GI50	TGI	LC50	
		Ctrl	-9.0	-8.0	-7.0	-6.0	-5.0	-9.0	-8.0	-7.0	-6.0				-5.0
<b>Leukemia</b>															
CCRF-CEM	0.778	3.313	3.365	2.033	0.872	0.856	0.838	102	49	4	3	2	9.78E-9	> 1.00E-5	> 1.00E-5
HL-60(TB)	1.240	3.162	3.334	1.646	1.097	0.962	0.794	109	21	-12	-22	-36	4.69E-9	4.43E-8	> 1.00E-5
K-562	0.312	2.191	2.423	1.474	0.726	0.540	0.480	112	62	22	12	9	1.98E-8	> 1.00E-5	> 1.00E-5
MOLT-4	0.907	3.294	3.358	1.571	0.940	0.865	0.860	103	28	1	-5	-5	5.05E-9	1.69E-7	> 1.00E-5
RPMI-8226	0.943	3.133	3.120	2.301	0.898	0.896	0.796	99	62	-5	-5	-16	1.51E-8	8.47E-8	> 1.00E-5
SR	0.298	1.456	1.512	0.925	0.453	0.417	0.411	105	54	13	10	10	1.26E-8	> 1.00E-5	> 1.00E-5
<b>Non-Small Cell Lung Cancer</b>															
A549/ATCC	0.434	2.214	2.285	1.954	0.658	0.699	0.622	104	85	13	15	11	3.06E-8	> 1.00E-5	> 1.00E-5
EKVX	1.041	2.888	2.679	2.587	1.380	1.051	1.017	89	84	18	1	-2	3.28E-8	1.52E-6	> 1.00E-5
HOP-62	0.906	2.433	2.230	2.049	1.083	0.877	0.788	87	75	12	-3	-13	2.47E-8	6.04E-7	> 1.00E-5
HOP-92	1.115	1.768	1.753	1.540	1.099	1.068	1.095	98	65	-1	-4	-2	1.69E-8	9.50E-8	> 1.00E-5
NCI-H226	0.953	2.553	2.440	2.487	1.276	0.981	0.971	93	96	20	2	1	4.04E-8	> 1.00E-5	> 1.00E-5
NCI-H23	0.661	2.293	2.203	1.796	0.820	0.654	0.592	94	70	10	-1	-10	2.12E-8	7.97E-7	> 1.00E-5
NCI-H322M	0.782	2.031	2.002	1.536	0.924	0.762	0.827	98	60	11	-3	4	1.63E-8	> 1.00E-5	> 1.00E-5
NCI-H460	0.245	2.430	2.541	2.589	0.435	0.352	0.219	105	107	9	5	-11	3.81E-8	2.05E-6	> 1.00E-5
NCI-H522	0.929	2.408	2.393	0.979	0.955	0.849	0.840	99	3	2	-9	-10	3.26E-9	1.47E-7	> 1.00E-5
<b>Colon Cancer</b>															
COLO 205	0.638	2.249	2.175	1.629	0.387	0.286	0.324	95	62	-39	-55	-49	1.30E-8	4.07E-8	> 1.00E-5
HCC-2998	0.800	2.837	2.808	2.253	1.163	0.978	0.887	99	71	18	9	4	2.50E-8	> 1.00E-5	> 1.00E-5
HCT-116	0.274	2.476	2.149	1.938	0.406	0.395	0.379	85	76	6	5	5	2.33E-8	> 1.00E-5	> 1.00E-5
HCT-15	0.347	1.139	2.081	2.155	2.056	1.074	0.420	97	101	96	41	4	6.72E-7	> 1.00E-5	> 1.00E-5
HT29	0.322	2.030	2.061	0.800	0.405	0.368	0.324	102	28	5	3		5.03E-9	> 1.00E-5	> 1.00E-5
KM12	0.457	2.664	2.632	1.840	0.695	0.644	0.554	99	63	10	8	4	1.74E-8	> 1.00E-5	> 1.00E-5
SW-620	0.386	2.356	2.377	1.441	0.564	0.500	0.391	101	54	9	6		1.20E-8	> 1.00E-5	> 1.00E-5
<b>CNS Cancer</b>															
SF-268	0.646	2.043	2.006	1.214	0.783	0.734	0.639	97	41	10	6	-1	6.84E-9	7.12E-6	> 1.00E-5
SF-295	0.819	2.532	2.318	2.368	1.200	0.788	0.733	87	90	22	-4	-11	3.91E-8	7.12E-7	> 1.00E-5
SF-539	1.125	3.054	2.960	3.059	1.115	0.693	0.433	95	100		-38	-62	3.14E-8	9.79E-8	3.17E-6
SNB-19	0.980	2.703	2.643	2.047	1.185	1.134	1.102	97	62	12	9	7	1.73E-8	> 1.00E-5	> 1.00E-5
SNB-75	0.929	1.736	1.571	1.261	0.577	0.260	0.077	80	41	-38	-72	-92	5.87E-9	3.31E-8	2.26E-7
U251	0.476	2.238	2.228	1.872	0.720	0.680	0.622	99	79	14	12	8	2.80E-8	> 1.00E-5	> 1.00E-5
<b>Melanoma</b>															
LOX IMVI	0.174	1.338	1.284	0.573	0.209	0.234	0.162	95	34	3	5	-7	5.53E-9	2.62E-6	> 1.00E-5
MALME-3M	0.845	1.579	1.517	1.339	0.377	0.462	0.276	92	67	-55	-45	-67	1.38E-8	3.54E-8	> 1.00E-5
M14	0.439	1.716	1.605	1.213	0.502	0.339	0.129	91	61	5	-23	-71	1.55E-8	1.51E-7	3.70E-6
MDA-MB-435	0.479	2.411	2.336	0.911	0.485	0.519	0.197	96	22	2	-69		4.22E-9	1.08E-6	7.13E-6
SK-MEL-2	1.025	2.471	2.535	2.420	1.039	0.581	0.345	104	95	1	-43	-66	3.06E-8	1.05E-7	1.94E-6
SK-MEL-28	0.880	2.572	2.508	2.022	1.017	0.647	0.552	96	67	8	-27	-37	1.97E-8	1.71E-7	> 1.00E-5
SK-MEL-5	0.795	3.278	3.264	3.195	0.775	1.228	0.653	99	97	-3	17	-18	2.95E-8	> 1.00E-5	> 1.00E-5
UACC-257	0.955	2.280	2.197	2.183	1.267	1.067	1.017	94	93	24	8	5	4.14E-8	> 1.00E-5	> 1.00E-5
UACC-62	0.894	3.023	2.974	2.698	0.549	0.417	0.280	98	85	-39	-53	-69	1.91E-8	4.86E-8	5.87E-7
<b>Ovarian Cancer</b>															
IGROV1	0.693	2.284	2.254	1.830	0.804	0.822	0.725	98	71	7	8	2	2.15E-8	> 1.00E-5	> 1.00E-5
OVCAR-3	0.434	1.602	1.653	1.213	0.509	0.489	0.469	104	67	6	5	3	1.89E-8	> 1.00E-5	> 1.00E-5
OVCAR-4	0.700	1.565	1.491	1.024	0.740	0.678	0.525	91	37	5	-3	-25	5.85E-9	3.94E-7	> 1.00E-5
OVCAR-5	0.681	1.905	1.854	1.889	1.005	0.950	0.899	96	99	26	22	18	4.72E-8	> 1.00E-5	> 1.00E-5
OVCAR-8	0.675	2.598	2.648	2.416	1.091	0.909	0.917	103	91	22	12	13	3.87E-8	> 1.00E-5	> 1.00E-5
NCI/ADR-RES	0.552	2.124	2.100	2.136	2.058	1.836	1.112	98	101	96	82	36	4.87E-6	> 1.00E-5	> 1.00E-5
SK-OV-3	0.888	2.227	2.133	2.141	1.224	1.084	1.136	93	94	25	15	19	4.33E-8	> 1.00E-5	> 1.00E-5
<b>Renal Cancer</b>															
786-0	0.886	2.620	2.438	2.491	1.913	0.891	0.713	90	93	59		-20	1.43E-7	1.03E-6	> 1.00E-5
A498	1.496	2.523	2.498	2.586	1.352	0.870	0.630	98	106	-10	-42	-68	3.06E-8	8.26E-8	3.22E-6
ACHN	0.462	2.009	1.944	2.032	1.832	0.465	0.536	96	102	89		5	2.73E-7	> 1.00E-5	> 1.00E-5
CAKI-1	0.593	3.040	2.928	2.957	2.910	2.430	0.868	95	97	95	75	11	2.47E-6	> 1.00E-5	> 1.00E-5
RFX 393	0.632	1.304	1.274	1.121	0.459	0.337	0.279	95	73	-27	-47	-66	1.69E-8	5.32E-8	2.27E-6
SN12C	1.145	3.322	3.361	2.653	1.540	1.433	1.253	102	69	18	13	5	2.38E-8	> 1.00E-5	> 1.00E-5
UO-31	0.822	2.371	2.290	2.265	2.078	0.539	0.650	95	93	81	-34	-21	1.86E-7	5.03E-7	> 1.00E-5
<b>Prostate Cancer</b>															
PC-3	0.504	1.789	1.793	1.501	0.638	0.547	0.494	100	78	10	3	-2	2.57E-8	4.11E-6	> 1.00E-5
DU-145	0.490	1.963	2.001	1.883	0.770	0.610	0.568	103	95	19	8	5	3.89E-8	> 1.00E-5	> 1.00E-5
<b>Breast Cancer</b>															
MCF7	0.427	2.233	2.073	0.841	0.567	0.473	0.408	91	23	8	3	-5	4.01E-9	2.28E-6	> 1.00E-5
MDA-MB-231/ATCC	0.877	1.930	1.951	1.160	0.929	0.781	0.756	102	27	5	-11	-14	4.92E-9	2.05E-7	> 1.00E-5
HS 578T	1.166	2.116	2.068	1.729	1.240	1.209	1.094	95	59	8	4	-6	1.51E-8	2.62E-6	> 1.00E-5
BT-549	1.282	2.428	2.292	2.334	1.391	0.868	0.488	88	92	9	-32	-62	3.22E-8	1.68E-7	3.95E-6
T-47D	1.047	2.069	1.880	1.718	1.103	1.063	1.058	82	66	5	2	1	1.82E-8	> 1.00E-5	> 1.00E-5
MDA-MB-468	0.746	1.455	1.459	0.776	0.473	0.436	0.470	101	4	-37	-42	-37	3.35E-9	1.27E-8	> 1.00E-5



**Supplementary Figure S6:** Effect of **4.35** on apoptosis in lymphoma cell lines. Annexin V/PI assay was carried out as described in Methods.



**Supplementary Figure S7:** Fluorometric assay of caspase-3 and caspase-7 activity in lysates prepared from treated cells. The activities were measured in the presence of the fluorogenic substrate Ac-DEVD-AMC (gray columns) or the fluorogenic caspase inhibitor Ac-DEVD-CHO (white columns) as a control and normalized to an untreated control.



**Supplementary Figure S8:** Induction of apoptosis in UPF1H and MAVER-1 cancer cells treated with pyrazolo[4,3-*d*]pyrimidine **4.35** for 24 h. Actin level is included as a loading control.

## 5. Physicochemical and pharmacological properties of 4.35

Aqueous solubility (200 $\mu$ M in PBS, pH 7.4)	91%	
Aqueous solubility (200 $\mu$ M in simulated intestinal fluid)	91%	
Aqueous solubility (200 $\mu$ M in simulated gastric fluid)	91%	
Plasma protein binding (10 $\mu$ M, 4 h at 37 °C)	94%	
In vitro absorption Caco-2 (A-B permeability @ 10 $\mu$ M)	0.0 ( $10^{-6}$ cm/s)	
In vitro absorption Caco-2 (B-A permeability @ 10 $\mu$ M)	15.8 ( $10^{-6}$ cm/s)	
Intrinsic clearance (0.1 $\mu$ M with human liver microsomes)	0 min	100%
	15 min	92%
	30 min	82%
	45 min	63%
	60 min	61%

Physicochemical and pharmacological properties were determined by Eurofin Panlabs.

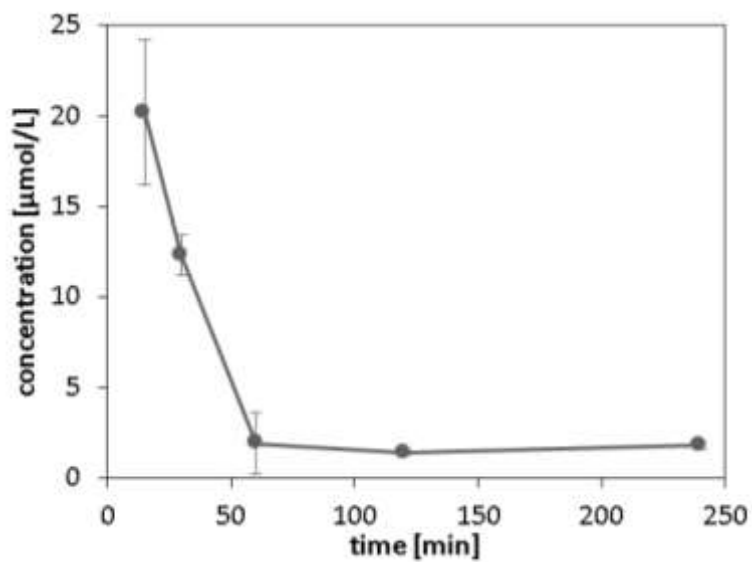
**Aqueous solubility.** The solubility was determined by comparing the peak area of the compound standard solution (200  $\mu$ M, methanol/water, 60/40, v/v) with the peak area of the compound in a buffer sample. In addition, chromatographic purity (%) was defined as the peak area of the principal peak relative to the total integrated peak area in the HPLC chromatogram of the calibration standard.

**Plasma protein binding.** The peak areas of the test compound in the buffer and test samples were used to calculate percent binding.

**Caco-2 permeability.** The apparent permeability coefficient ( $P_{app}$ ) of the test compound was determined. Fluorescein permeability assessment (in the A-B direction at pH 7.4 on both sides) was performed after the permeability assay for the test compound. The percent of inhibition was calculated by subtracting the percent of control from 100.

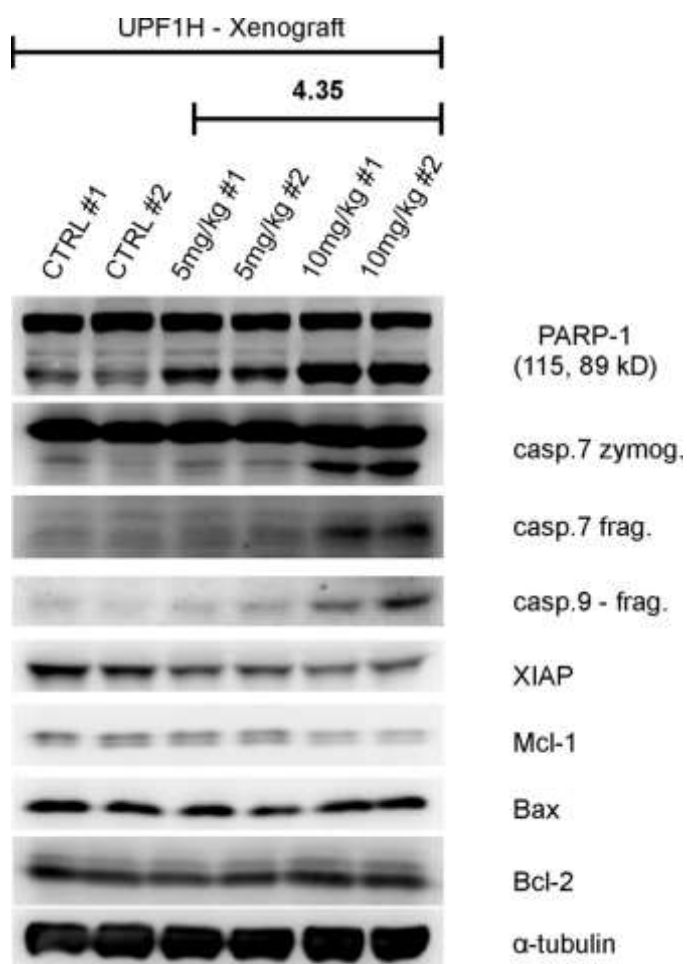
**Intrinsic Clearance.** Intrinsic clearance was determined with human liver microsomes.

Metabolic stability, expressed as percent of the parent compound remaining, was calculated by comparing the peak area of the compound at the time point relative to that at time-0.

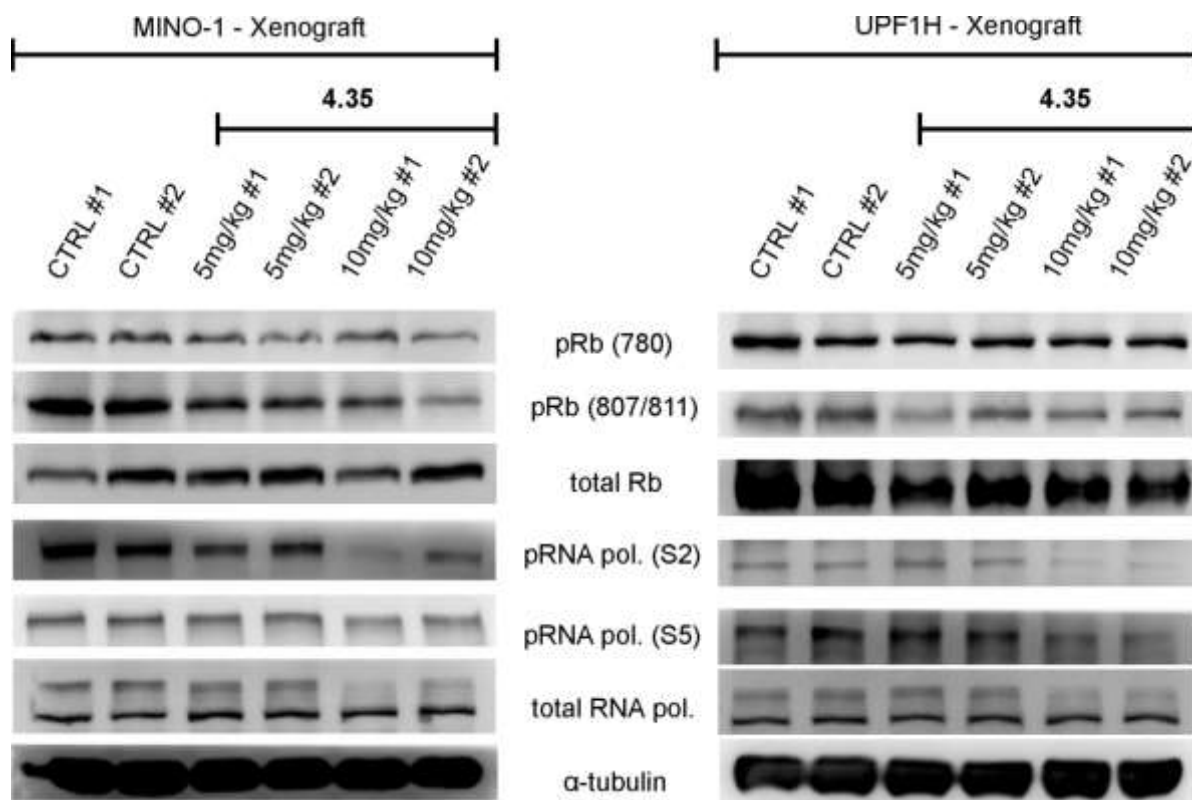


**Supplementary Figure S9:** Mean plasma concentration-time profile ( $\pm$  SD) of **4.35** in mice following 10 mg/kg i.v. administration (n=3). See Methods for experimental details

## 6. Additional in vivo data



**Supplementary Figure S10.** Inhibitory effect of pyrazolo[4,3-*d*]pyrimidine **4.35** on apoptosis in lymphoma xenografts derived from the UPF1H cell line. Tumor-bearing mice were intravenously injected with **4.35**. Twenty-four hours after injection, the mice were euthanized, and the tumors were removed and analyzed. Tubulin level is included as a loading control.



**Supplementary Figure S10.** Inhibitory effect of pyrazolo[4,3-*d*]pyrimidine **4.35** on some proteins in lymphoma xenografts derived from MINO-1 and UPF1H cell lines. Tumor-bearing mice were intravenously injected with **4.35**. Twenty-four hours after injection, the mice were euthanized, and the tumors were removed and analyzed. Tubulin level is included as a loading control.

## 7. Additional Methods

### Annexin V/PI Assay

Number of apoptotic and/or necrotic cells was determined by flow cytometry (BD FACS Canto II) using Annexin V FITC (Apronex, Czech Republic) and propidium iodide (Sigma). Percentage of cell death was calculated from the proportion of the living cells only using the following formula: % cell death = ((Agent induced apoptosis - basal apoptosis)/(100 - basal apoptosis))\*100

### Caspase activity assay

The cells were homogenized in an extraction buffer (10 mM KCl, 5 mM HEPES, 1 mM EDTA, 1 mM EGTA, 0.2% CHAPS, inhibitors of proteases, pH 7.4) on ice for 20 min. The homogenates were clarified by centrifugation at 10 000 x g for 30 min at 4 °C, and then the proteins were quantified and diluted to equal concentrations. Lysates were then incubated for 4 h with 100 mM Ac-DEVD-AMC (Enzo Life Sciences) as a substrate of caspases 3 and 7 in the assay buffer (25 mM PIPES, 2 mM EGTA, 2 mM MgCl<sub>2</sub>, 5 mM DTT, pH 7.3). The fluorescence of the product was measured using a Fluoroskan Ascent microplate reader (Labsystems) at 355/460 nm (excitation/emission).

### Pharmacokinetic analysis in mice

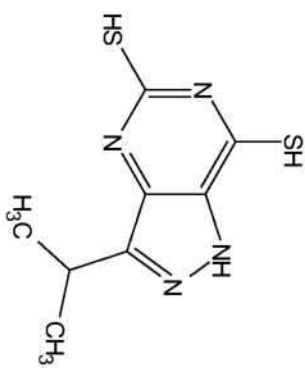
Compound **4.35** was dissolved in DMSO at 100 mM. Mice were i.v. administered 10 mg/kg compound **4.35**. Three mice were sacrificed at each time point, and blood samples were collected by cardiac puncture into heparinized tubes at 15, 30, 60, 120 and 240 min after drug administration. Blood samples were centrifuged immediately after collection at 1000 g and 4 °C for 5 min, and the supernatants were collected and frozen at -20 °C. Before analysis, the plasma samples were thawed at room temperature, precipitated in methanol (plasma/methanol, 1/3, v/v), spiked with the internal standard (IS, roscovitine), vortexed and then centrifuged (4 °C, 9000 g, 10 min). The supernatants were transferred to Eppendorf tubes with microspin filters (0.2 µm, NY) and centrifuged (4 °C, 9000 g, 5 min). The filtrates were evaporated under nitrogen and reconstructed in 50% methanol. A total of 10 µL of the filtrate was injected in an Acquity BEH C18 column (100 × 2.1 mm, 1.7 µm) (Waters, Ireland) maintained at 40 °C. The analyses were performed on a liquid chromatography system (Acquity UPLC System, Waters, Milford, MA, USA) coupled to a Micromass Quattro Micro<sup>TM</sup> API (Waters MS Technologies, Manchester, UK) detector. A gradient of 15 mM ammonium formate at pH 4.0 (A) and methanol (B) at a flow rate of 0.25 mL/min was

employed (0-6 min linear gradient 35–100% B, 6-6.5 min 100% B, 6.5-7 min linear gradient 100–35%, 7-8 min 35% B). The mass spectrometry system was operated in positive ionization mode using multiple reaction monitoring and scanning a transition of 420.2 > 403 (collision energy 18 V) for **4.35** and a transition of 355.5 > 90.86 (collision energy 40 V) for IS. The source and analyzer parameters were set as follows: capillary voltage 1000 V; cone voltage 30 V; extractor 2 V; RF lens 0.2 V; cone and desolvation gas was nitrogen at 100 and 350 °C and flow rates 2.0 and 550 L/h; LM/HM resolution 12.5; ion energy 1, 0.3 V; ion energy 2, 1.5 V; entrance, exit and multiplier voltages, 2.0 V, 2.0 V and 650 V, respectively. Argon was used as the collision gas. The quantification of the analyte in mouse plasma samples was based on a subsequently measured matrix-matched calibration curve in the range of 0.025–25 µmol/L (7 calibration concentration levels) constructed by plotting the analyte response (analyte/IS peak area ratio multiplied by IS concentration) against the analyte concentration by applying a logarithmic transformation. The obtained slope, intercept and  $r^2$  of the calibration curve were 0.8726, 0.1938 and 0.9979, respectively. More than 75% of the back calculated concentrations of the calibration standards were within the  $\pm 15\%$  of the nominal concentration.

## 8. NMR Spectra of Prepared Compounds

3-Isopropyl-1(2)H-pyrazolo[4,3-d]pyrimidin-5,7-dithiol (2)

— 13.84  
— 13.45  
— 13.33



— 3.30

— 2.50 DMSO-d6

— 1.21  
— 1.20

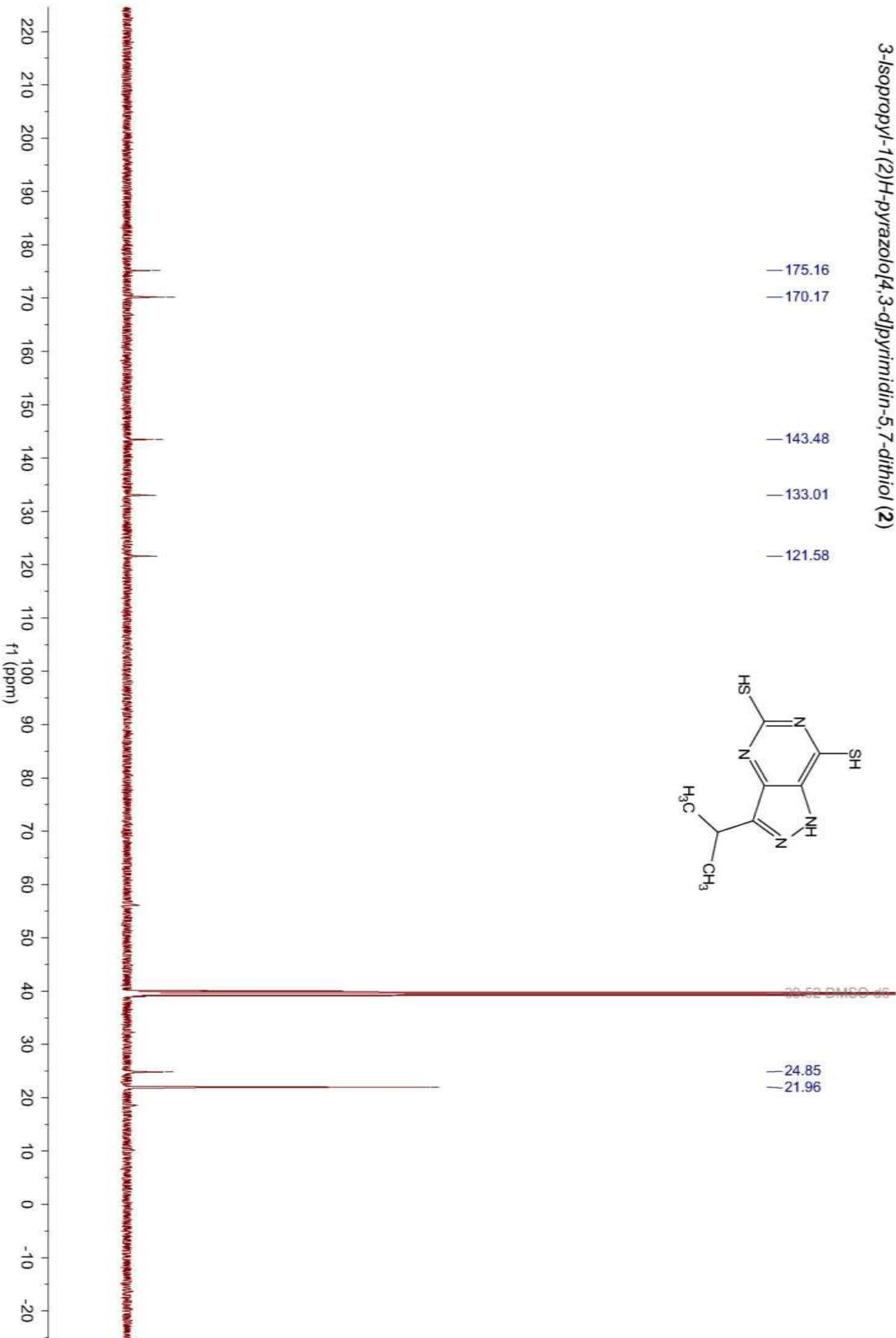
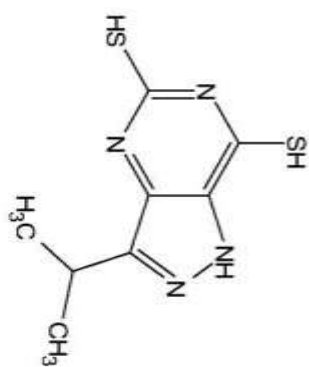
14.0 14.5 13.5 13.0 12.5 12.0 11.5 11.0 10.5 10.0 9.5 9.0 8.5 8.0 7.5 7.0 6.5 6.0 5.5 5.0 4.5 4.0 3.5 3.0 2.5 2.0 1.5 1.0 0.5 0.

0.83  
0.84  
0.84

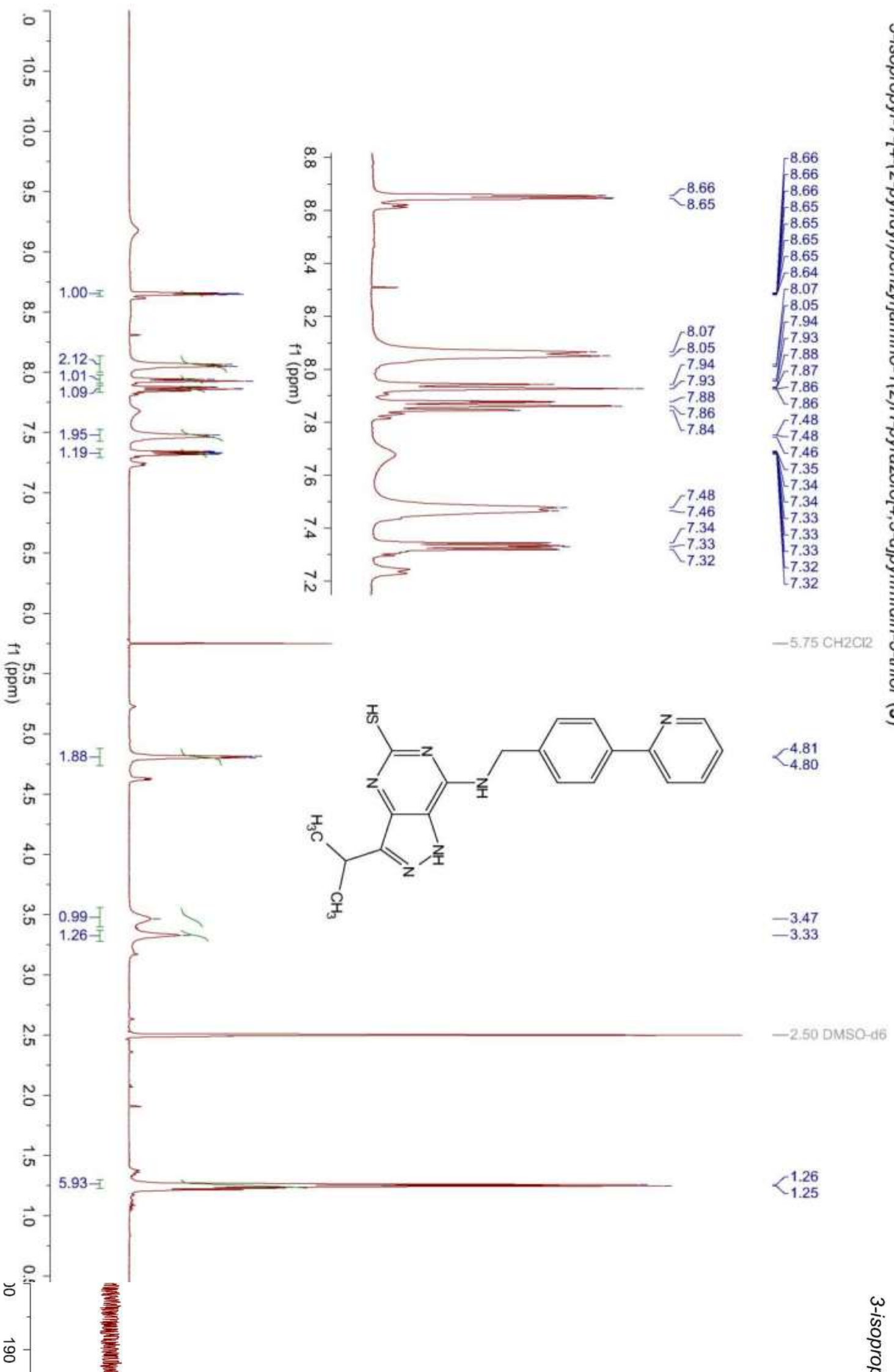
0.91

6.00

3-Isopropyl-1(2*H*)-pyrazolo[4,3-*d*]pyrimidin-5,7-dithiol (2)

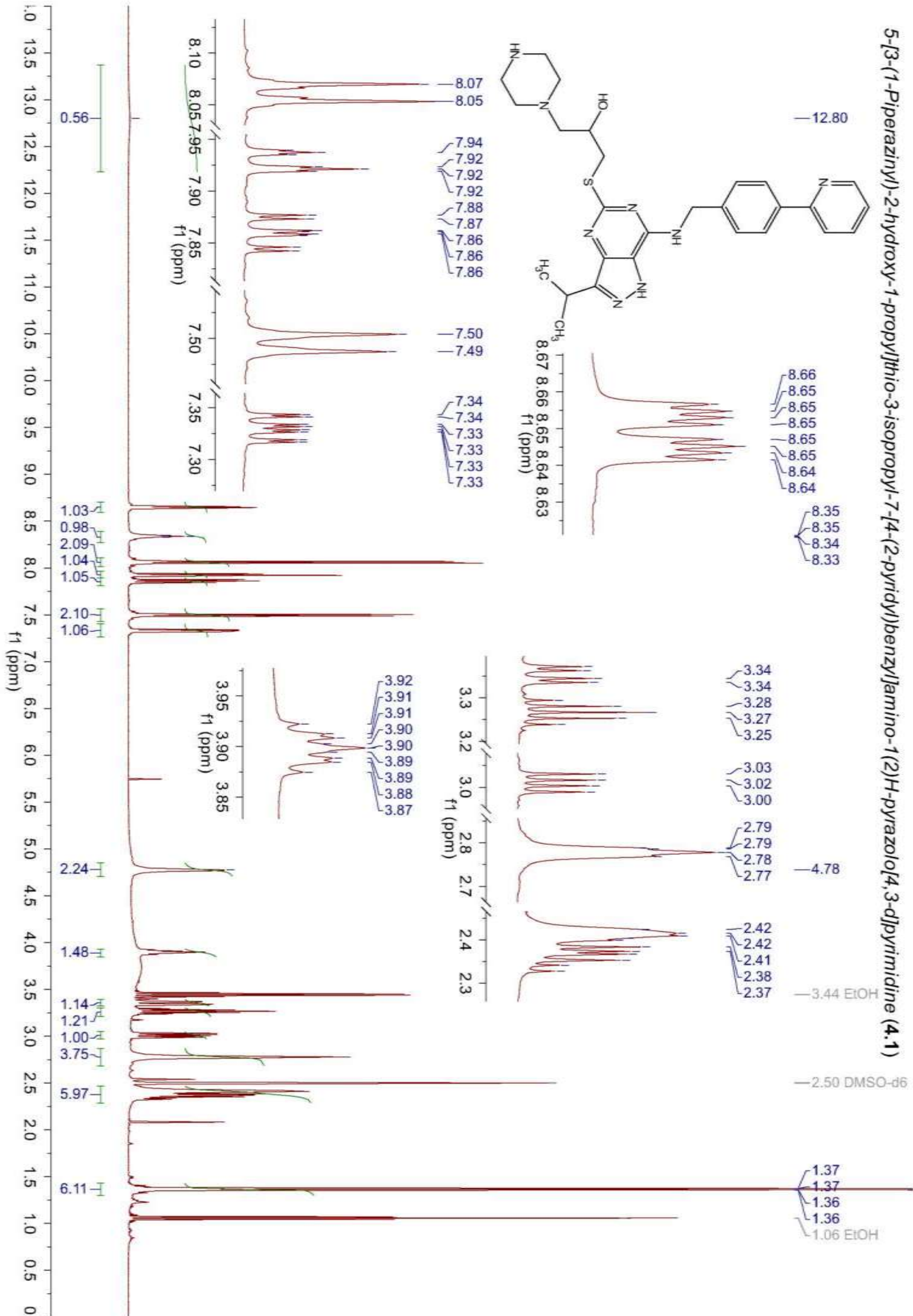
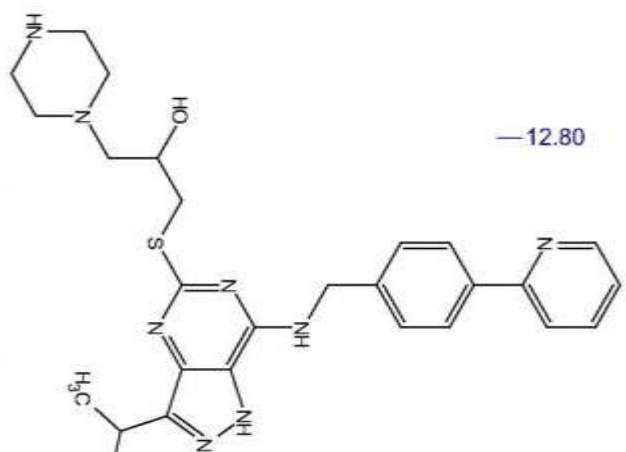


3-isopropyl-7-[4-(2-pyridyl)benzyl]amino-1(2H)-pyrazolo[4,3-d]pyrimidin-5-thiol (3)

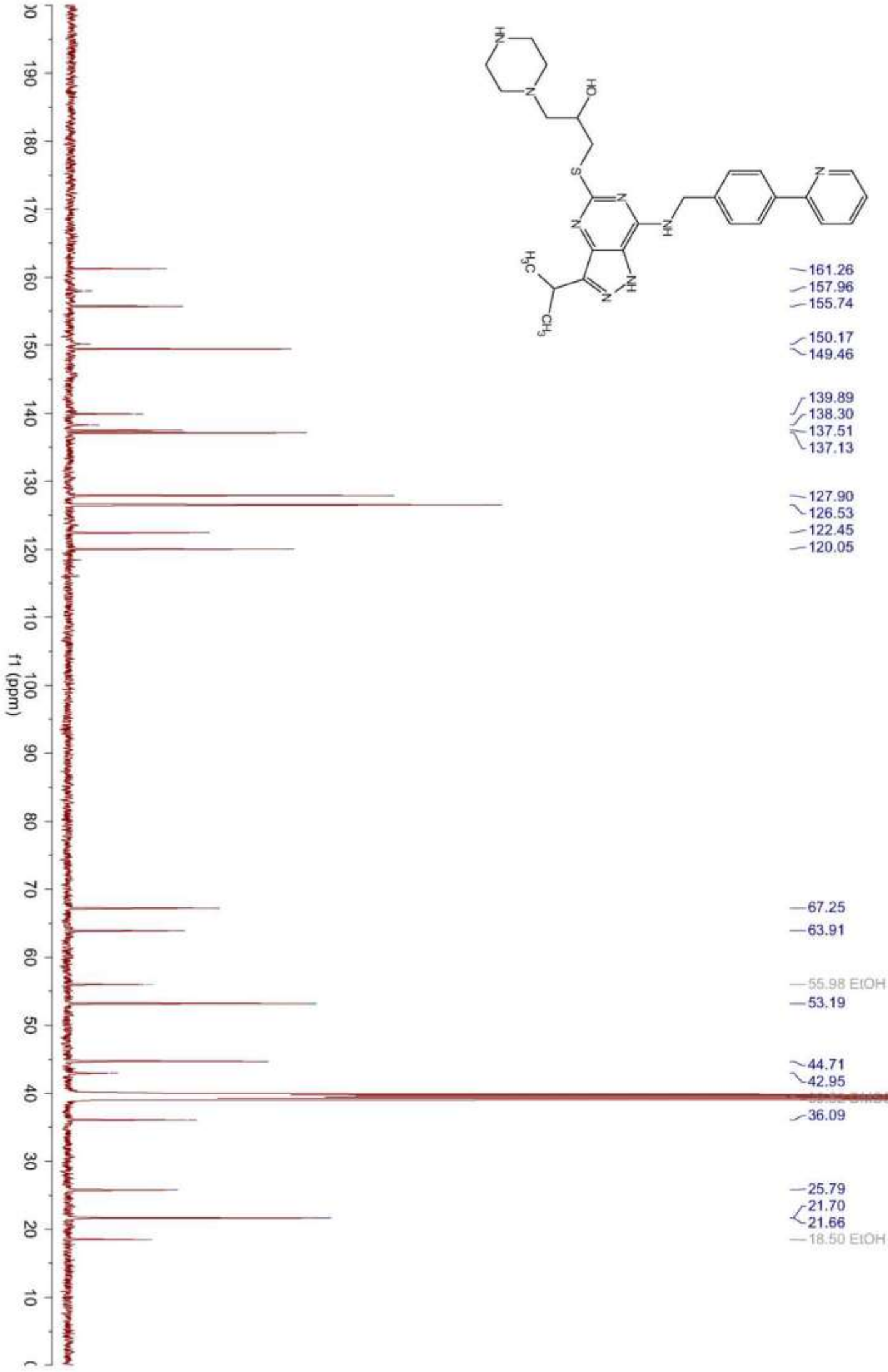
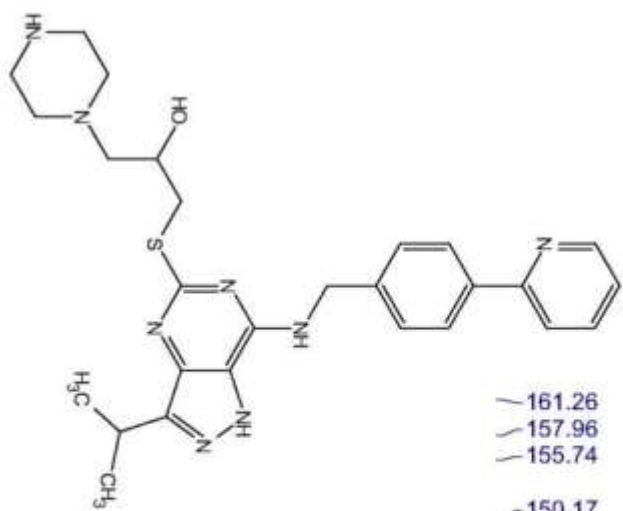


3-isoprop

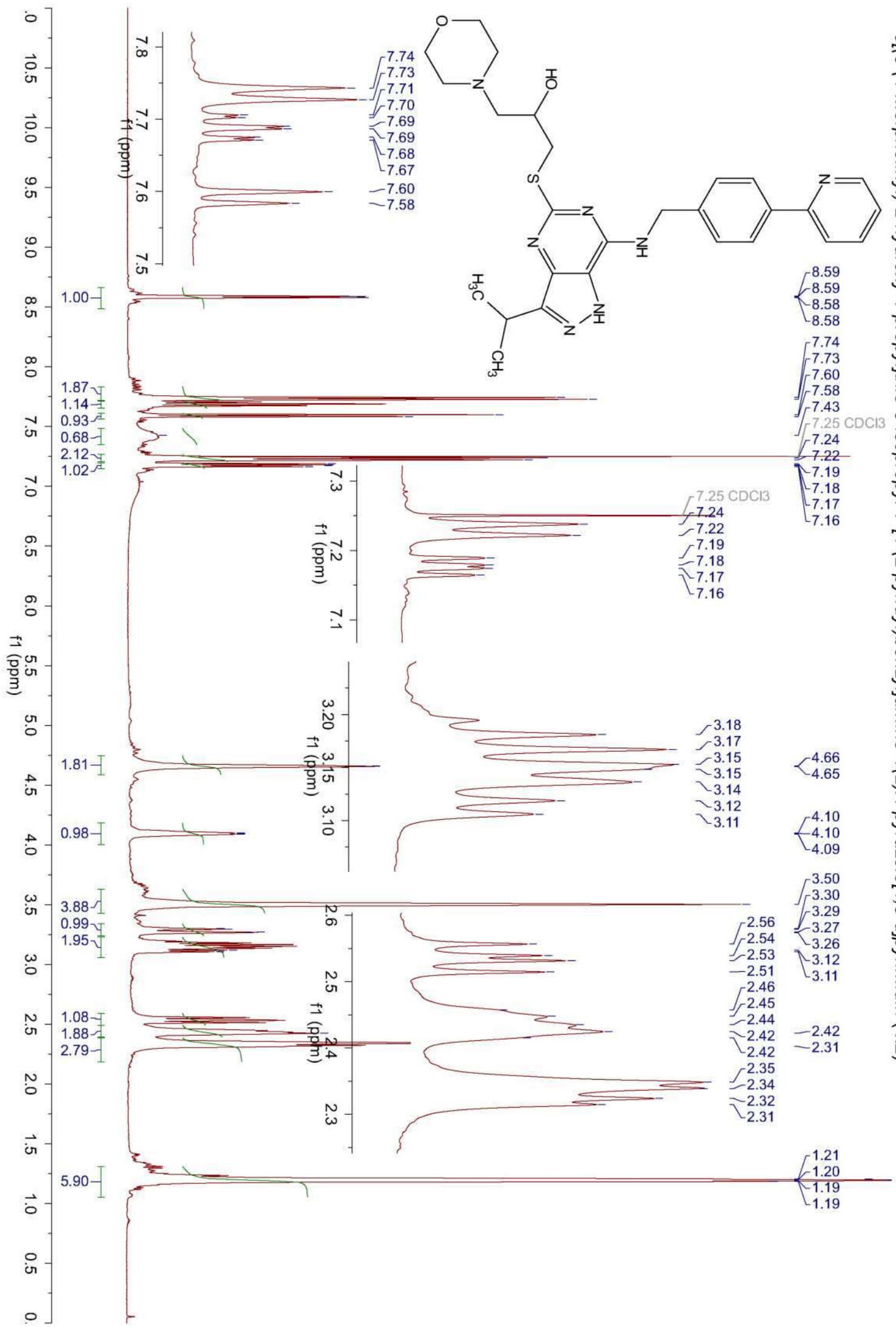
5-[3-(1-Piperazinyl)-2-hydroxy-1-propyl]thio-3-isopropyl-7-[4-(2-pyridyl)benzyl]amino-1(2H)-pyrazolo[4,3-d]pyrimidine (4.1)



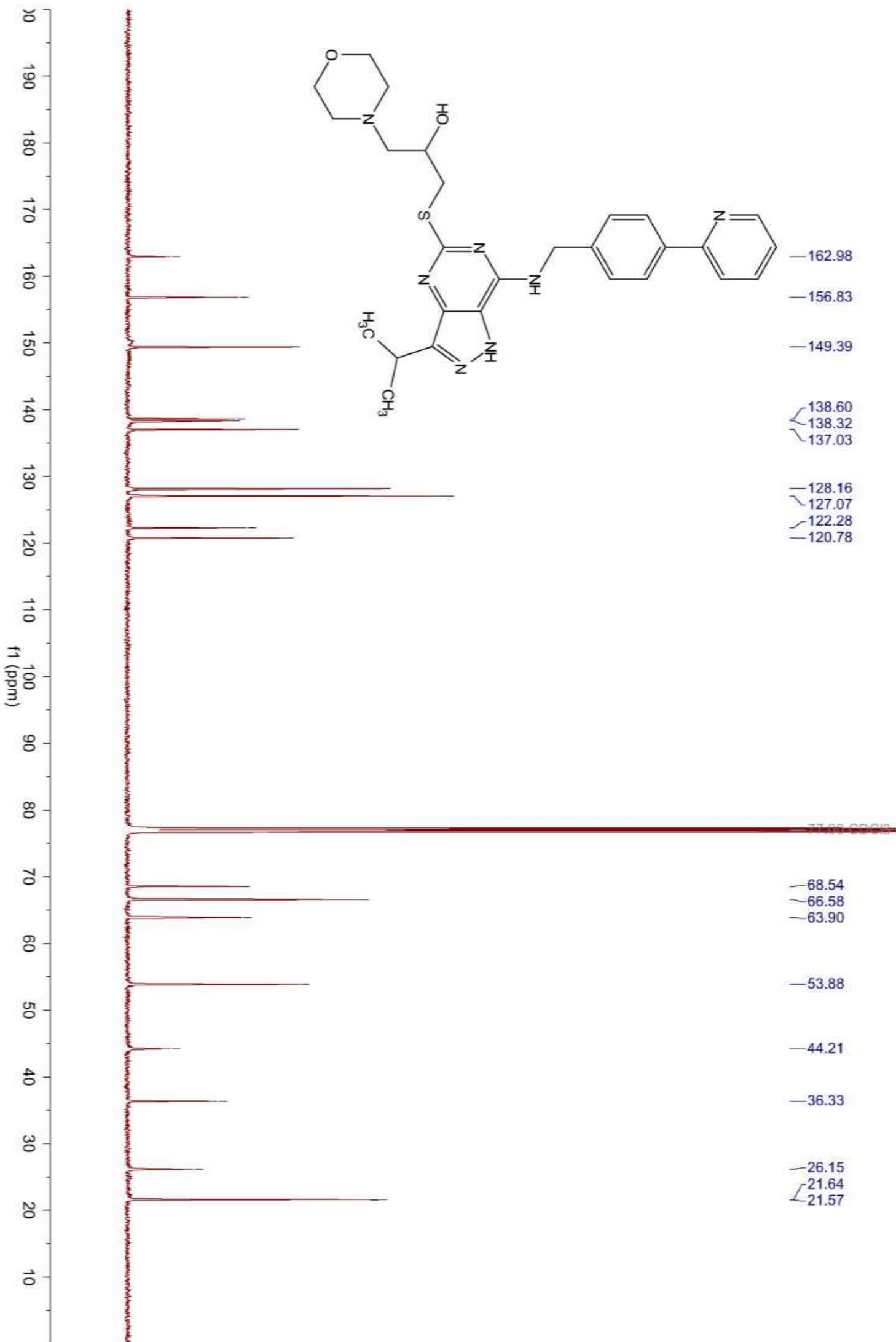
5-[3-(1-Piperazinyl)-2-hydroxy-1-propyl]thio-3-isopropyl-7-[4-(2-pyridyl)benzyl]amino-1(2H)-pyrazolo[4,3-d]pyrimidine (4.1)



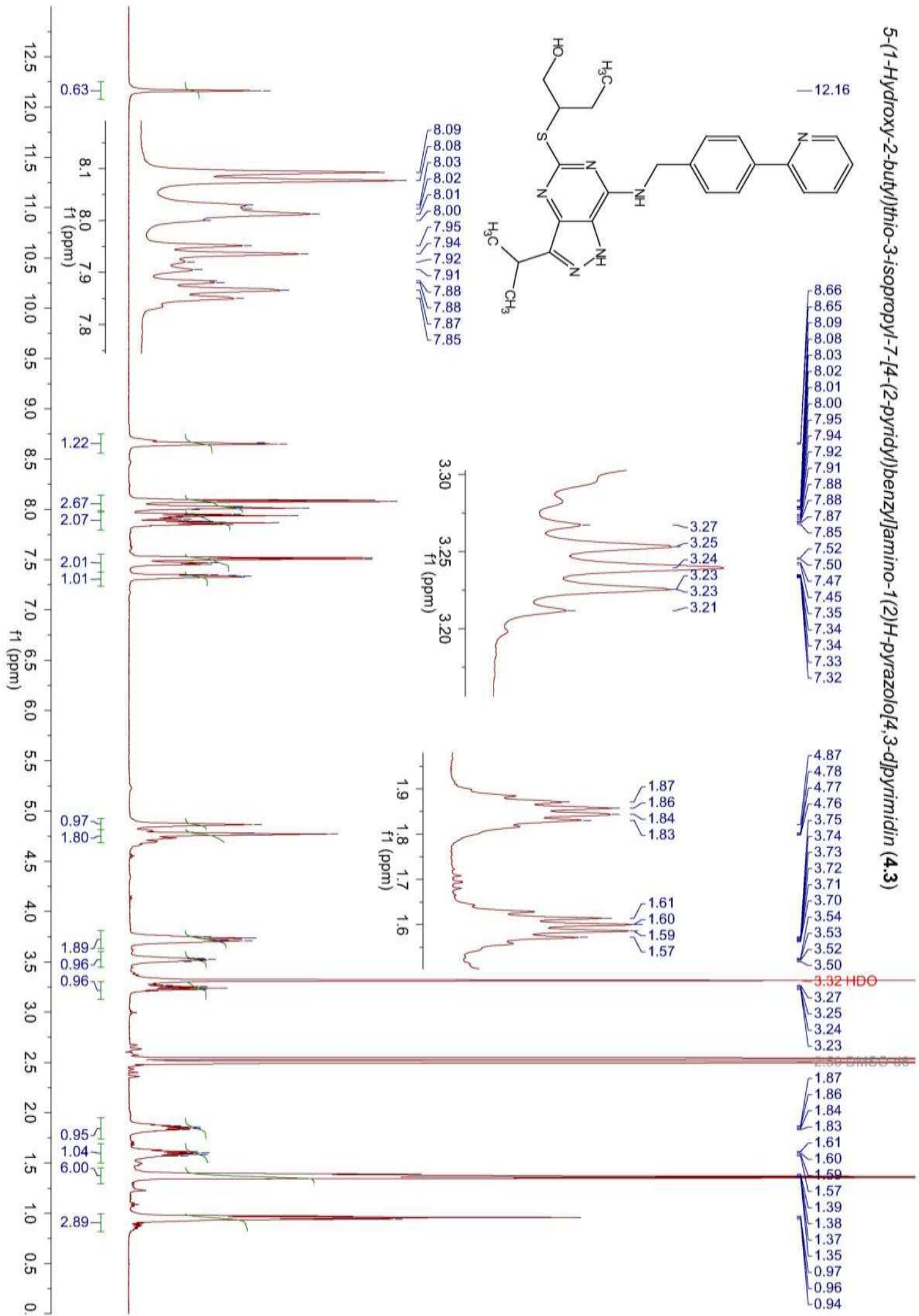
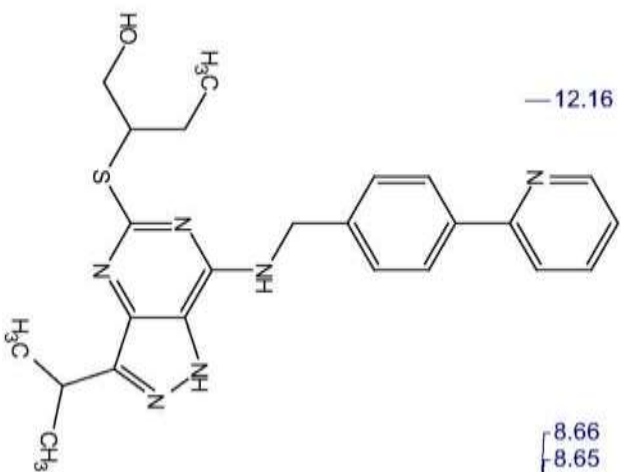
5[(3-(4-Morpholinyl)-2-hydroxy-1-propyl)thio-3-isopropyl-7-[4-(2-pyridyl)benzylamino-1(2H)-pyrazolo[4,3-d]pyrimidin (4.2)



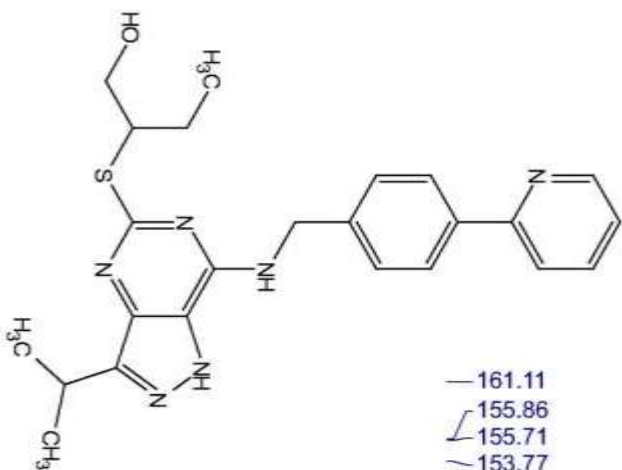
5[(3-(4-Morpholinyl)-2-hydroxy-1-propyl]thio-3-isopropyl-7-[4-(2-pyridyl)benzyl]amino-1(2H)-pyrazolo[4,3-d]pyrimidin (4.2)



5-(1-Hydroxy-2-butyl)thio-3-isopropyl-7-[4-(2-pyridyl)benzyl]amino-1(2)H-pyrazolo[4,3-d]pyrimidin (4.3)



5-(1-Hydroxy-2-butyl)thio-3-isopropyl-[4-(2-pyridyl)benzyl]amino-1(2H)-pyrazolo[4,3-d]pyrimidin (4.3)



- 161.11
- 155.86
- 155.71
- 153.77
- 149.49
- 148.77
- 148.60
- 140.60
- 139.99
- 139.61
- 138.66
- 137.69
- 137.18
- 130.47
- 128.07
- 127.71
- 126.63
- 126.36
- 122.52
- 122.38
- 120.40
- 120.10

63.11

48.52

43.15

40.43

26.39

24.92

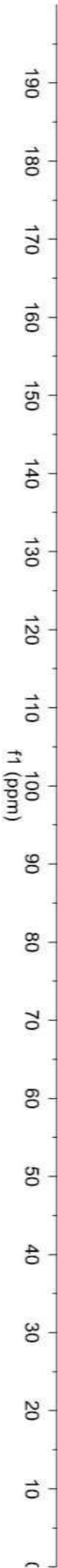
23.61

21.75

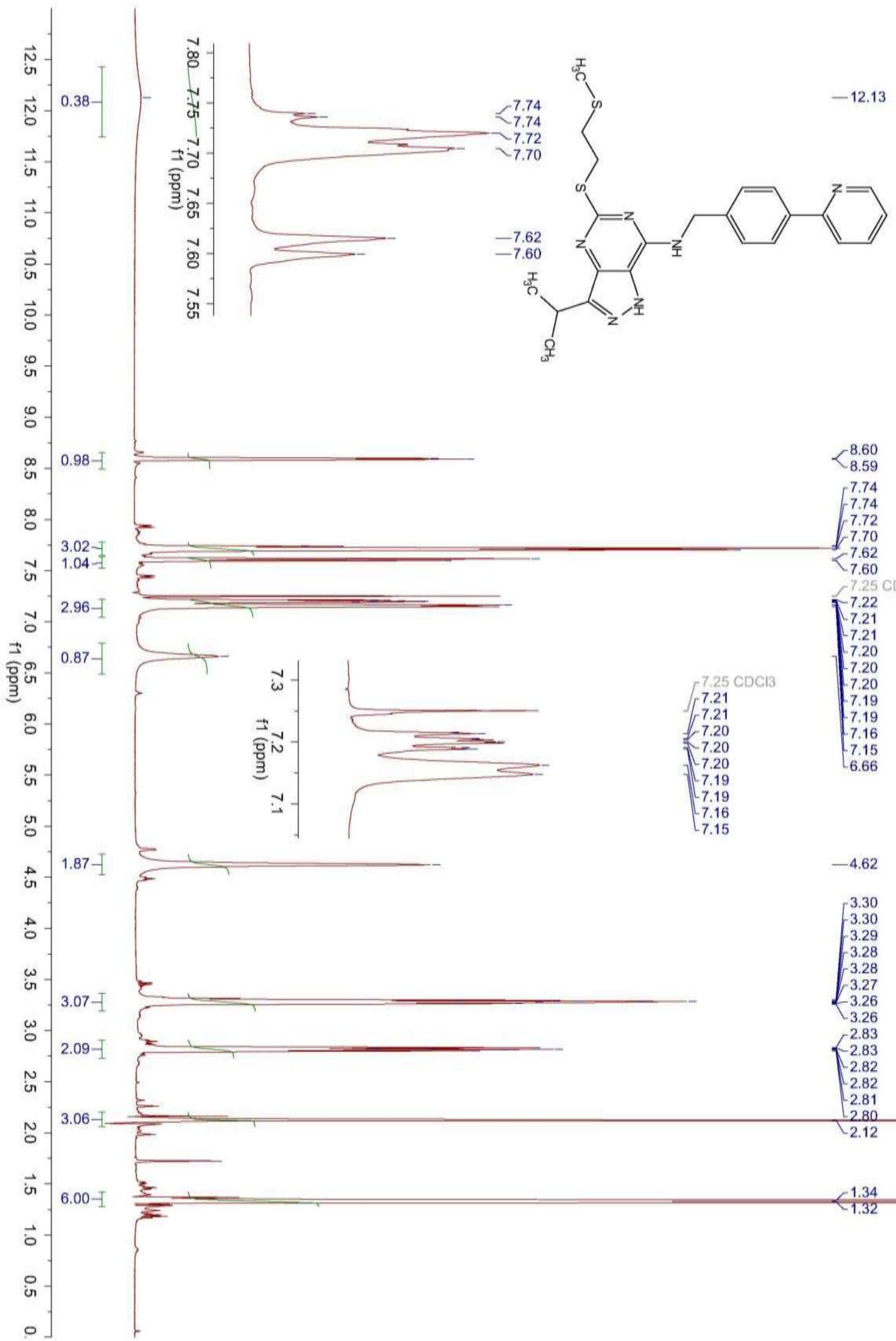
21.63

21.58

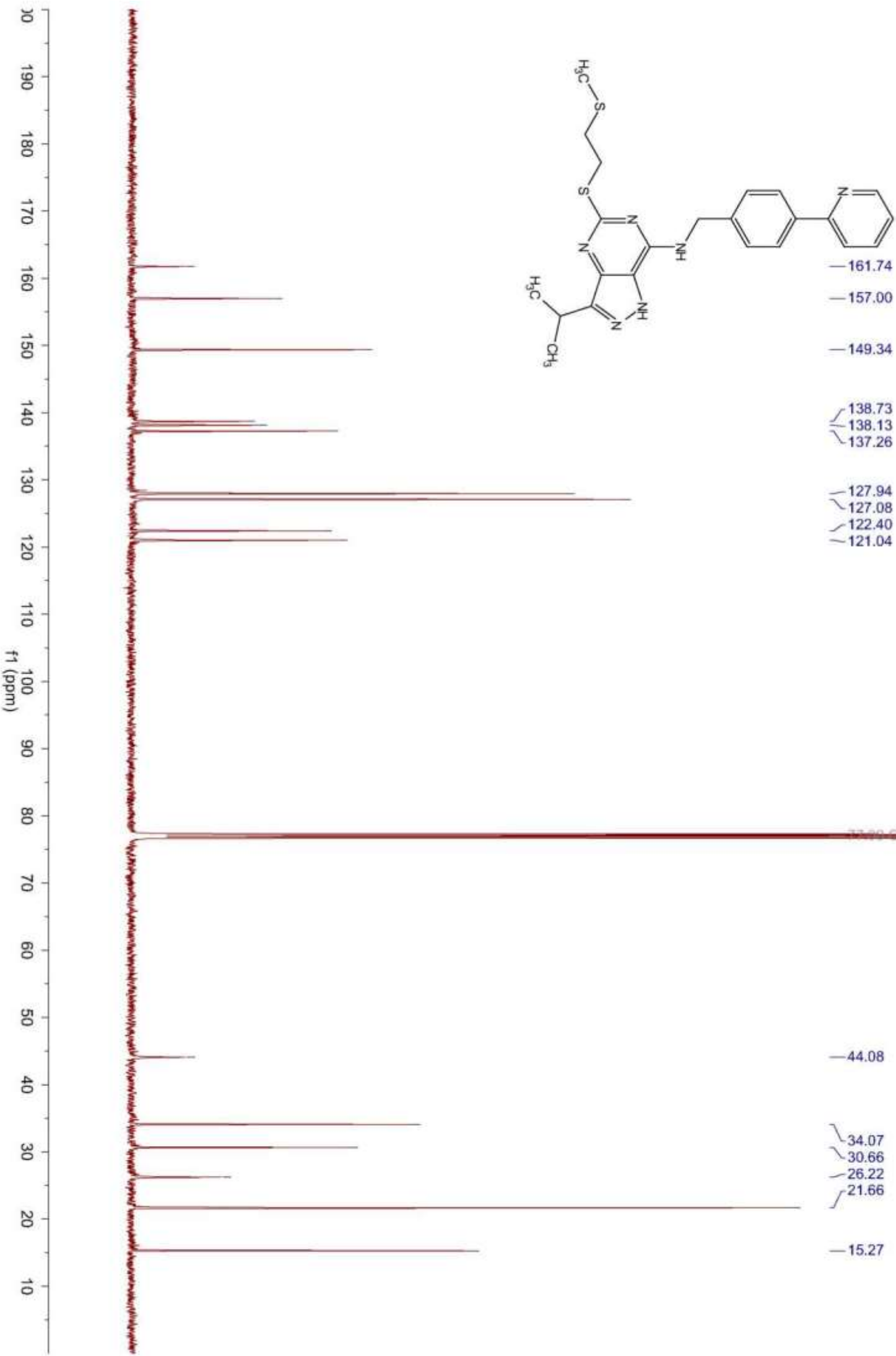
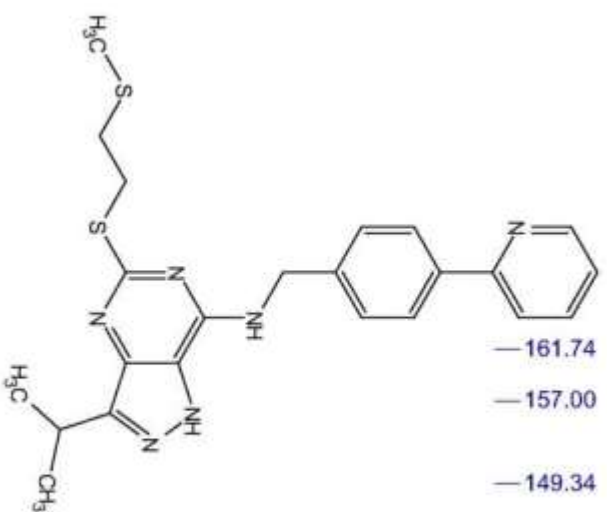
11.37



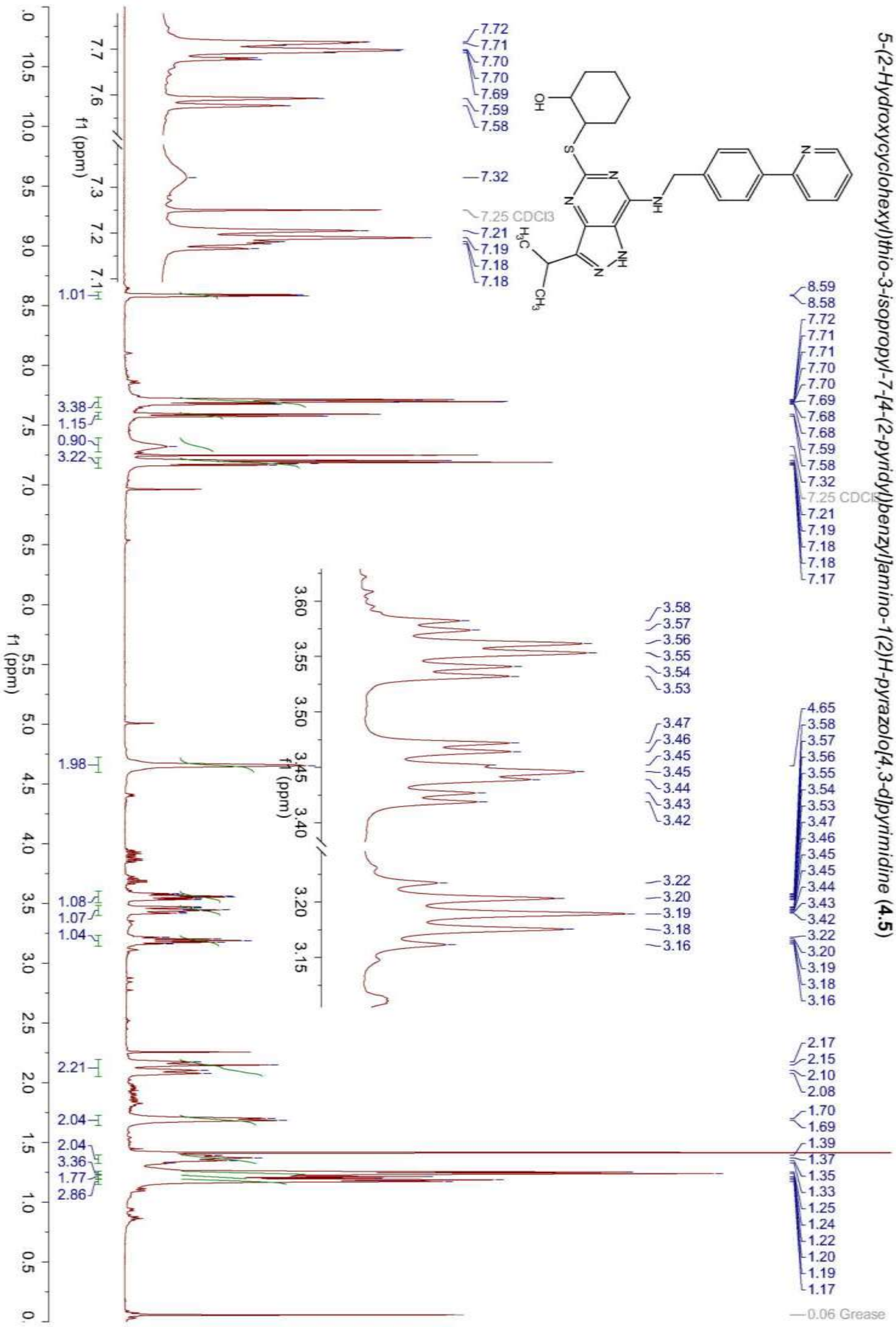
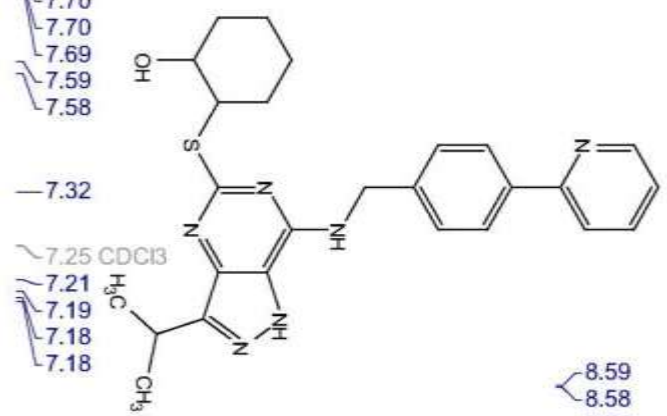
5-(2-Methylthio-1-ethyl)thio-3-isopropyl-7-[4-(2-pyridyl)benzyl]amino-1(2H)-pyrazolo[4,3-d]pyrimidine (4.4)



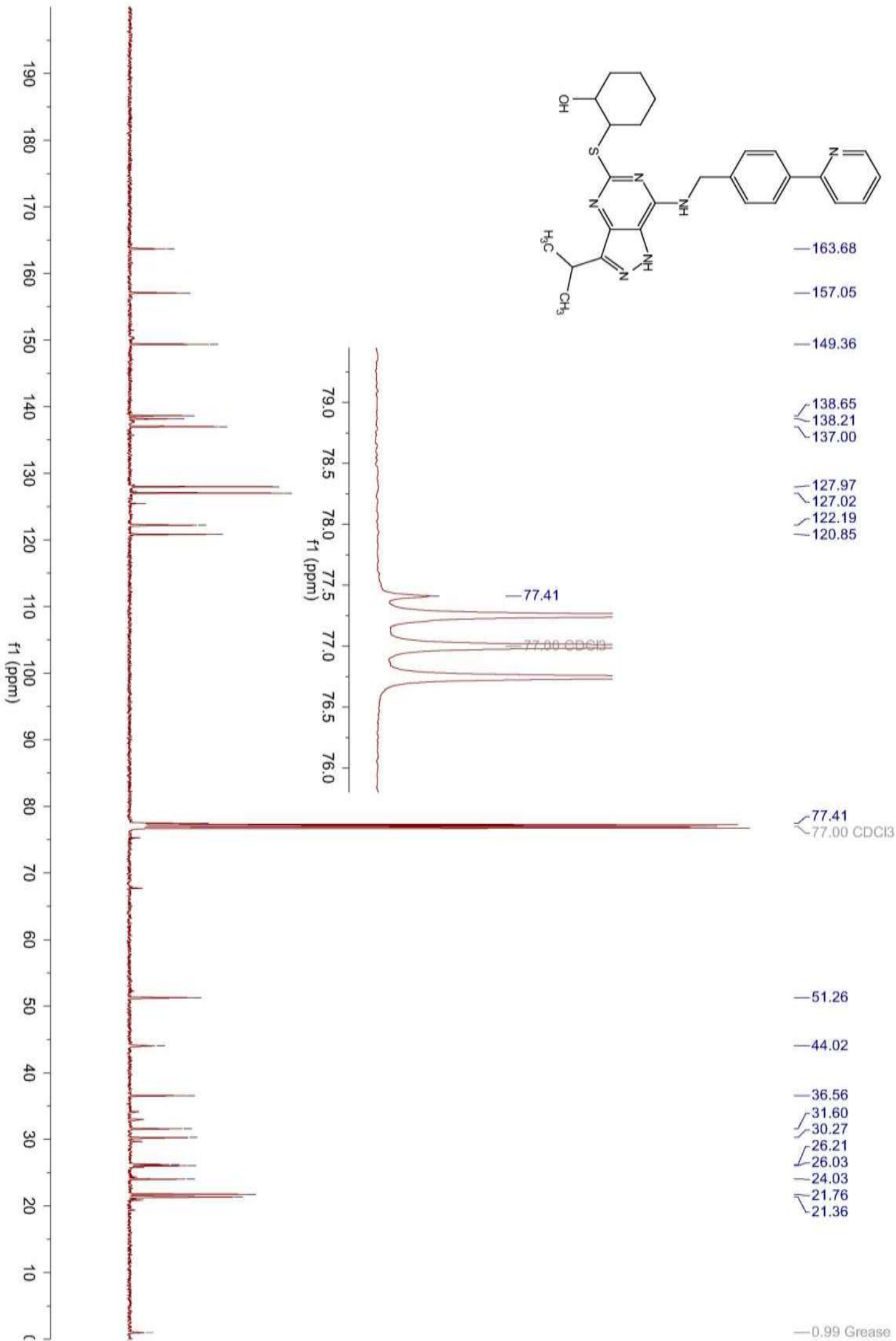
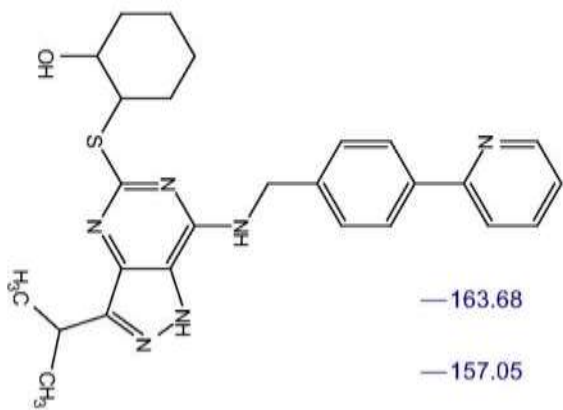
5-(2-Methylthio-1-ethyl)thio-3-isopropyl-7-[4-(2-pyridyl)benzyl]amino-1(2*H*)-pyrazolo[4,3-*d*]pyrimidine (4.4)



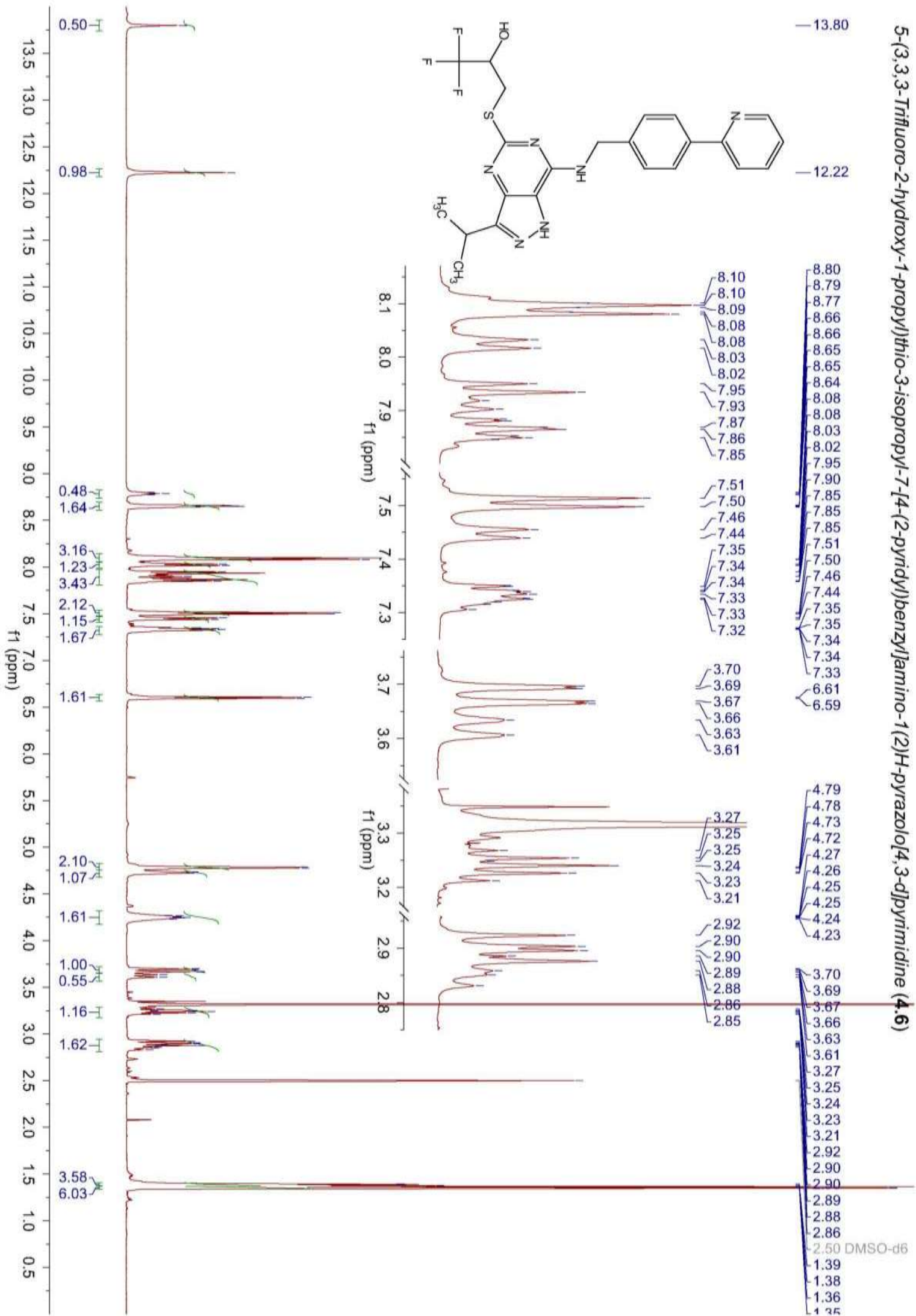
5-(2-Hydroxycyclohexyl)thio-3-isopropyl-7-[4-(2-pyridyl)benzyl]amino-1(2H)-pyrazolo[4,3-d]pyrimidine (4.5)



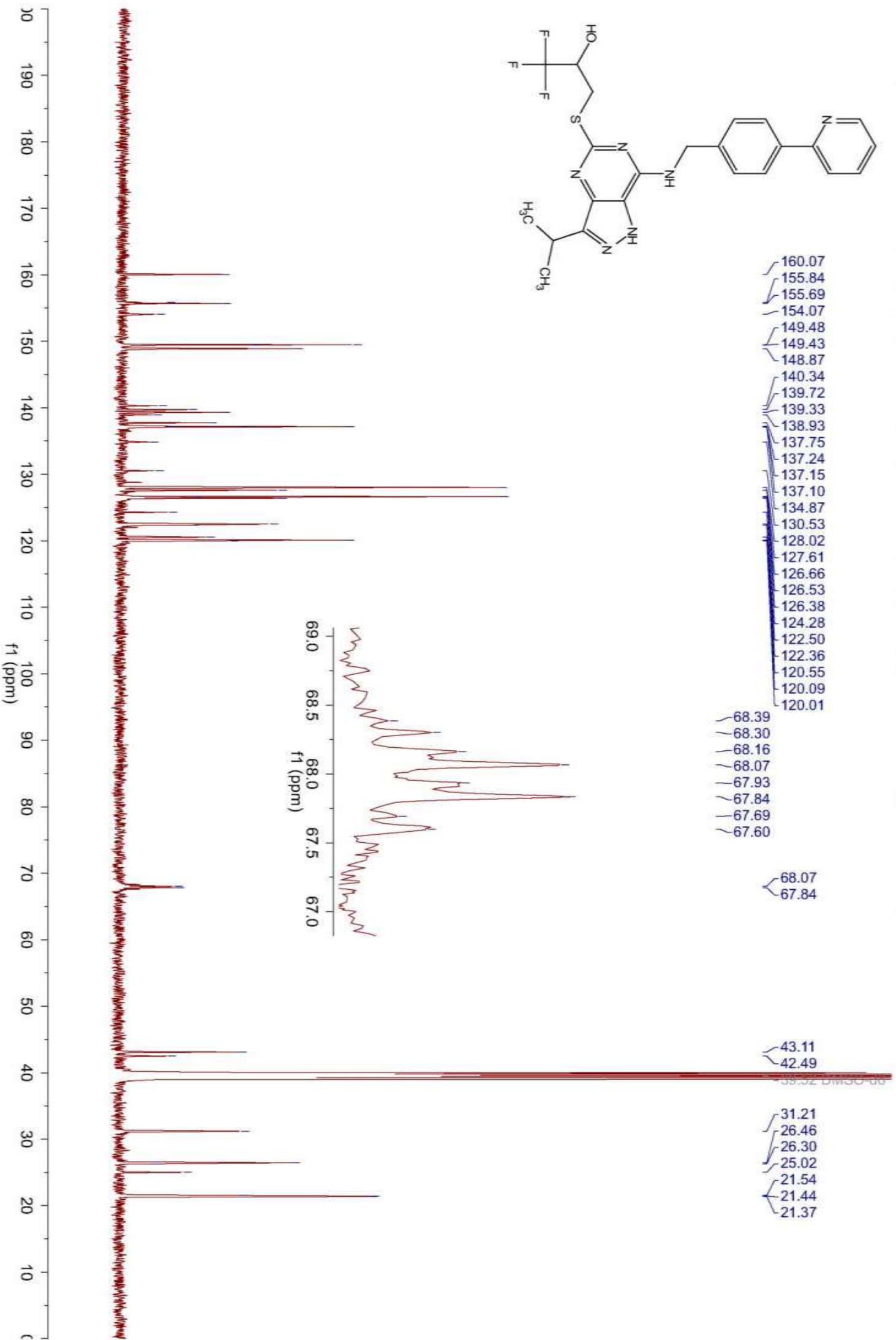
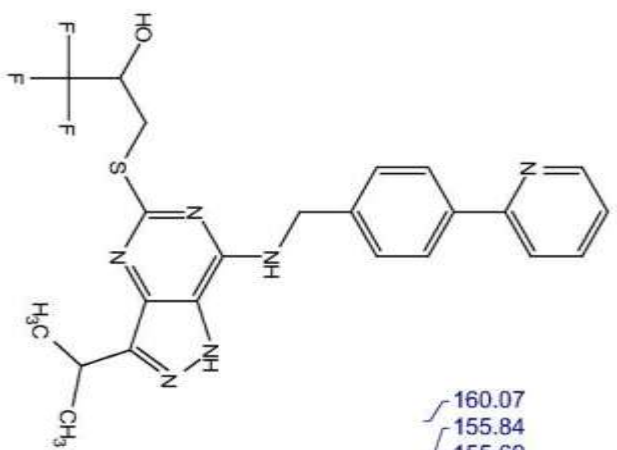
5-(2-Hydroxycyclohexyl)thio-3-isopropyl-7-[4-(2-pyridyl)benzyl]amino-1(2H)-pyrazolo[4,3-d]pyrimidine (4.5)



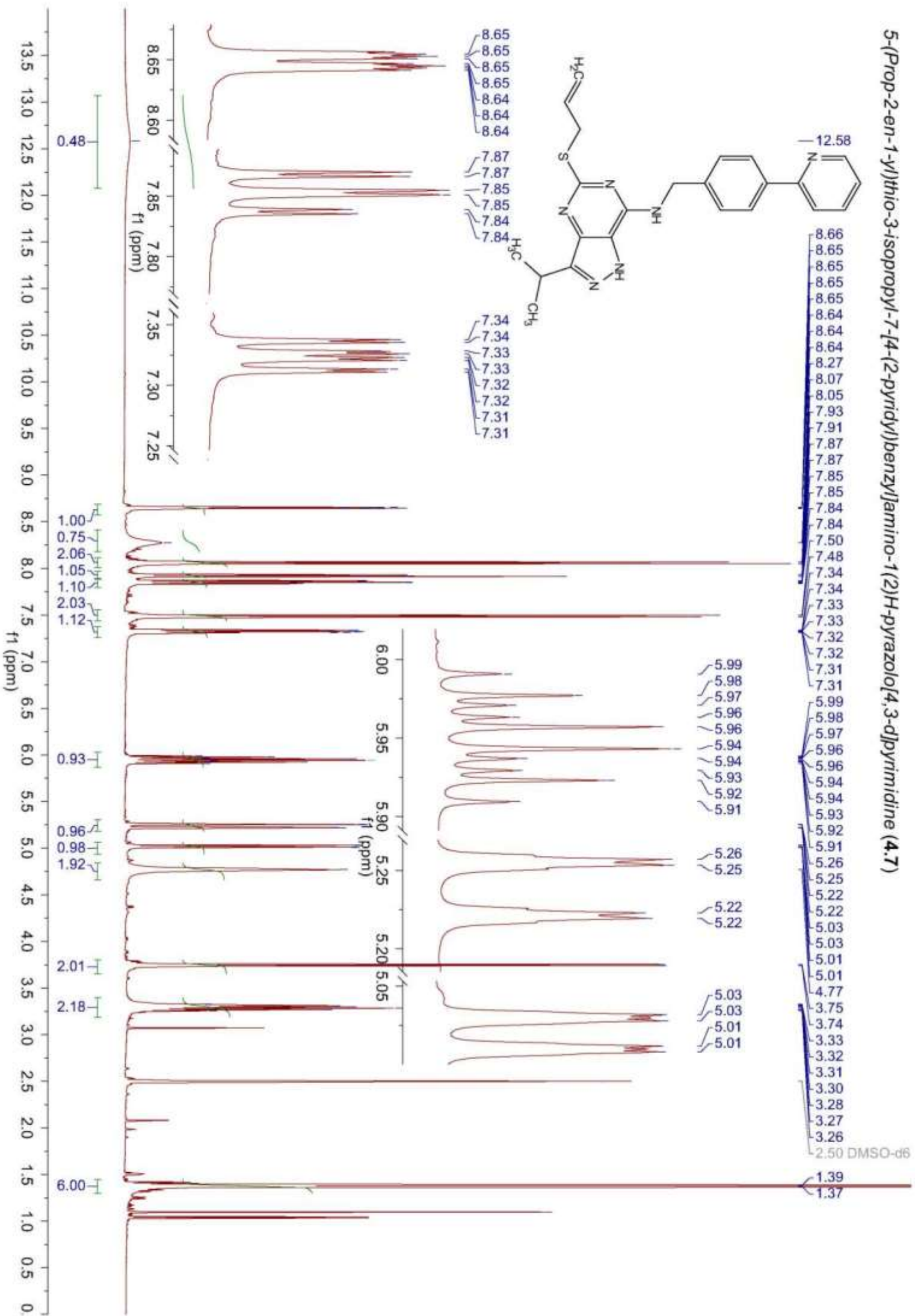
5-(3,3,3-Trifluoro-2-hydroxy-1-propyl)thio-3-isopropyl-7-[4-(2-pyridyl)benzyl]amino-1(2H)-pyrazolo[4,3-d]pyrimidine (4.6)



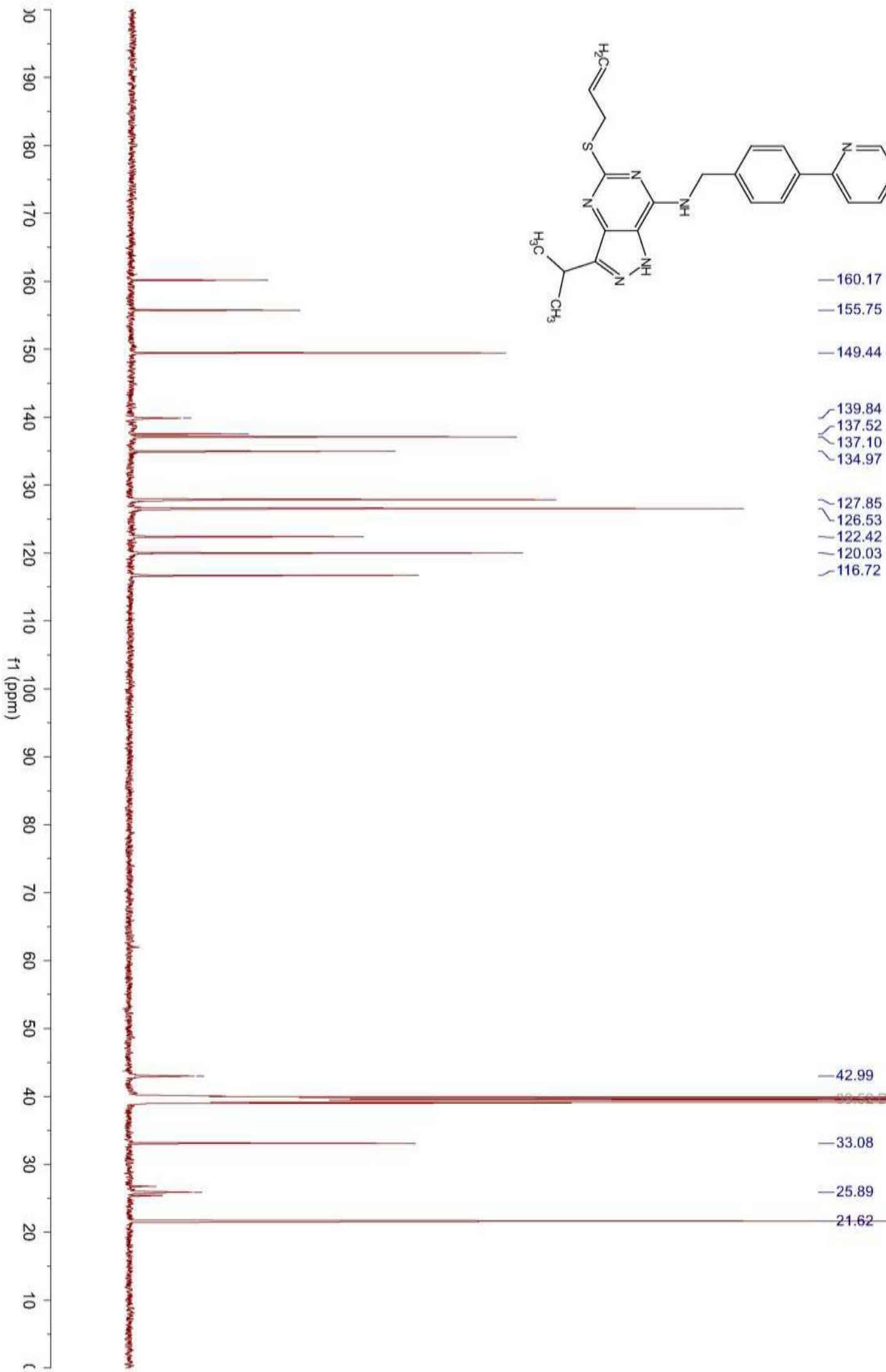
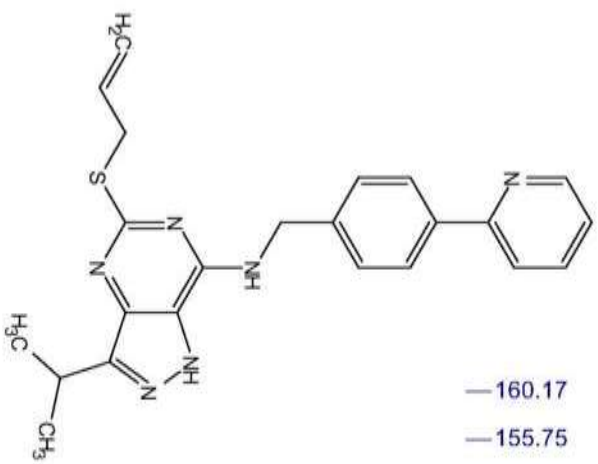
5-(3,3-Trifluoro-2-hydroxy-1-propyl)thio-3-isopropyl-7-[4-(2-pyridyl)benzylamino-1(2H)-pyrazolo[4,3-d]pyrimidine (4.6)



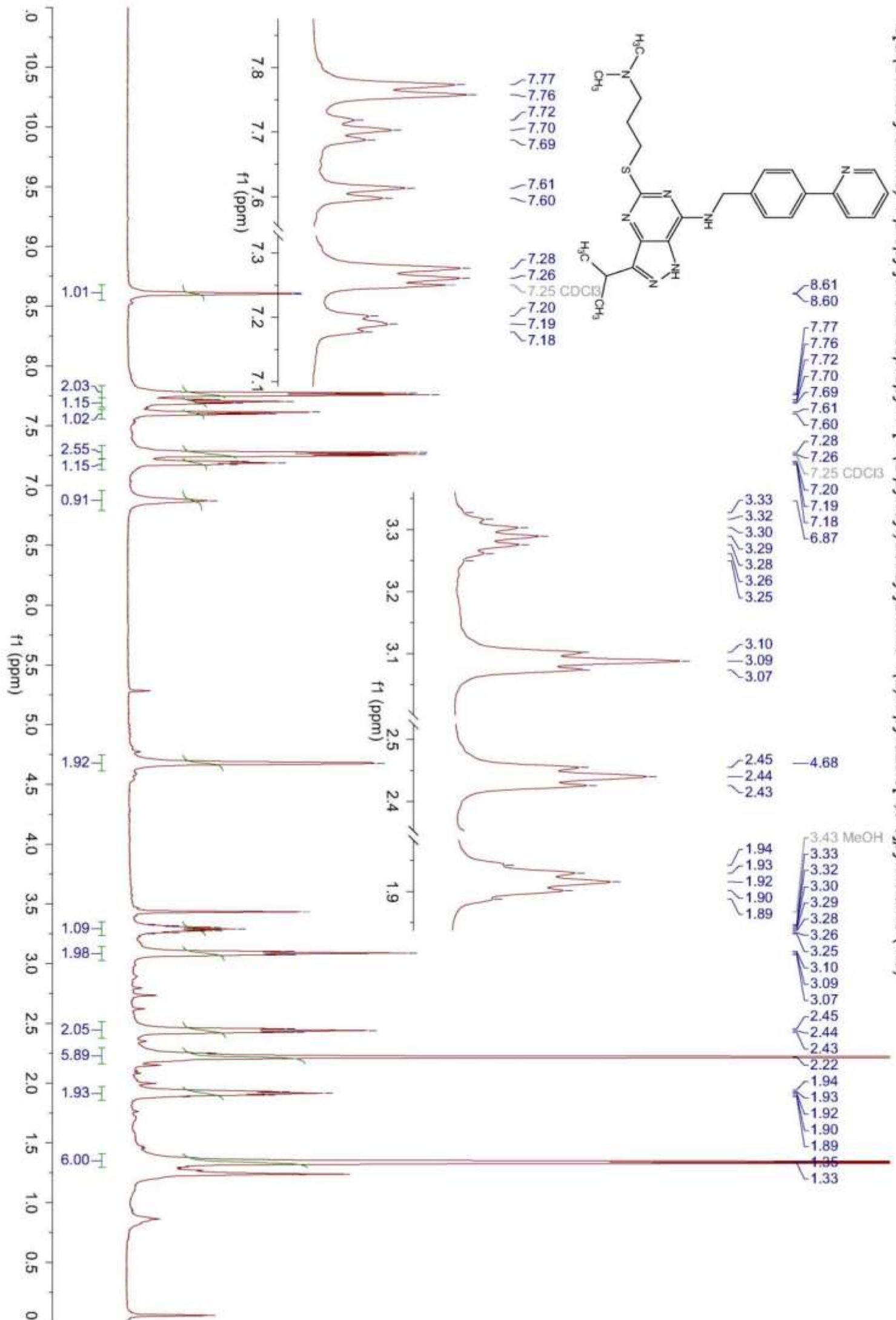
5-(Prop-2-en-1-yl)thio-1-ylthio-3-isopropyl-7-[4-(2-pyridyl)benzyl]amino-1(2H)-pyrazolo[4,3-d]pyrimidine (4.7)



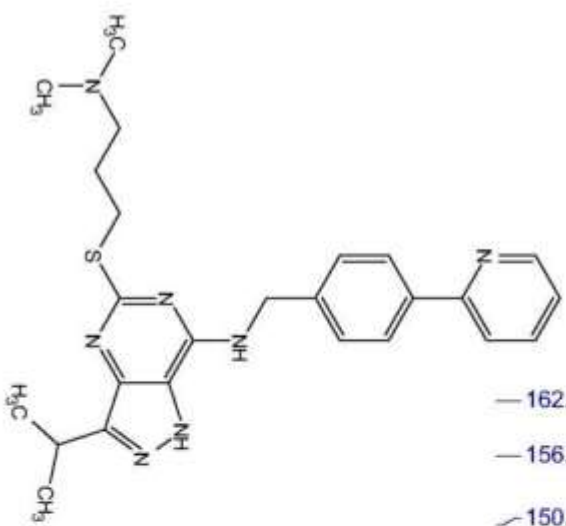
5-(Prop-2-en-1-yl)thio-3-isopropyl-7-[4-(2-pyridyl)benzyl]amino-1(2H)-pyrazolo[4,3-d]pyrimidine (4.7)



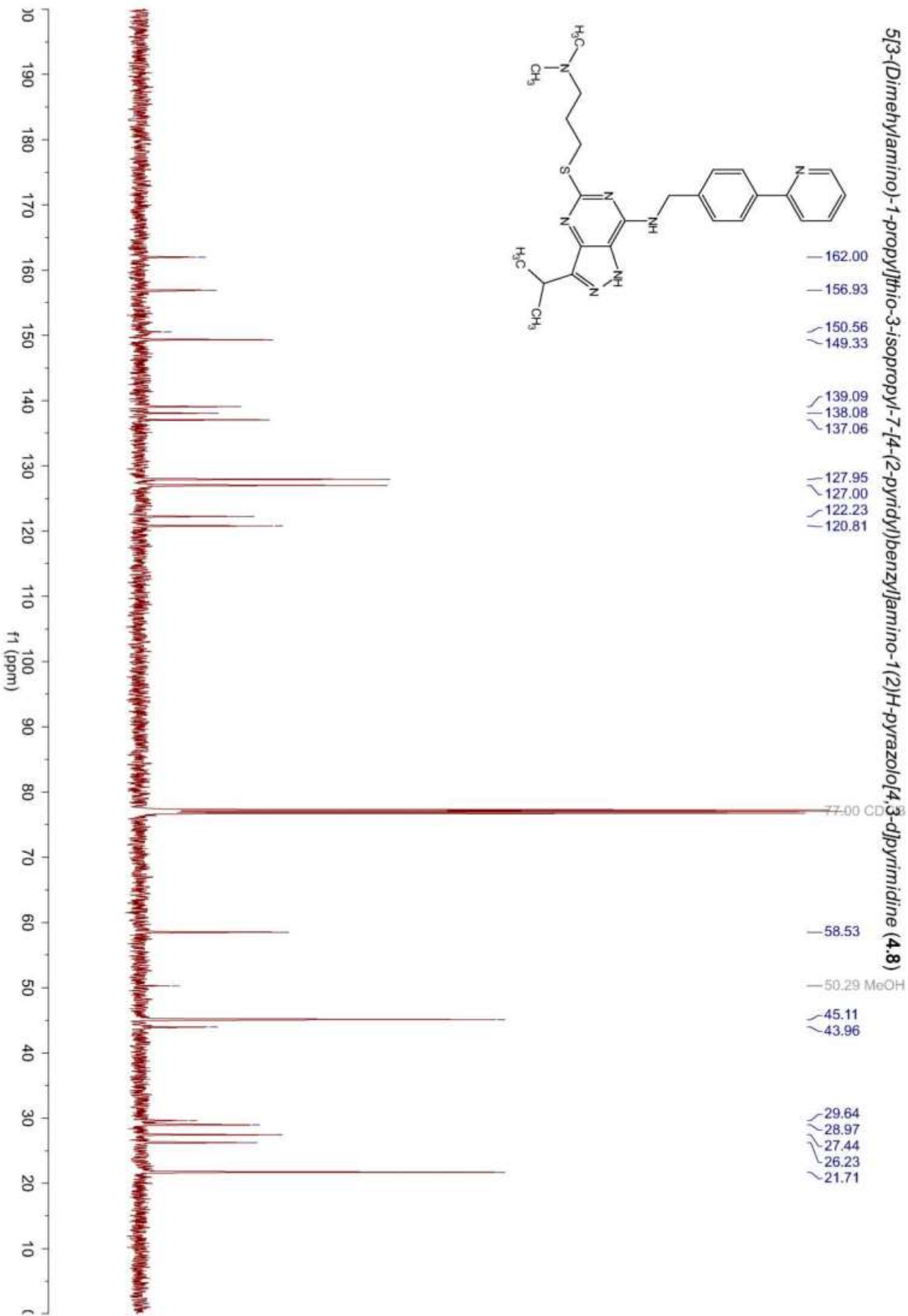
5[3-(Dimethylamino)-1-propyl]thio-3-isopropyl-7-[4-(2-pyridyl)benzylamino-1(2H)-pyrazolo[4,3-d]pyrimidine (4.8)



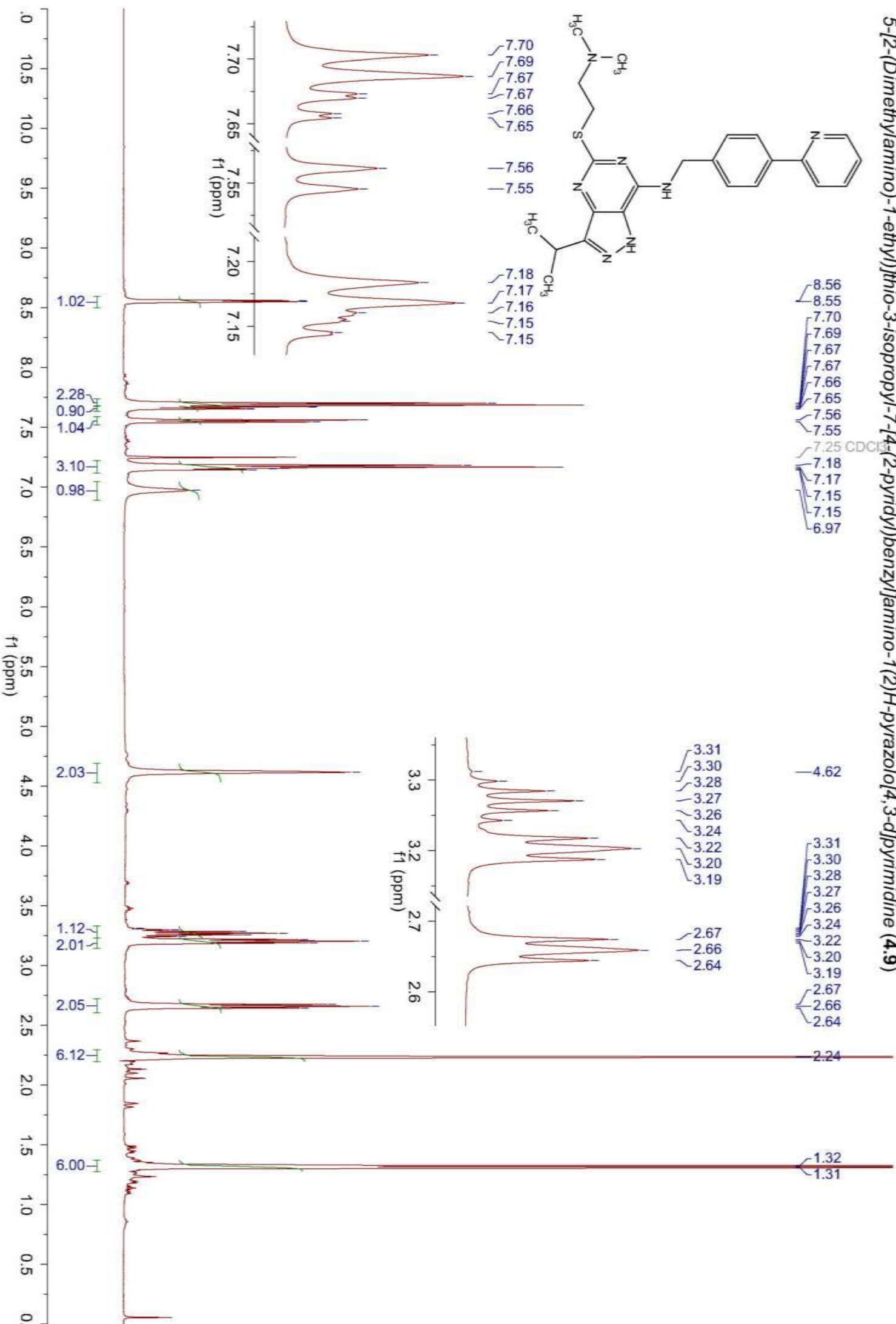
5[3-(Dimethylamino)-1-propyl]thio-3-isopropyl-7-[4-(2-pyridyl)benzyl]amino-1(2H)-pyrazolo[4,3-d]pyrimidine (4.8)



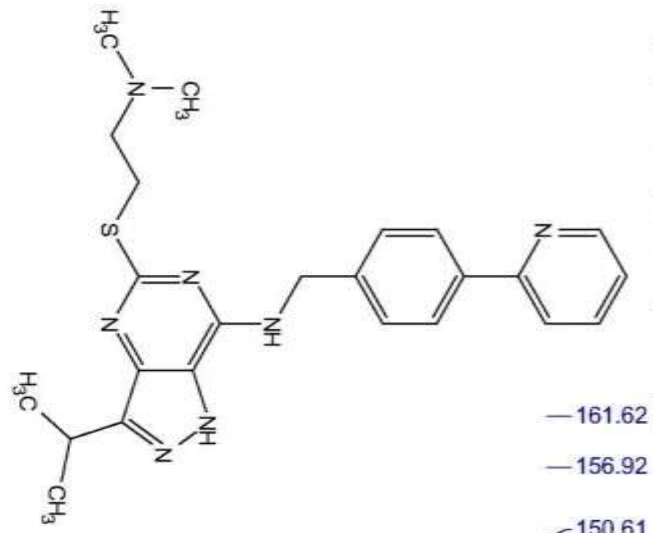
- 162.00
- 156.93
- 150.56
- 149.33
- 139.09
- 138.08
- 137.06
- 127.95
- 127.00
- 122.23
- 120.81



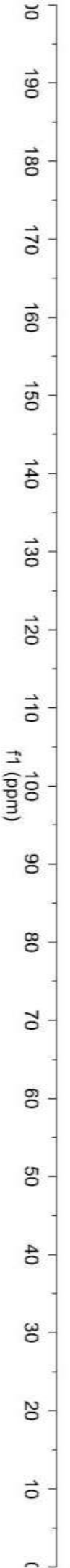
5-[2-(Dimethylamino)-1-ethyl]thio-3-isopropyl-7-[4-(2-pyridyl)benzyl]amino-1(2H)-pyrazolo[4,3-d]pyrimidine (4.9)



5-[2-(Dimethylamino)-1-ethyl]thio-3-isopropyl-7-[4-(2-pyridyl)benzylamino-1(2)H-pyrazolo[4,3-d]pyrimidine (4.9)



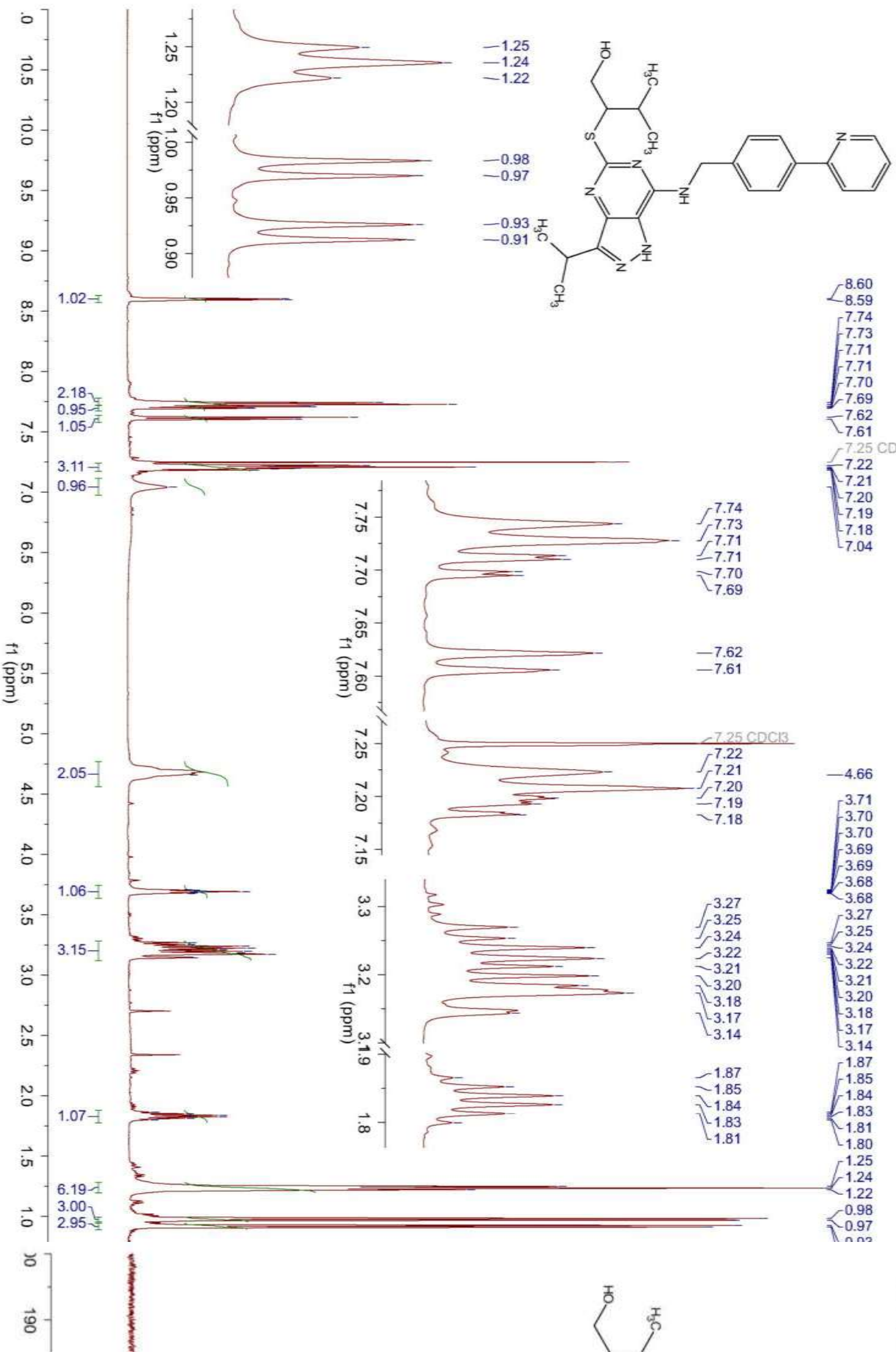
- 161.62
- 156.92
- 150.61
- 149.29
- 138.96
- 138.06
- 137.08
- 127.93
- 126.99
- 122.24
- 120.83



- 77.00 CDCl<sub>3</sub>
- 59.00
- 44.96
- 43.93
- 28.04
- 26.26
- 21.68

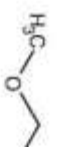
5-(1-Hydroxy-3-methyl-2-butyl)thio-3-isopropyl-7-[4-(2-pyridyl)benzylamino-1(2)H-pyrazolo[4,3-d]pyrimidine (4.10)

5-(1-Hydroxy-3-methyl-2-butyl)thio-3-isopropyl-7-[4-(2-pyridyl)benzylamino-1(2)H-pyrazolo[4,3-d]pyrimidine (4.10)



5-(Metho

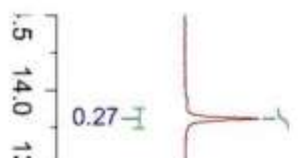
— 13.81



8.10

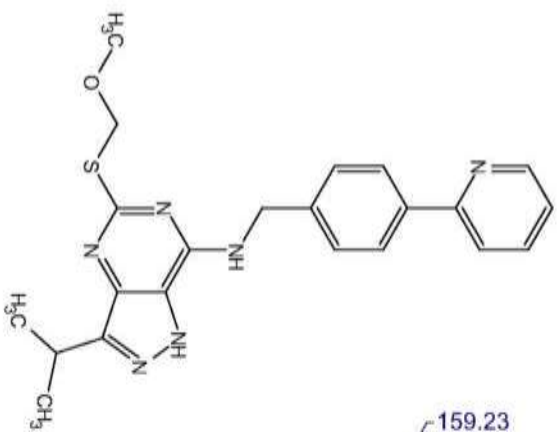
8.2

0.27





5-(Methoxymethyl)thio-3-isopropyl-7-[4-(2-pyridyl)benzyl]amino-1(2H)-pyrazolo[4,3-d]pyrimidine (4.11)



- 159.23
- 155.82
- 155.69
- 153.97
- 149.46
- 148.94
- 148.74
- 139.90
- 139.46
- 137.72
- 137.13
- 128.03
- 127.64
- 126.63
- 126.38
- 122.48
- 122.35
- 120.63
- 120.07

73.40

55.95

43.20

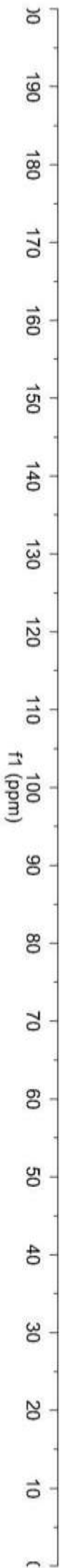
42.62

26.29

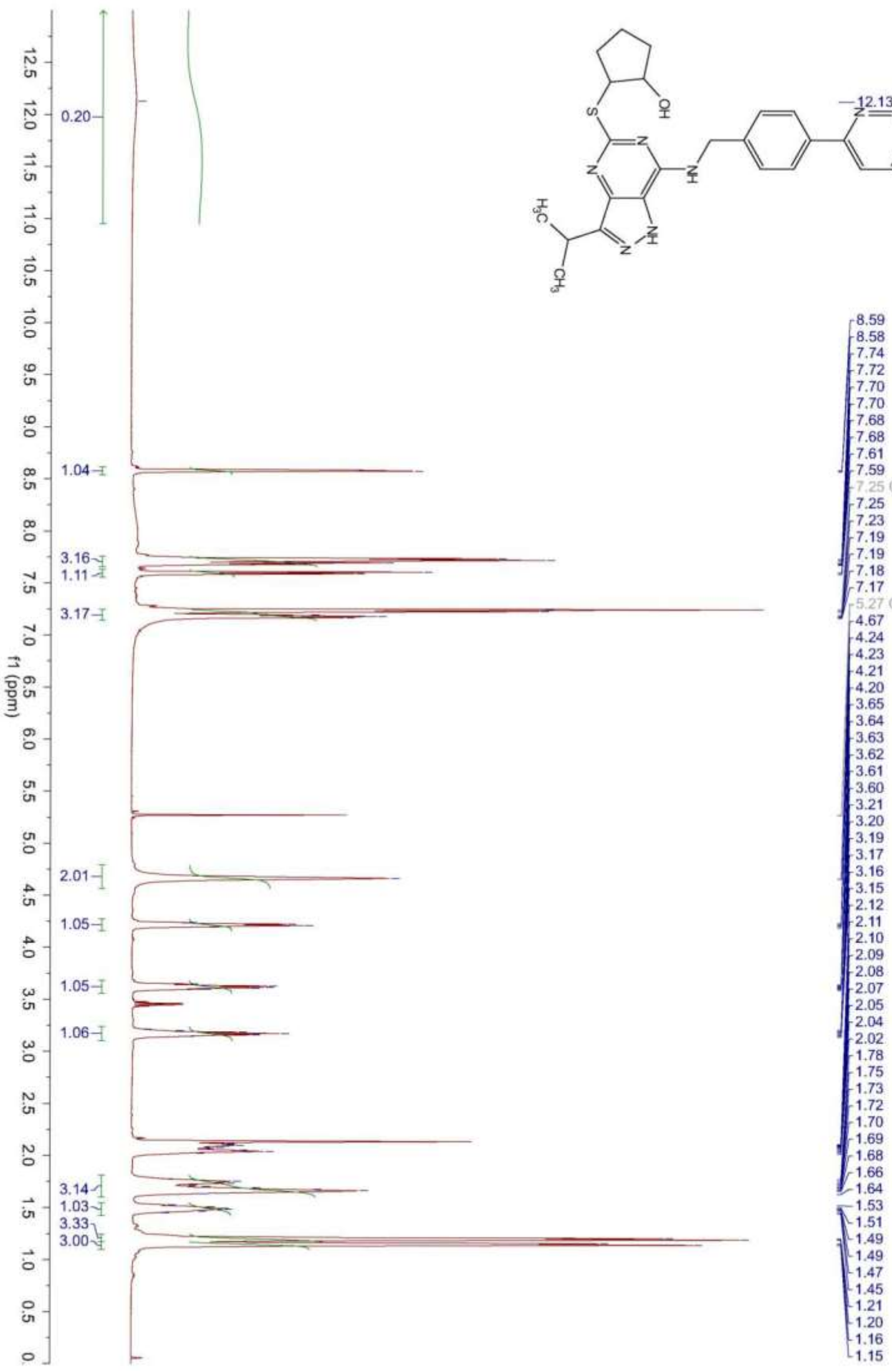
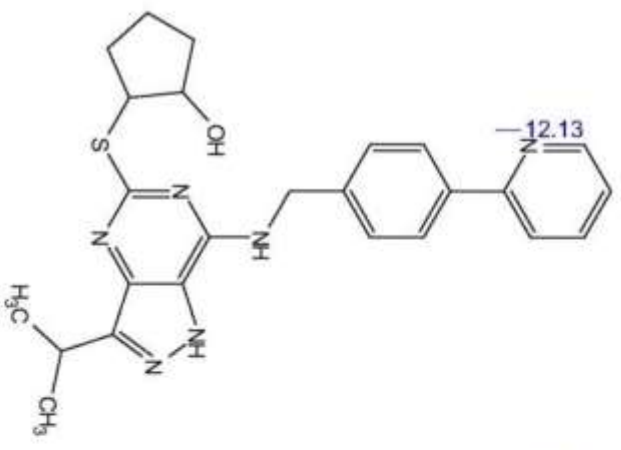
24.84

21.75

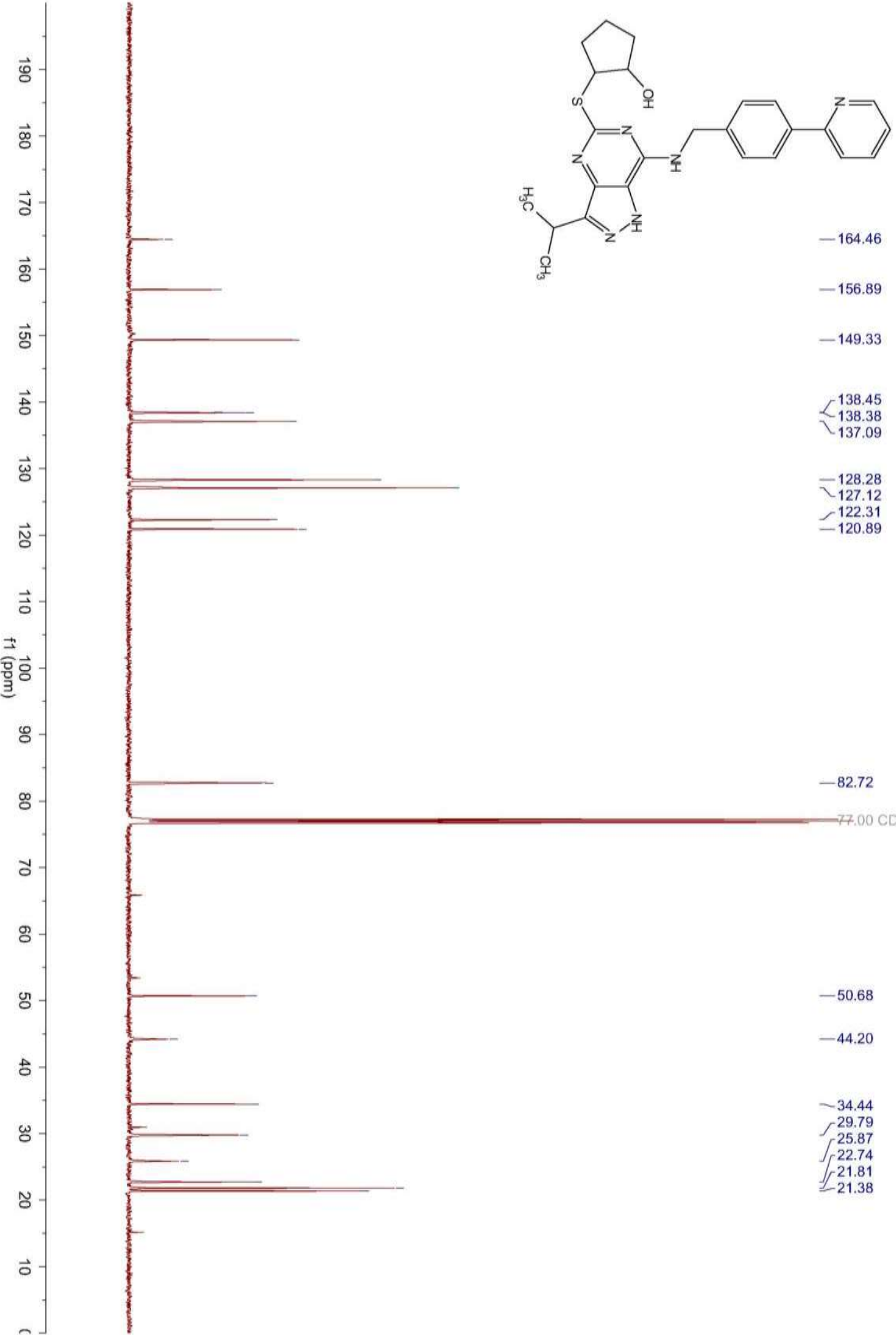
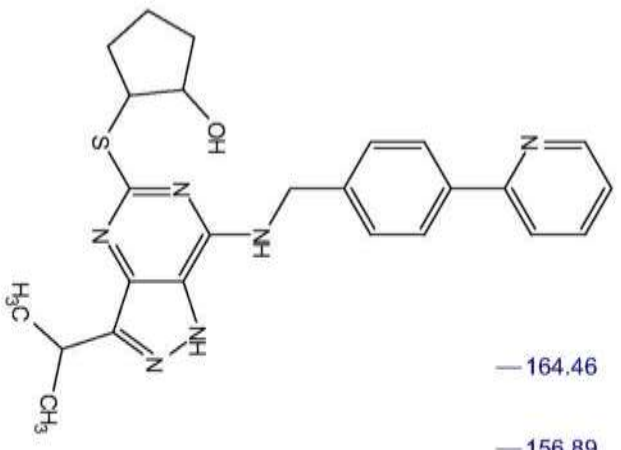
21.61



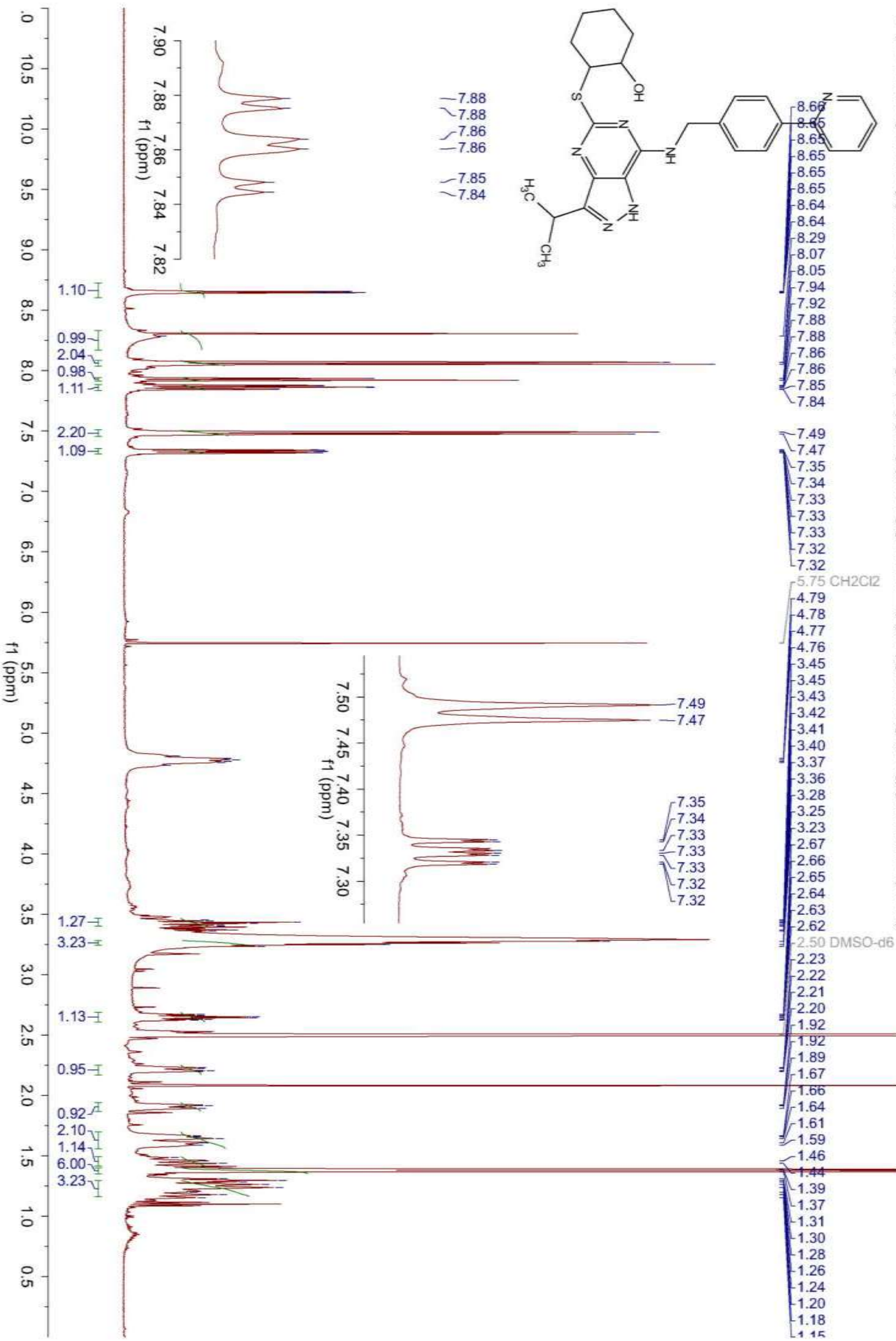
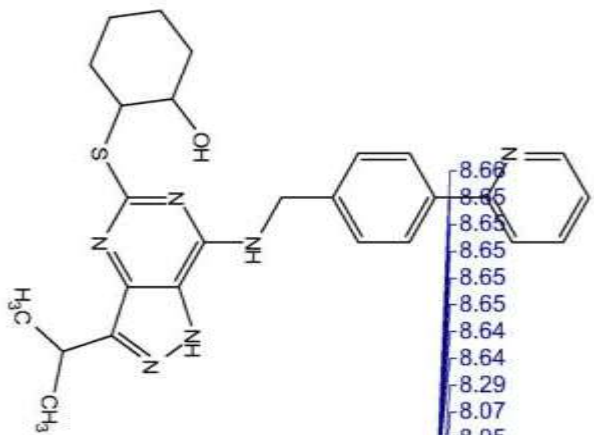
5-(2-Hydroxycyclopentyl)thio-3-isopropyl-7-[4-(2-pyridyl)benzyl]amino-1(2H)-pyrazolo[4,3-d]pyrimidine (4.12)



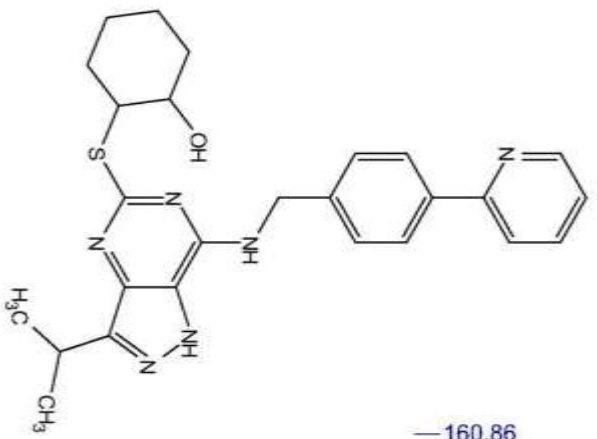
5-(2-Hydroxycyclopentyl)thio-3-isopropyl-[4-(2-pyridyl)benzyl]amino-1(2H)-pyrazolo[4,3-d]pyrimidine (4.12)



5-(2-Aminocyclohexyl)thio-3-isopropyl-7-[4-(2-pyridyl)benzylamino-1(2)H-pyrazolo[4,3-d]pyrimidine (4.13)



5-(2-Aminocyclohexyl)thio-3-isopropyl-7-[4-(2-pyridyl)benzyl]amino-1(2H)-pyrazolo[4,3-d]pyrimidine (4.13)



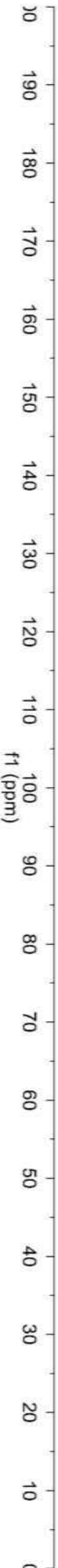
- 160.86
- 155.75
- 149.45
- 139.89
- 137.48
- 137.12
- 127.70
- 126.52
- 122.43
- 120.03

— 79.12

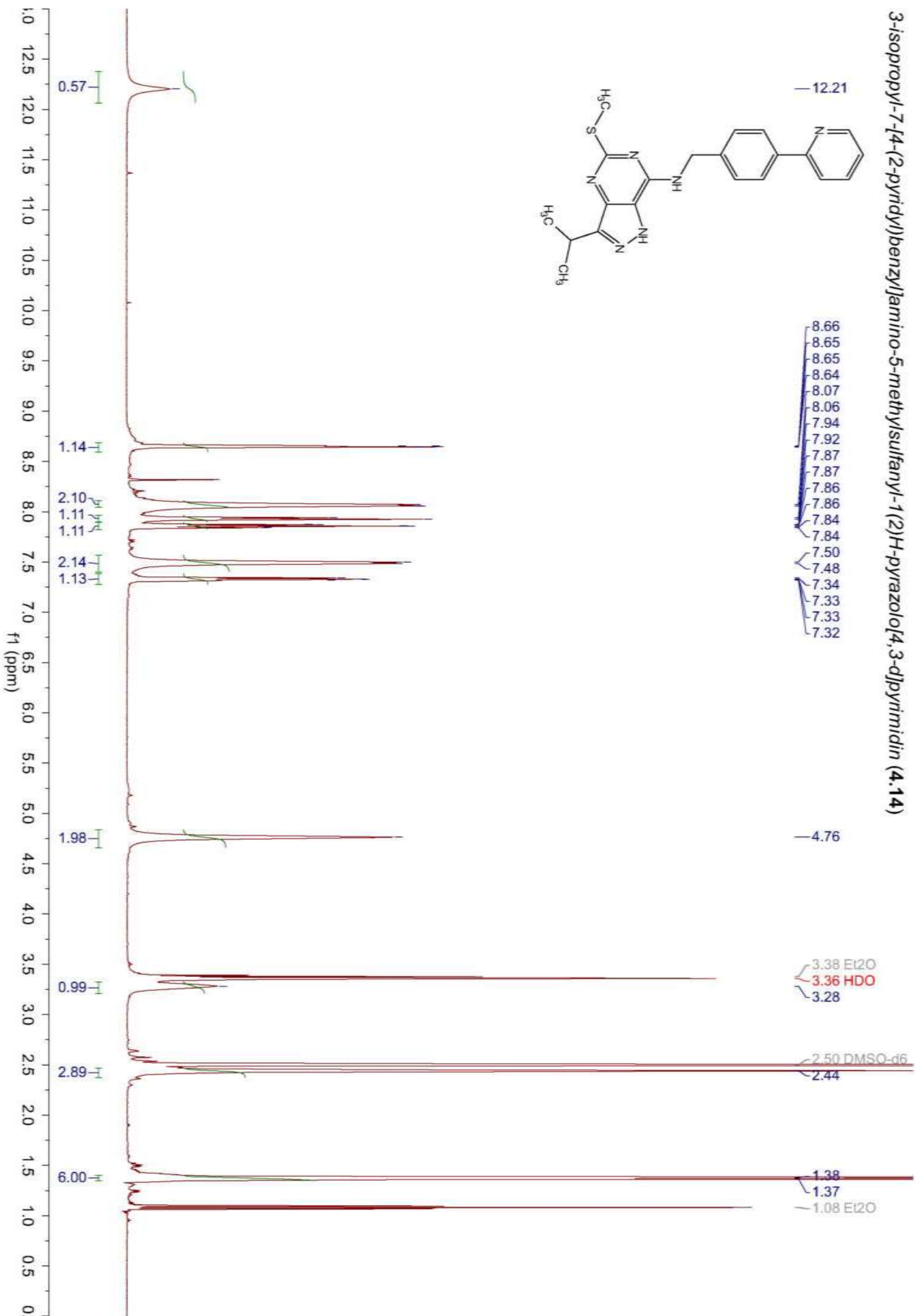
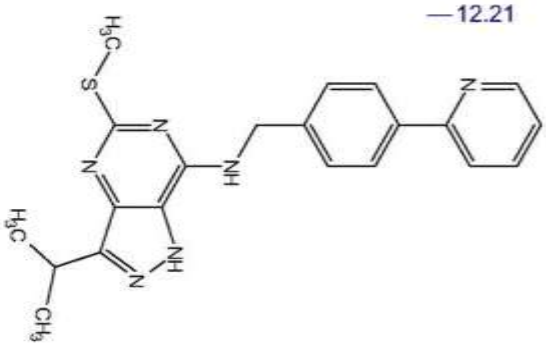
- 54.83 CH<sub>2</sub>Cl<sub>2</sub>
- 52.65
- 52.28

— 42.93

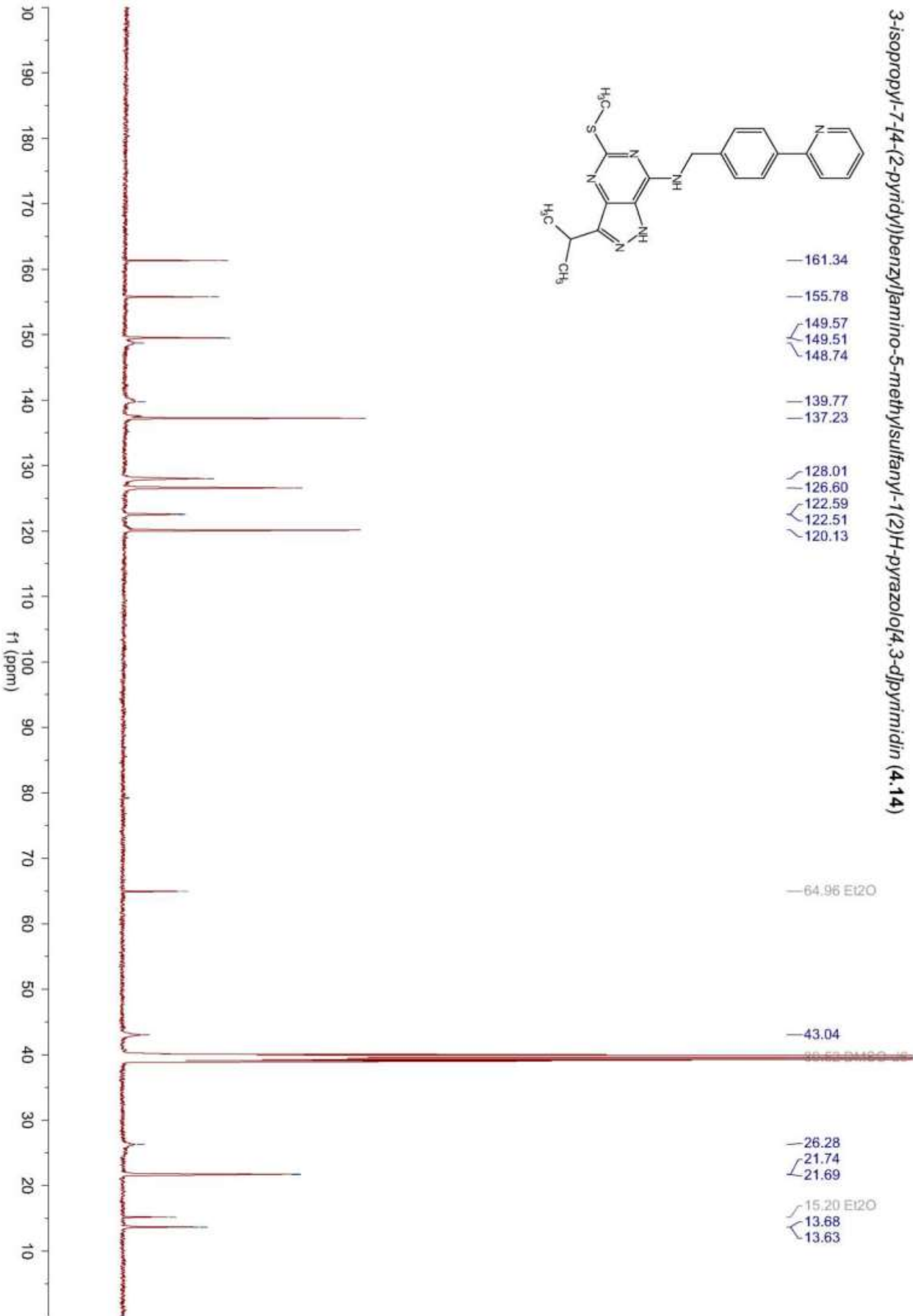
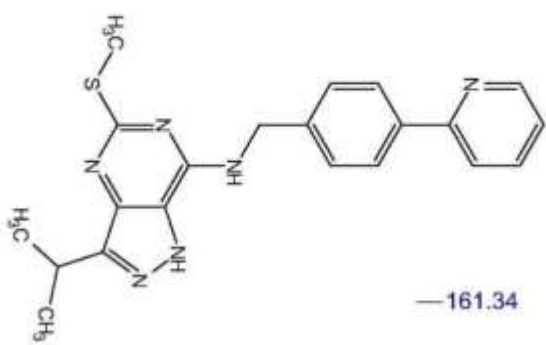
- 35.02
- 32.83
- 30.61
- 25.79
- 24.31
- 21.66
- 21.52



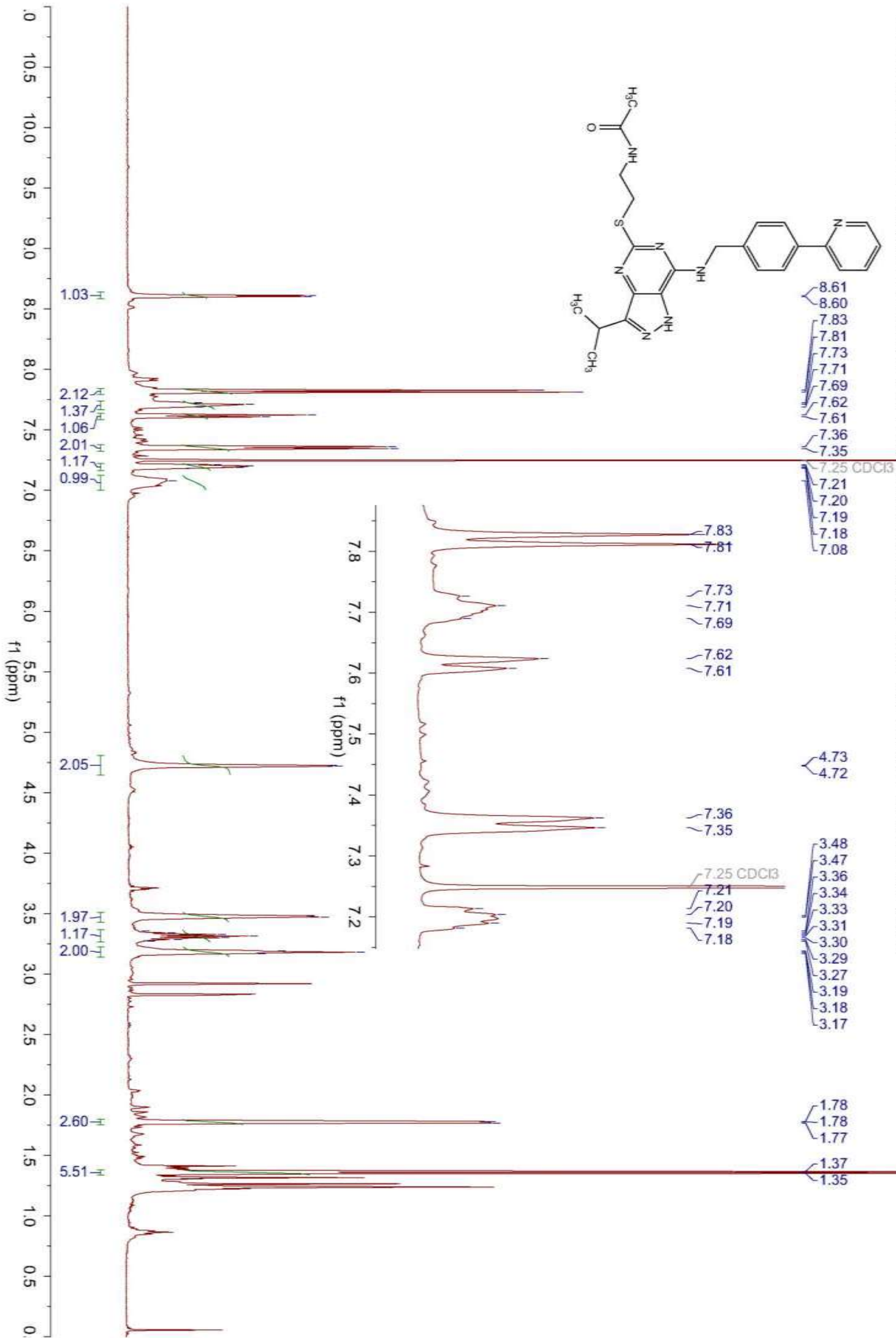
3-isopropyl-7-[4-(2-pyridyl)benzyl]amino-5-methylsulfanyl-1(2H)-pyrazolo[4,3-d]pyrimidin (4.14)



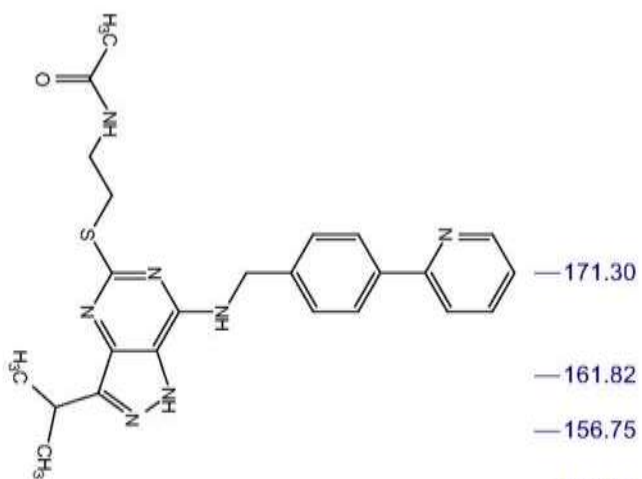
3-isopropyl-7-[4-(2-pyridyl)benzyl]amino-5-methylsulfanyl-1(2H)-pyrazolo[4,3-d]pyrimidin (4.14)



5-(2-Acetylamino-1-ethyl)thio-3-isopropyl-7-[4-(2-pyridyl)benzyl]amino-1(2H)-pyrazolo[4,3-d]pyrimidine (4.15)

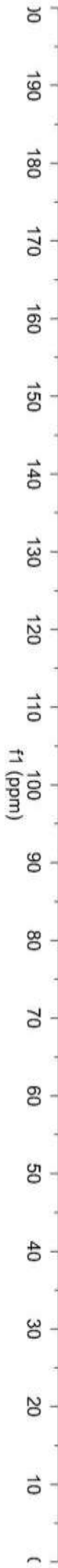


5-(2-Acetylamino-1-ethyl)thio-3-isopropyl-7-[4-(2-pyridyl)benzyl]amino-1(2)H-pyrazolo[4,3-d]pyrimidine (4.15)

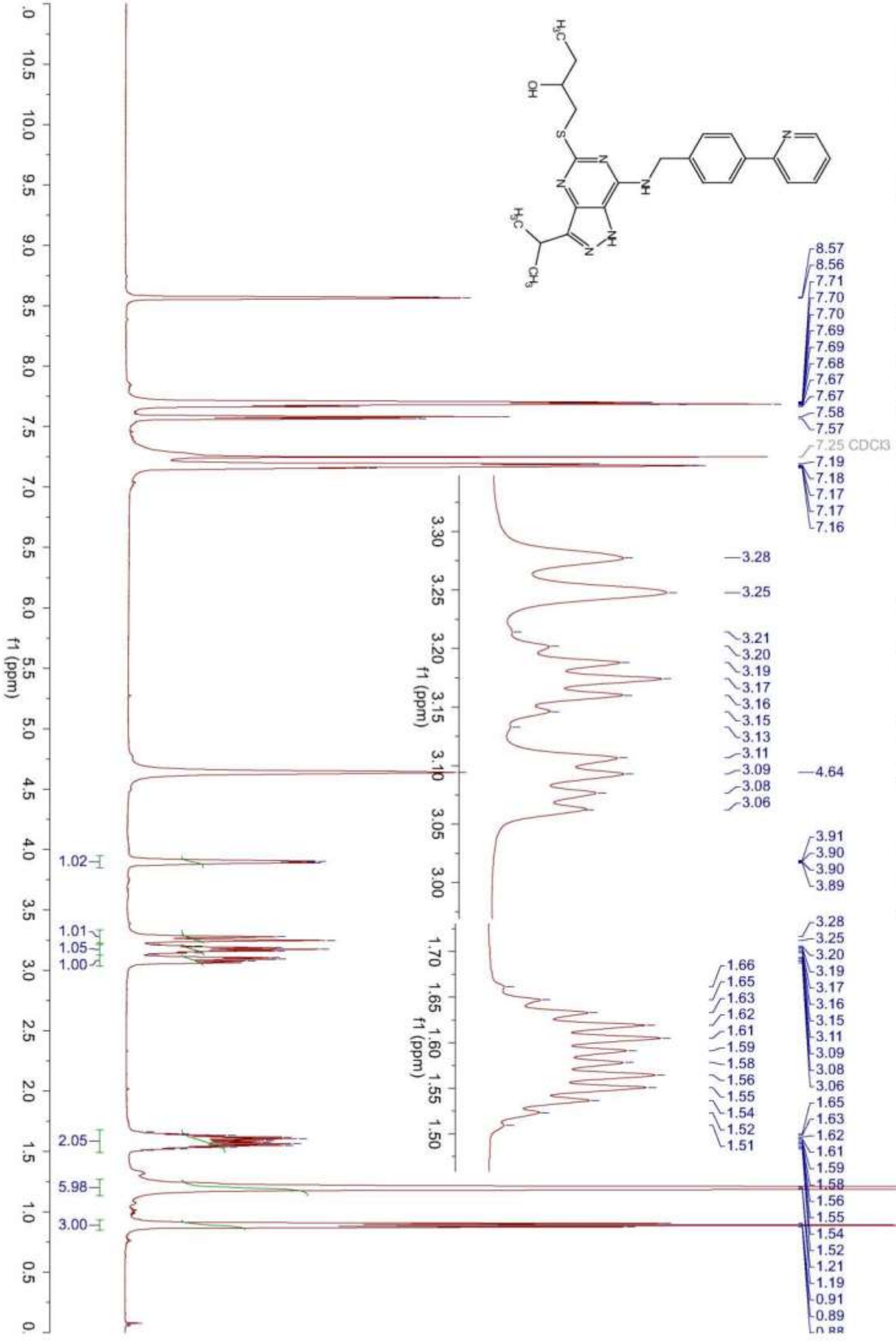
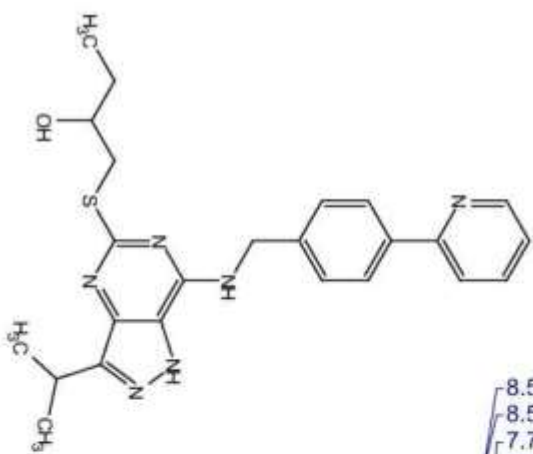


- 171.30
- 161.82
- 156.75
- 150.18
- 149.33
- 138.85
- 138.24
- 137.17
- 128.17
- 127.13
- 122.33
- 120.74

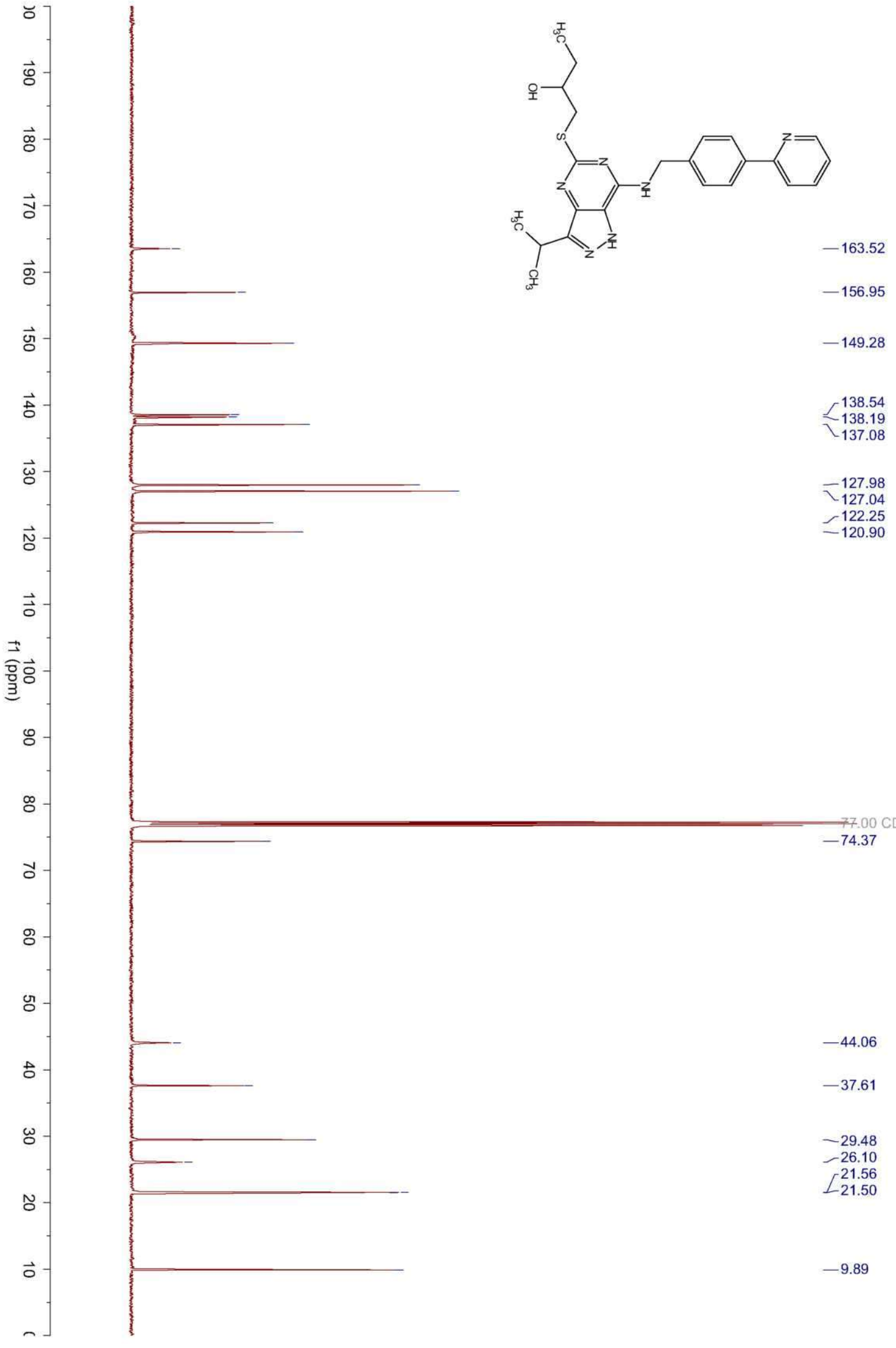
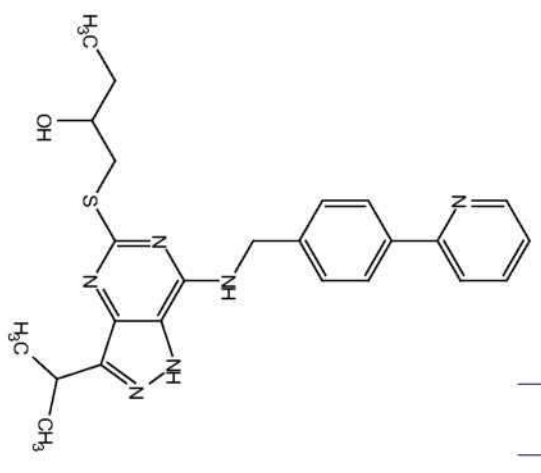
- 44.29
- 40.58
- 30.31
- 26.36
- 23.13
- 21.83



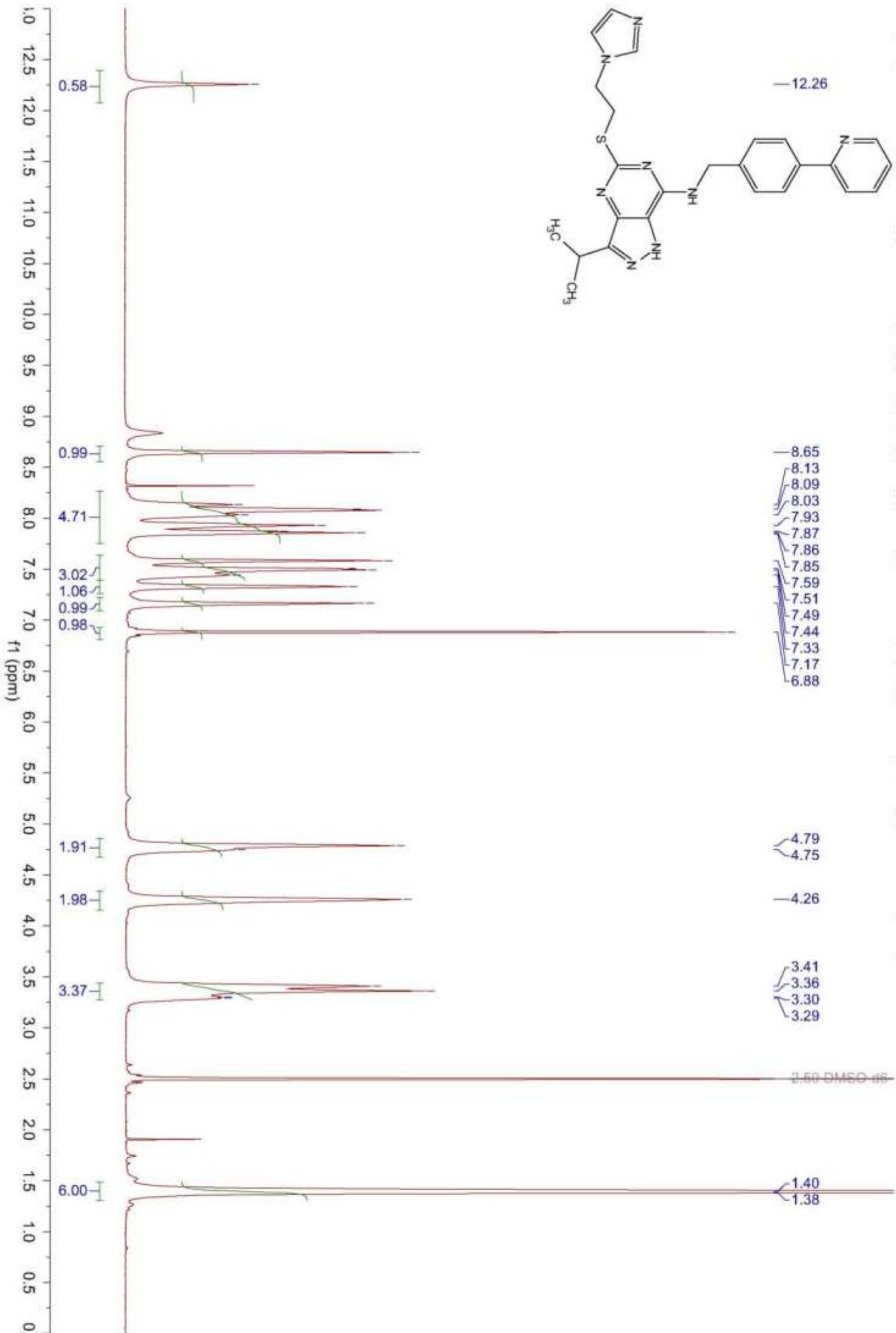
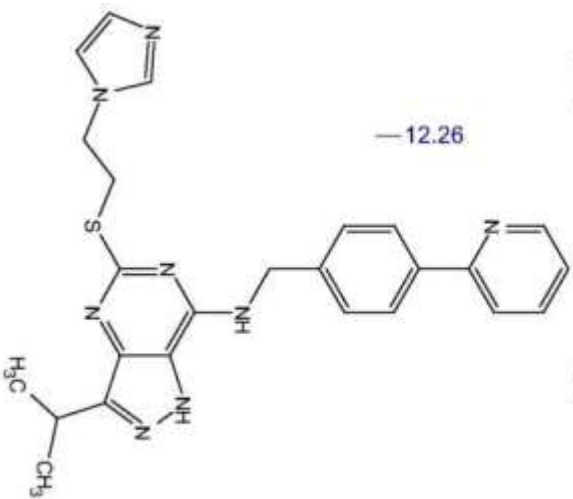
5-(2-Hydroxy-1-butyl)thio-3-isopropyl-7-[4-(2-pyridyl)benzylamino-1(2)H-pyrazolo[4,3-d]pyrimidine (4.16)



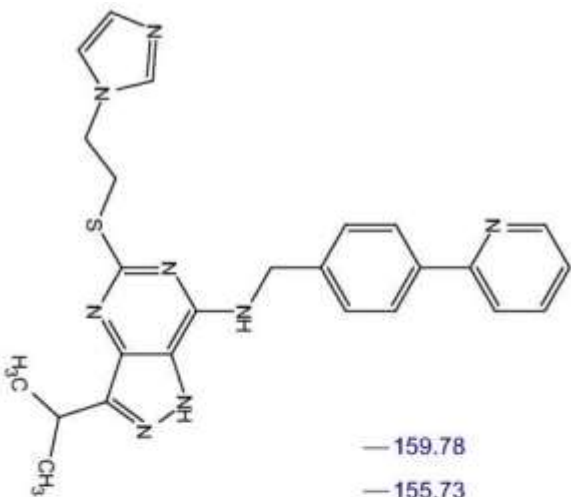
5-(2-Hydroxy-1-butyl)thio-3-isopropyl-7-[4-(2-pyridyl)benzyl]amino-1(2)H-pyrazolo[4,3-d]pyrimidine (4.16)



5-[2-(1-Imidazolyl)-1-ethyl]thio-3-isopropyl-7-[4-(2-pyridyl)benzyl]amino-1(2H)-pyrazolo[4,3-d]pyrimidine (4.17)



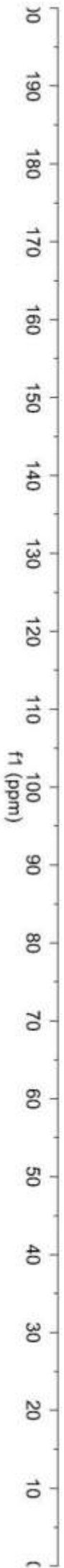
5-[2-(1-imidazolyl)-1-ethylthio-3-isopropyl-7-[4-(2-pyridyl)benzyl]amino-1(2H)-pyrazolo[4,3-d]pyrimidine (4.17)



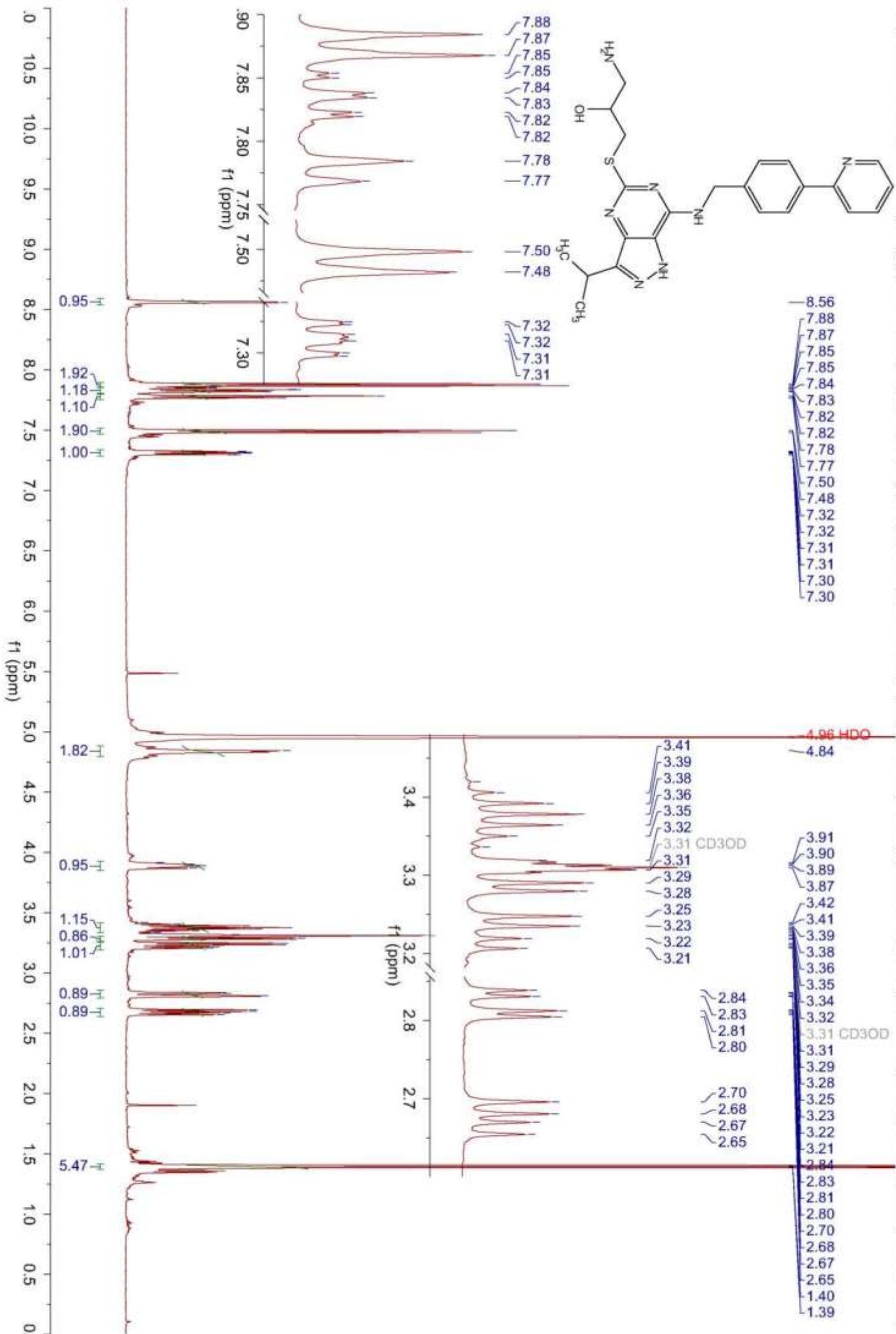
- 159.78
- 155.73
- ~ 149.53
- ~ 148.88
- ~ 139.47
- ~ 137.74
- ~ 137.22
- ~ 128.44
- ~ 128.03
- ~ 127.56
- ~ 126.70
- ~ 126.50
- ~ 122.56
- ~ 120.14
- ~ 119.20

- ~ 45.76
- ~ 43.25
- ~ 42.63

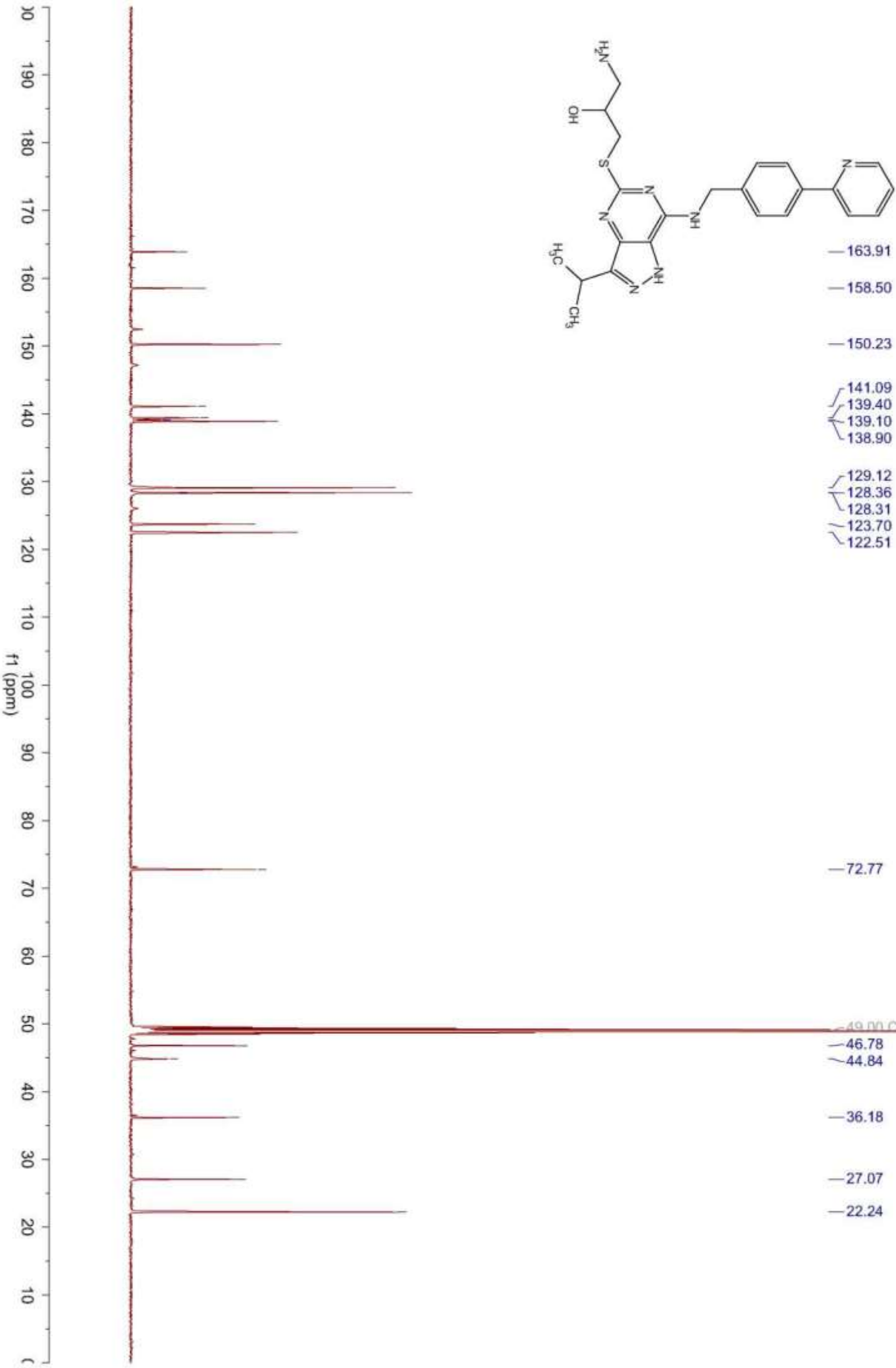
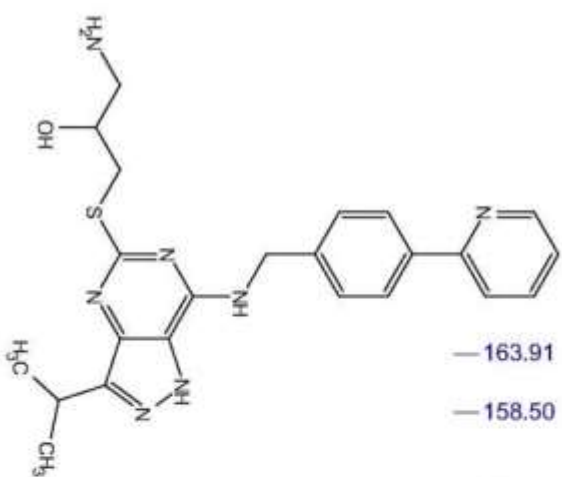
- ~ 31.19
- 26.42
- ~ 21.74



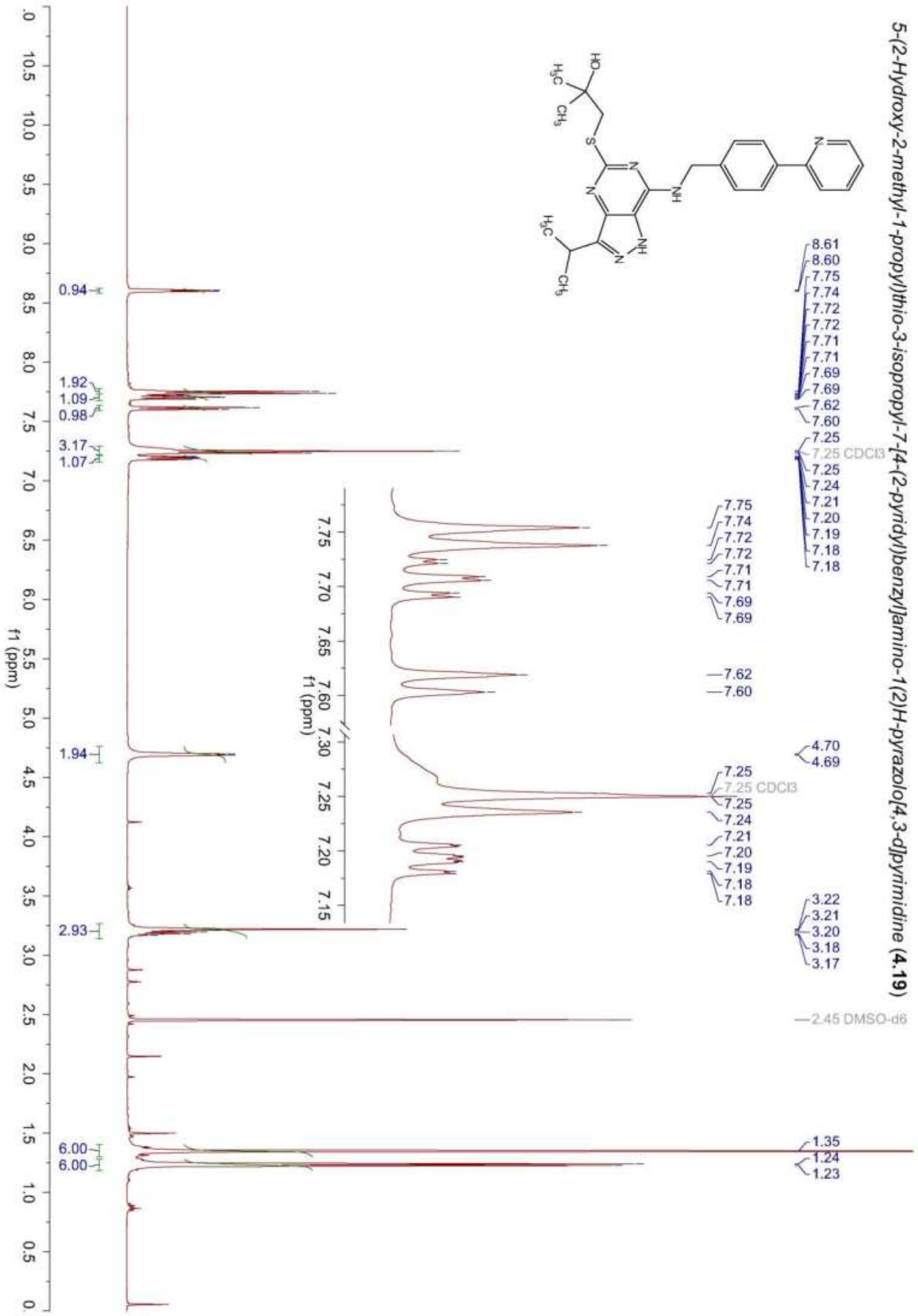
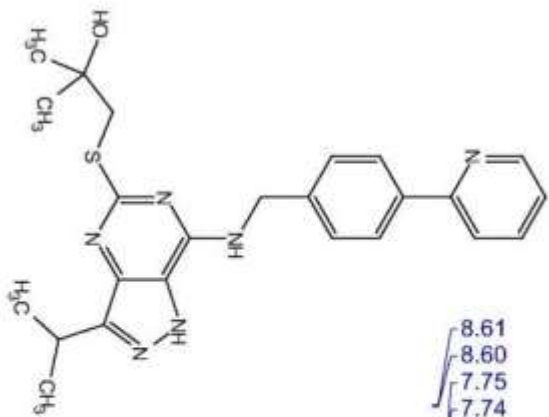
5-(3-Amino-2-hydroxy-1-propyl)thio-3-isopropyl-7-[4-(2-pyridyl)benzyl]amino-1(2H)-pyrazolo[4,3-d]pyrimidine, (R/S) mixture (4.18) and (R) antipode (4.31)



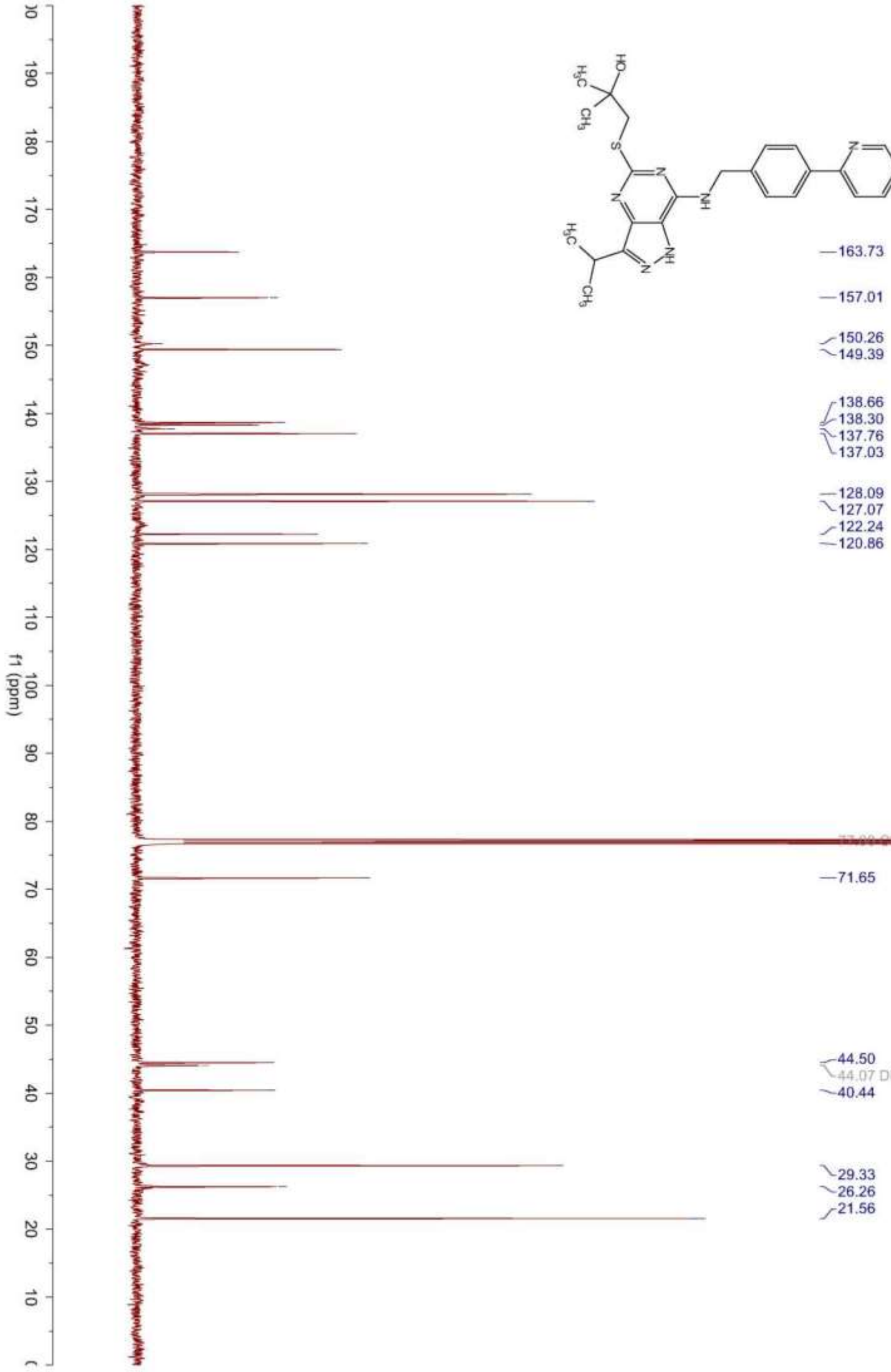
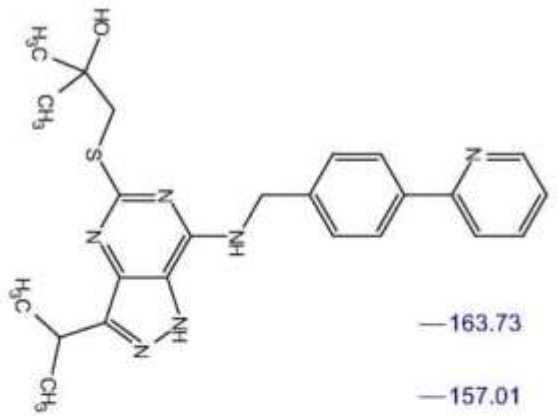
5-(3-Amino-2-hydroxy-1-propyl)thio-3-isopropyl-7-[4-(2-pyridyl)benzyl]amino-1(2H)-pyrazolo[4,3-d]pyrimidine, (R/S) mixture (4.18) and (R) antipode (4.31)



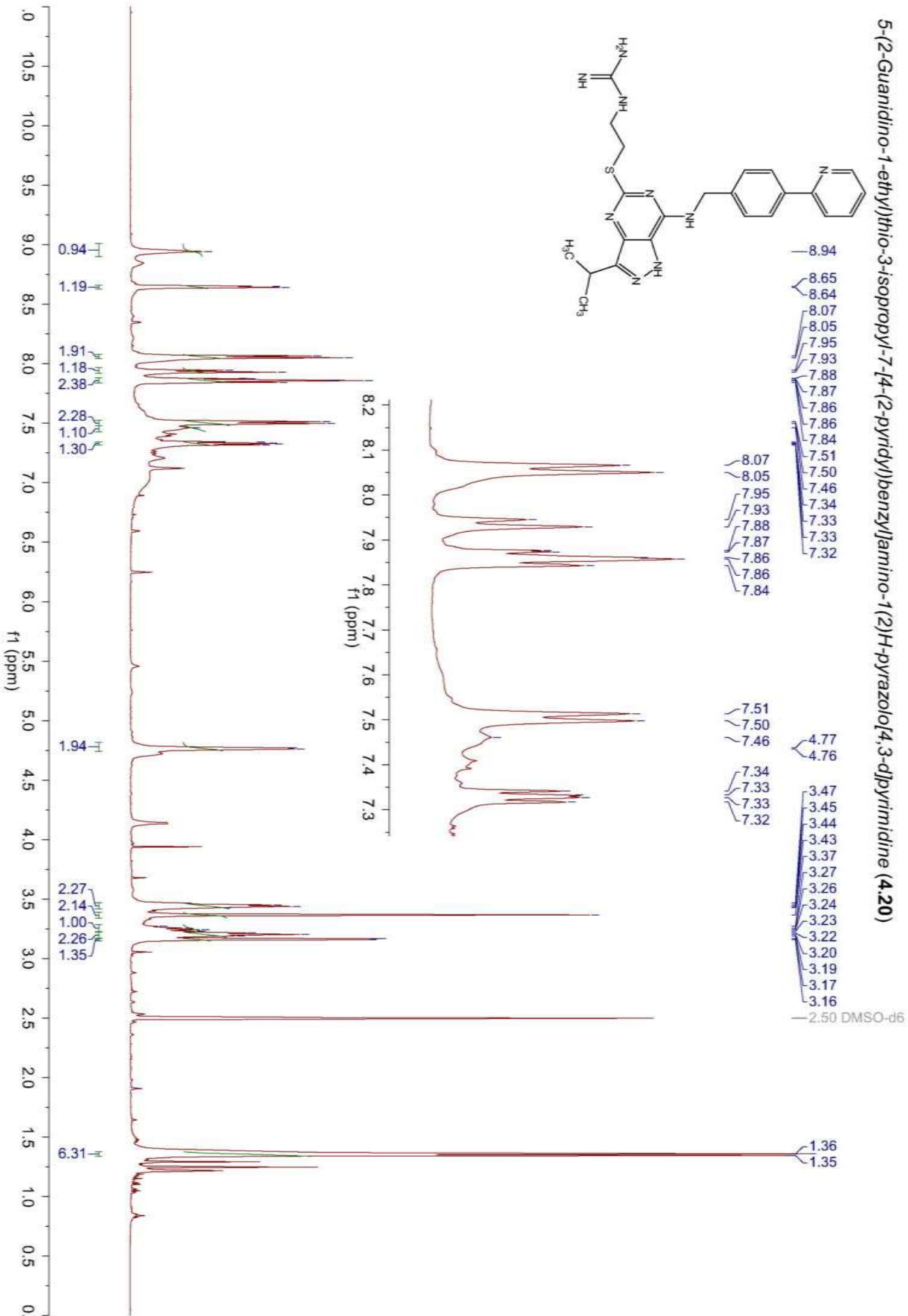
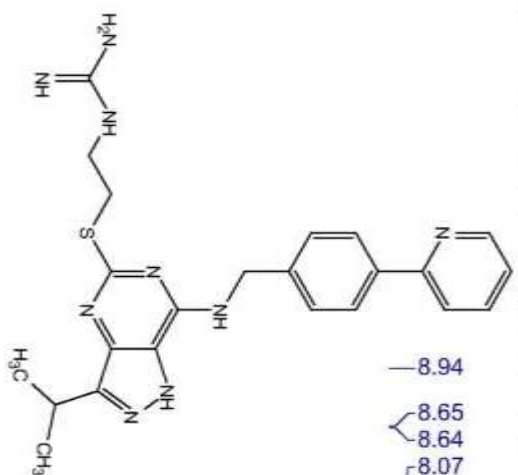
5-(2-Hydroxy-2-methyl-1-propyl)thio-3-isopropyl-7-[4-(2-pyridyl)benzyl]amino-1(2H)-pyrazolo[4,3-d]pyrimidine (4.19)



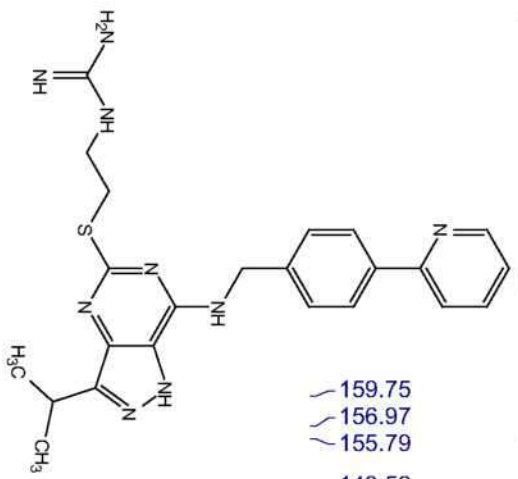
5-(2-Hydroxy-2-methyl-1-propyl)thio-3-isopropyl-7-[4-(2-pyridyl)benzylamino-1(2)H-pyrazolo[4,3-d]pyrimidine (4.19)



5-(2-Guanidino-1-ethyl)thio-3-isopropyl-7-[4-(2-pyridyl)benzyl]amino-1(2H)-pyrazolo[4,3-d]pyrimidine (4.20)

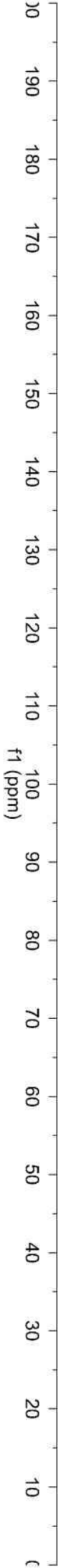


5-(2-Guanidino-1-ethyl)thio-3-isopropyl-7-[4-(2-pyridyl)benzyl]amino-1(2H)-pyrazolo[4,3-d]pyrimidine (4.20)



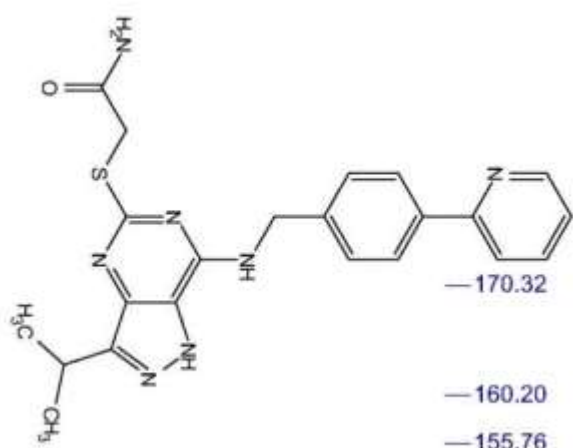
- 159.75
- 156.97
- 155.79
- 149.52
- 148.96
- 148.47
- 139.85
- 139.72
- 137.52
- 137.24
- 127.84
- 127.68
- 126.60
- 122.53
- 120.78
- 120.15

- 48.61
- 42.98
- 40.57
- 39.32 DMSO-d6
- 29.45
- 26.32
- 21.78

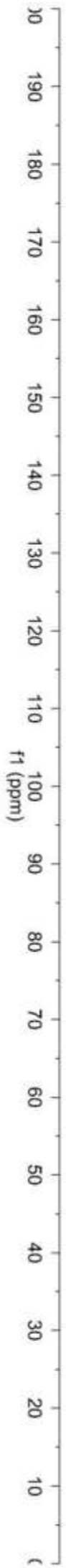




5-(Carbamoylmethyl)thio-3-isopropyl-7-[4-(2-pyridyl)benzyl]amino-1(2H)-pyrazolo[4,3-d]pyrimidine (4.21)

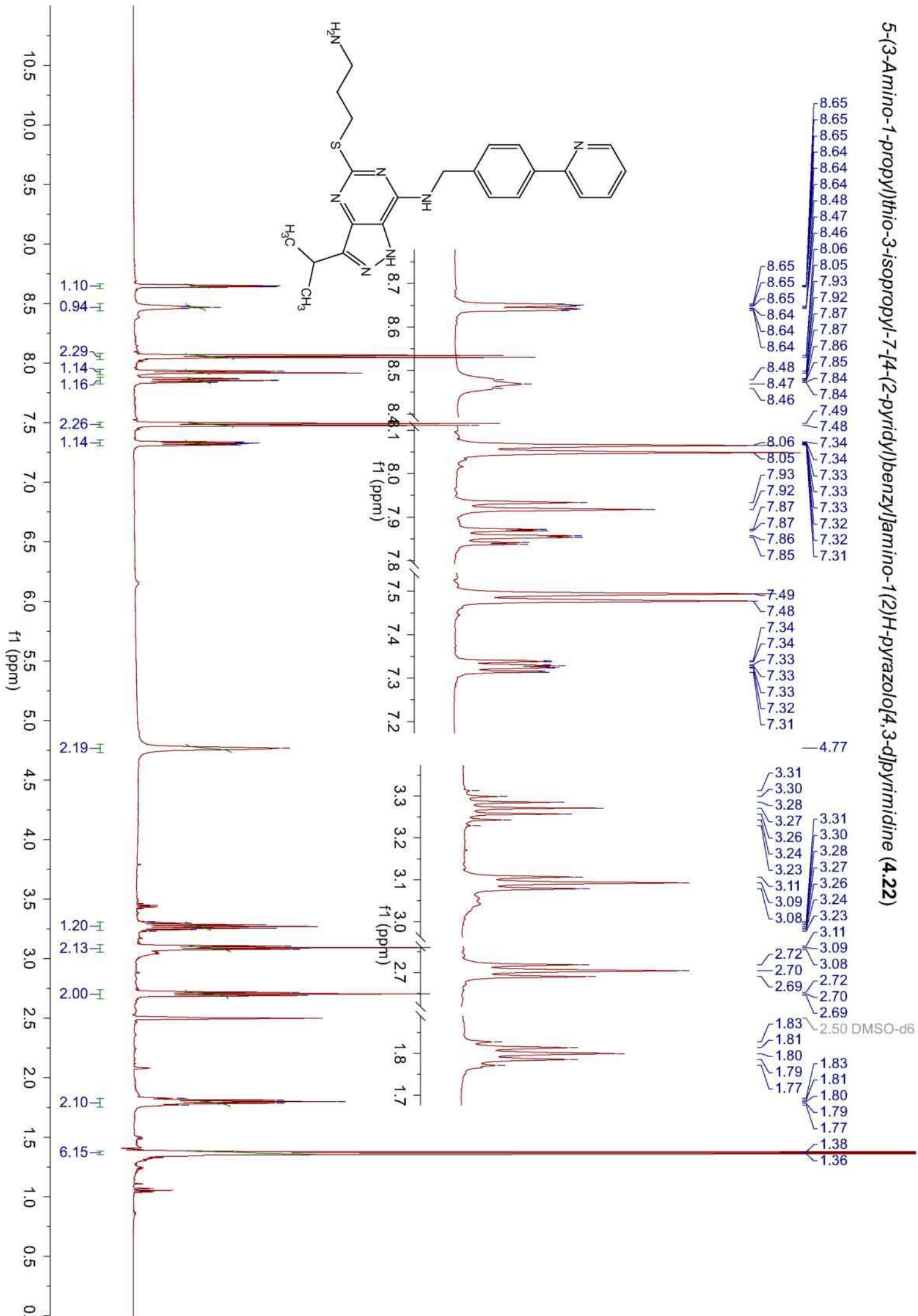


- 170.32
- 160.20
- 155.76
- 149.45
- 139.84
- 137.54
- 137.12
- 128.04
- 126.54
- 122.44
- 120.06

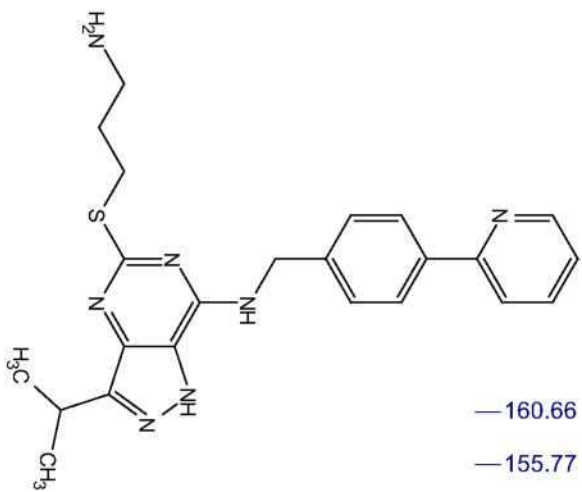


- 42.96
- 34.46
- 25.82
- 21.69

5-(3-Amino-1-propyl)thio-3-isopropyl-7-[4-(2-pyridyl)benzyl]amino-1(2H)-pyrazolo[4,3-d]pyrimidine (4.22)

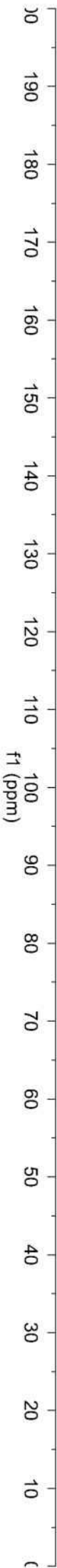


5-(3-Amino-1-propyl)thio-3-isopropyl-7-[4-(2-pyridyl)benzyl]amino-1(2)H-pyrazolo[4,3-d]pyrimidine (4.22)

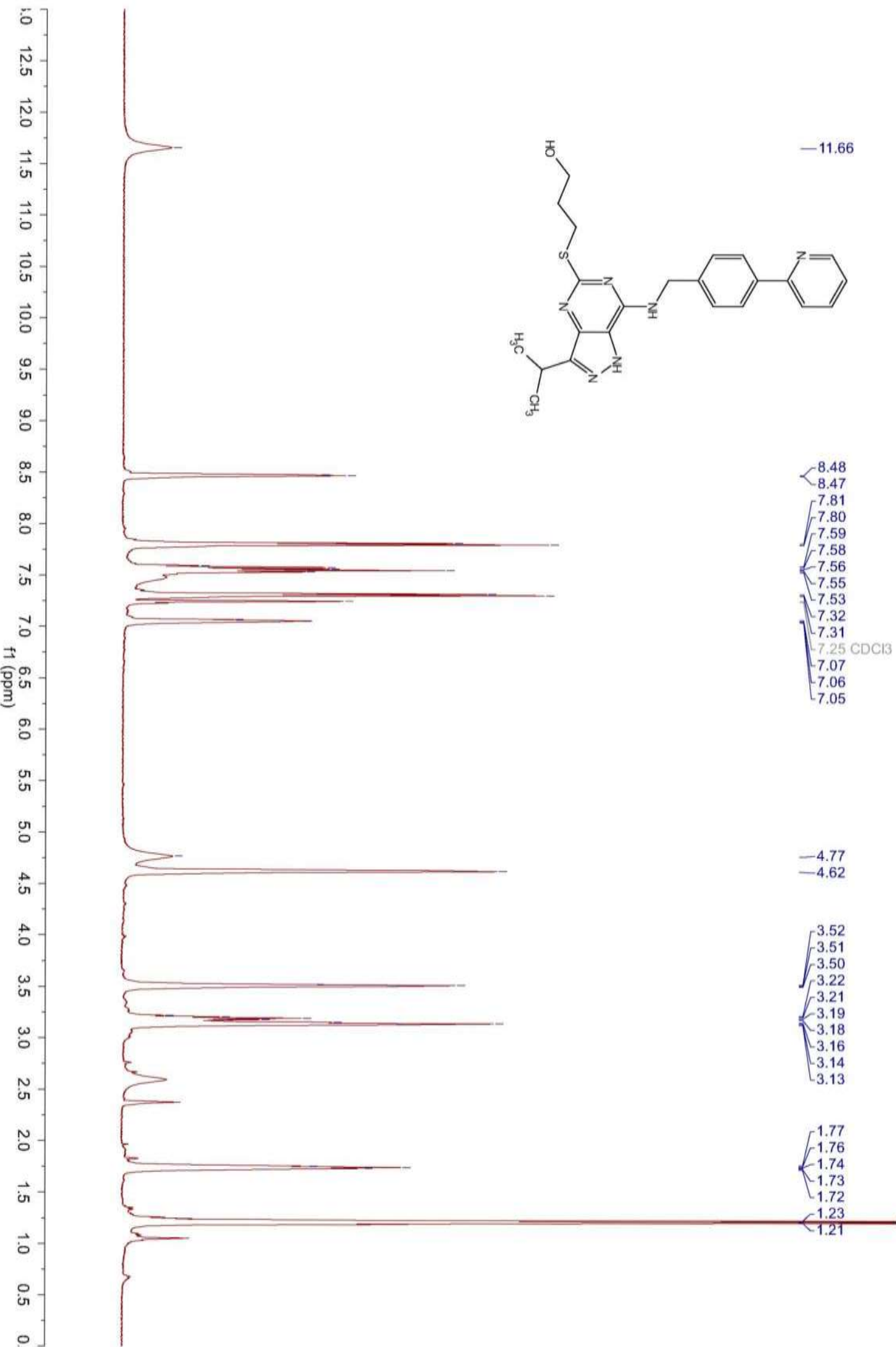
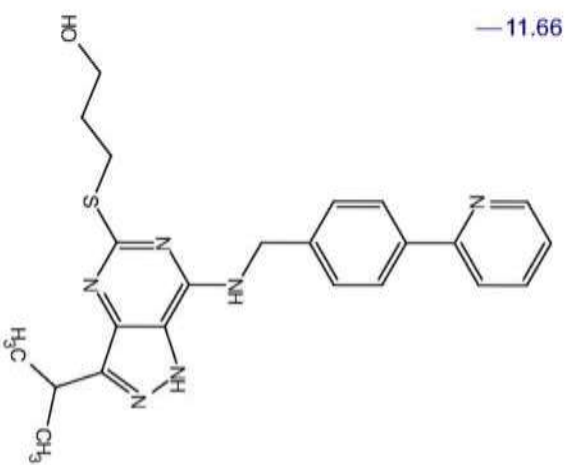


- 160.66
- 155.77
- 150.24
- 149.49
- 145.86
- 139.99
- 138.60
- 137.49
- 137.17
- 127.83
- 126.55
- 123.37
- 122.48
- 120.09

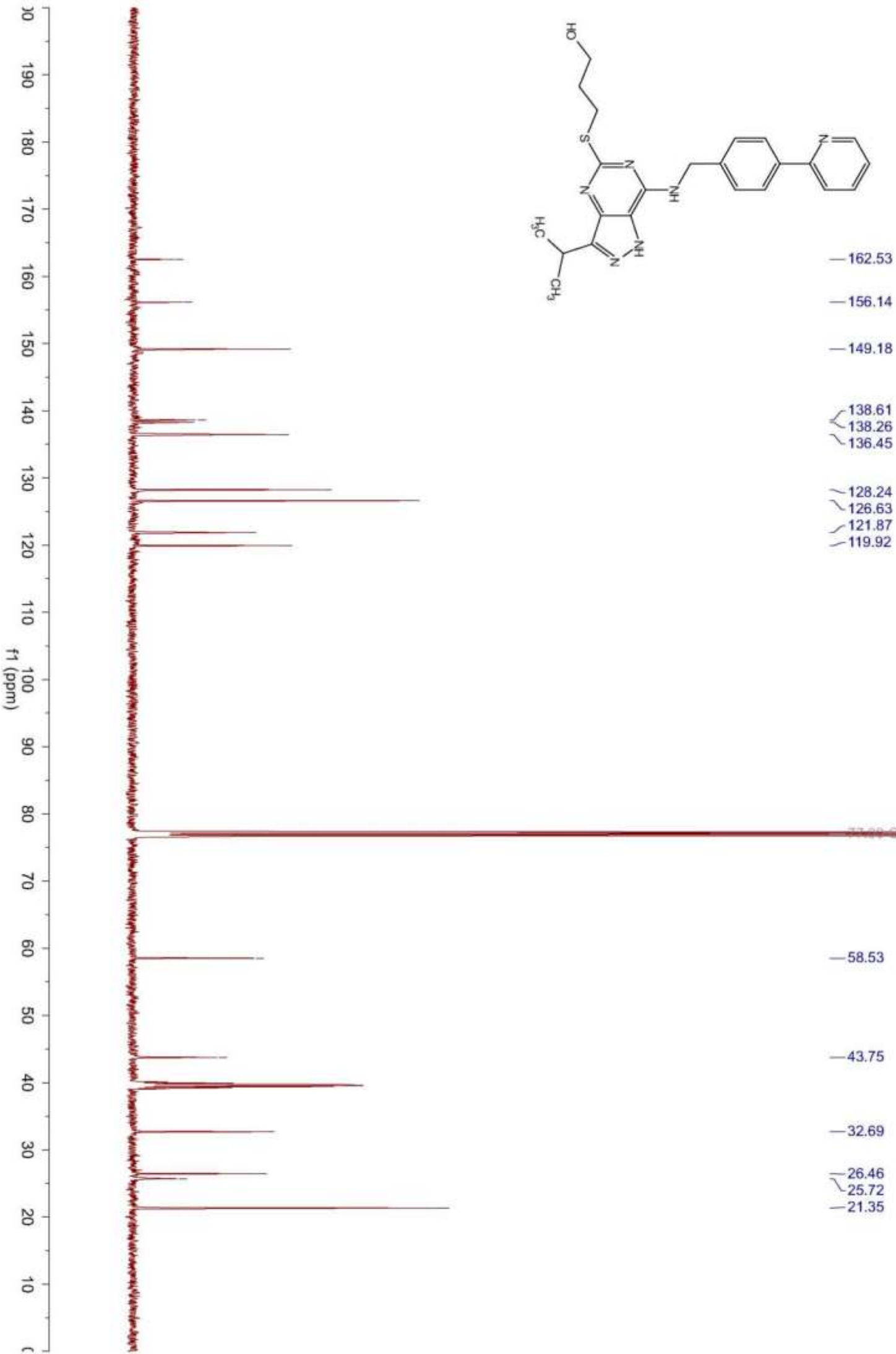
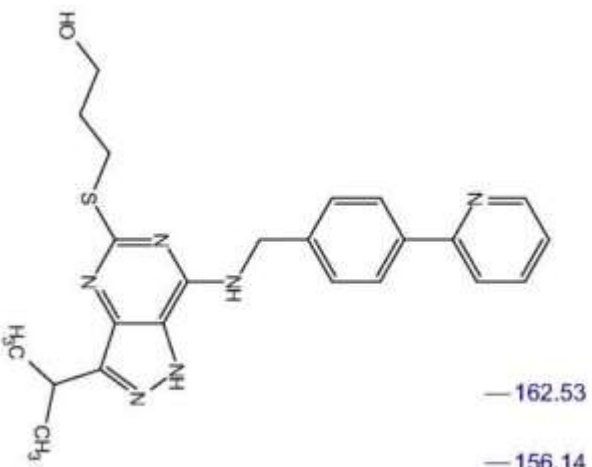
- 42.95
- 39.75
- 39.52 DMSO-d6
- 31.31
- 27.54
- 25.94
- 21.71



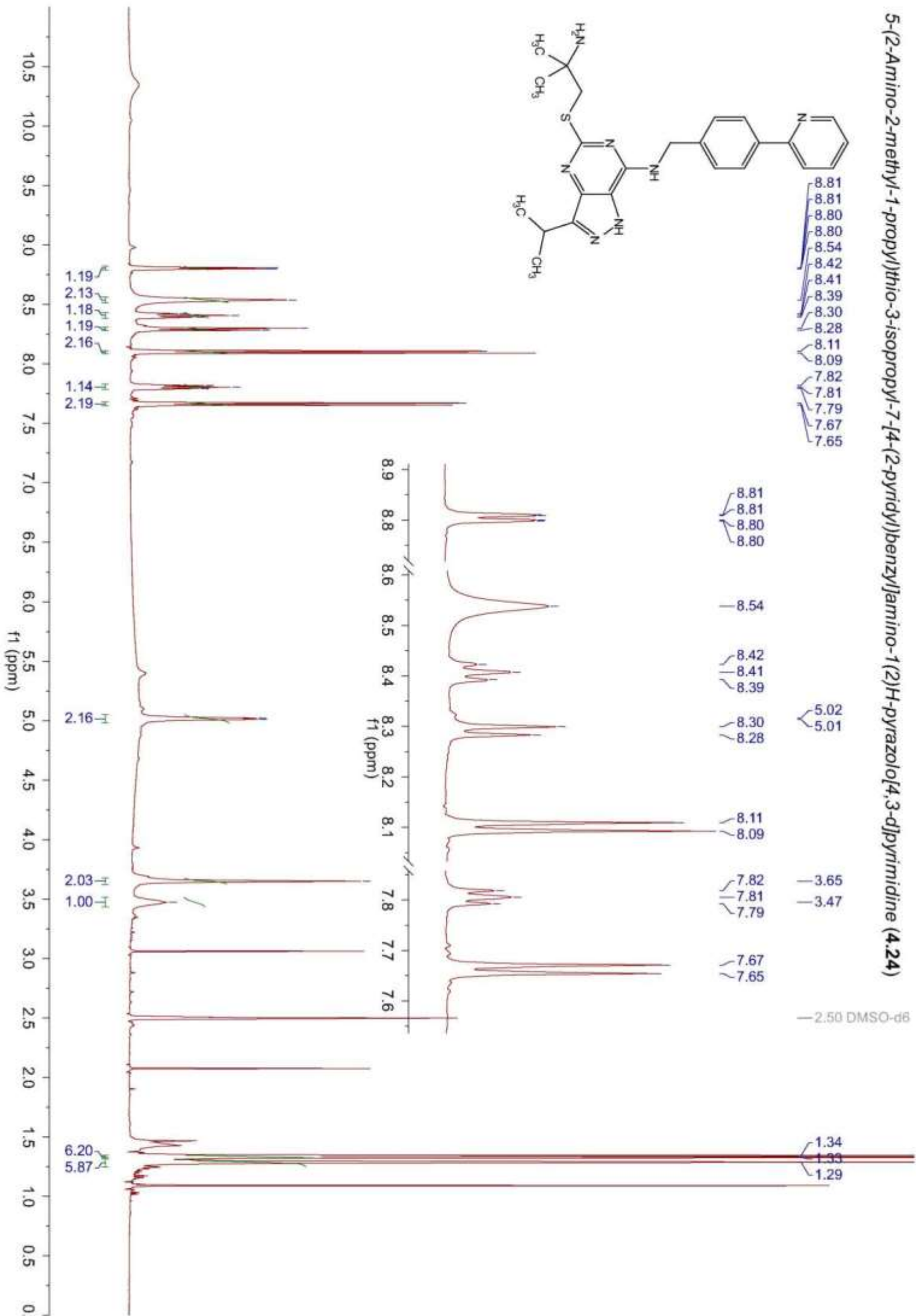
5-(3-Hydroxy-1-propyl)thio-3-isopropyl-7-[4-(2-pyridyl)benzyl]amino-1(2H)-pyrazolo[4,3-d]pyrimidine (4.23)



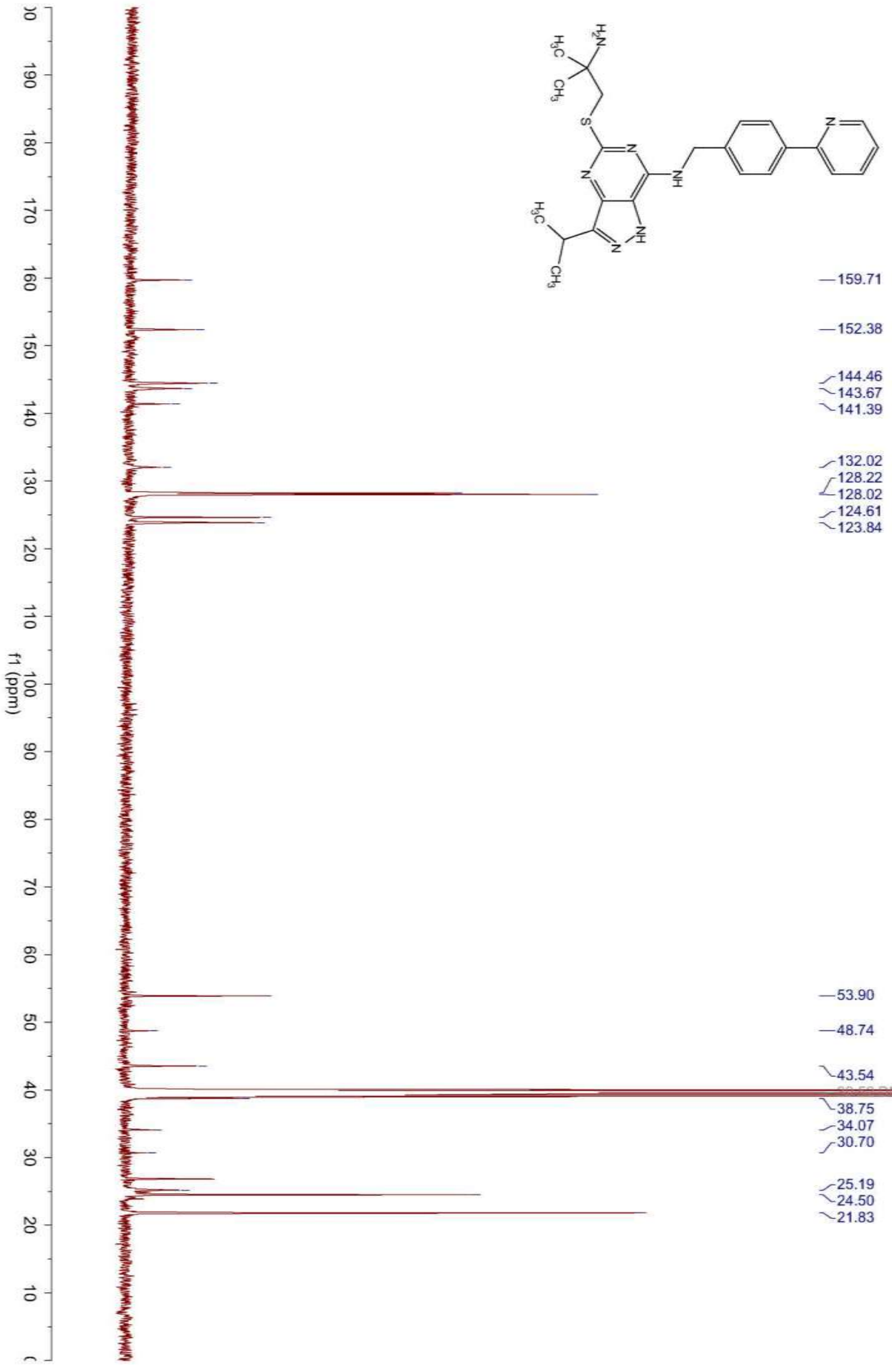
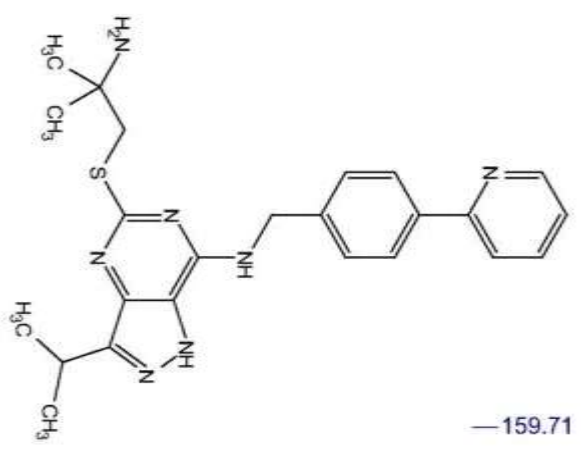
5-(3-Hydroxy-1-propyl)thio-3-isopropyl-7-[4-(2-pyridyl)benzyl]amino-1(2H)-pyrazolo[4,3-d]pyrimidine (4.23)



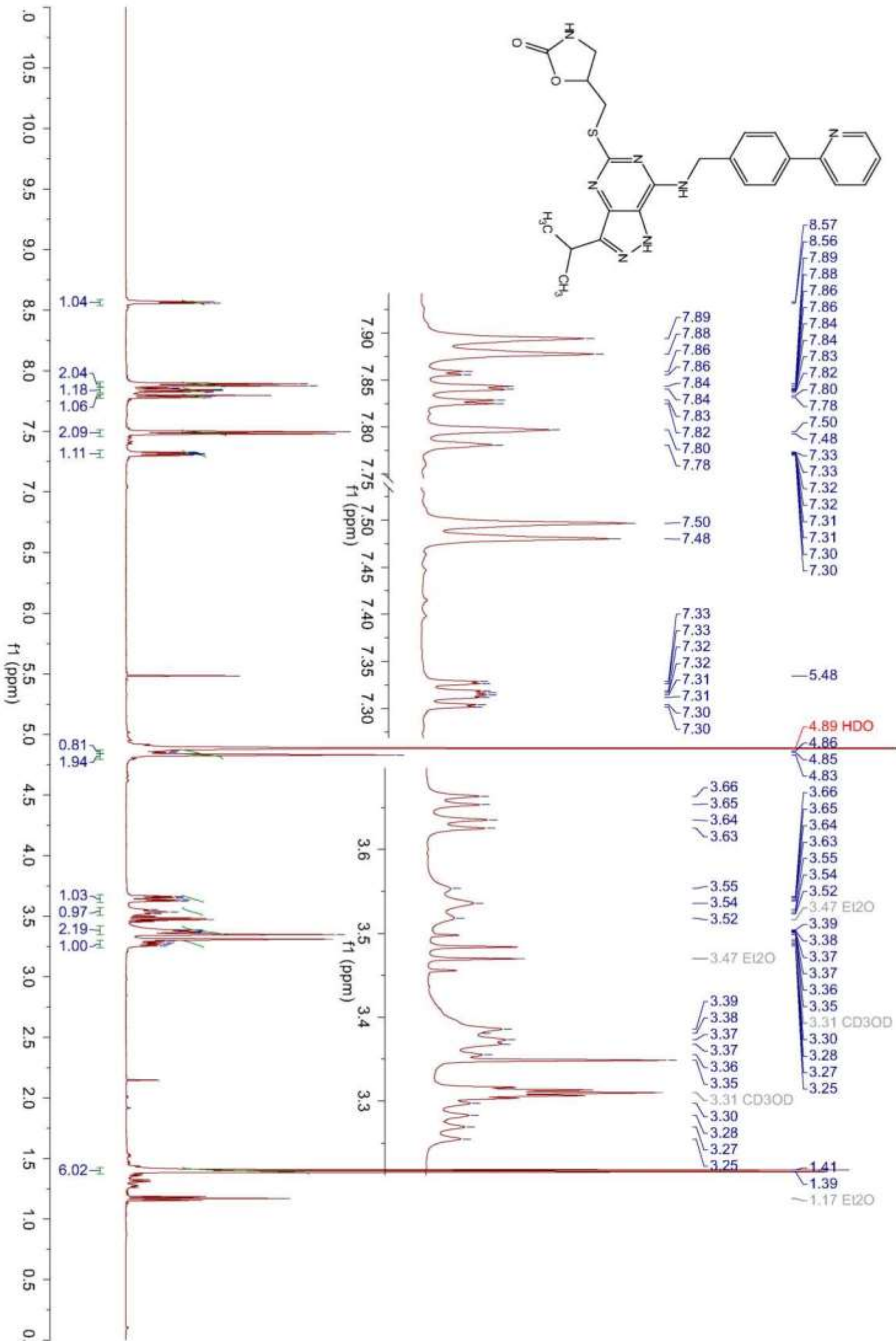
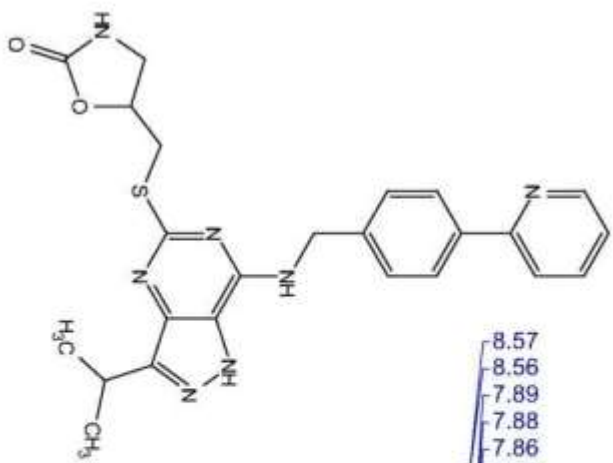
5-(2-Amino-2-methyl-1-propyl)thio-3-isopropyl-7-[4-(2-pyridyl)benzylamino-1(2H)-pyrazolo[4,3-d]pyrimidine (4.24)



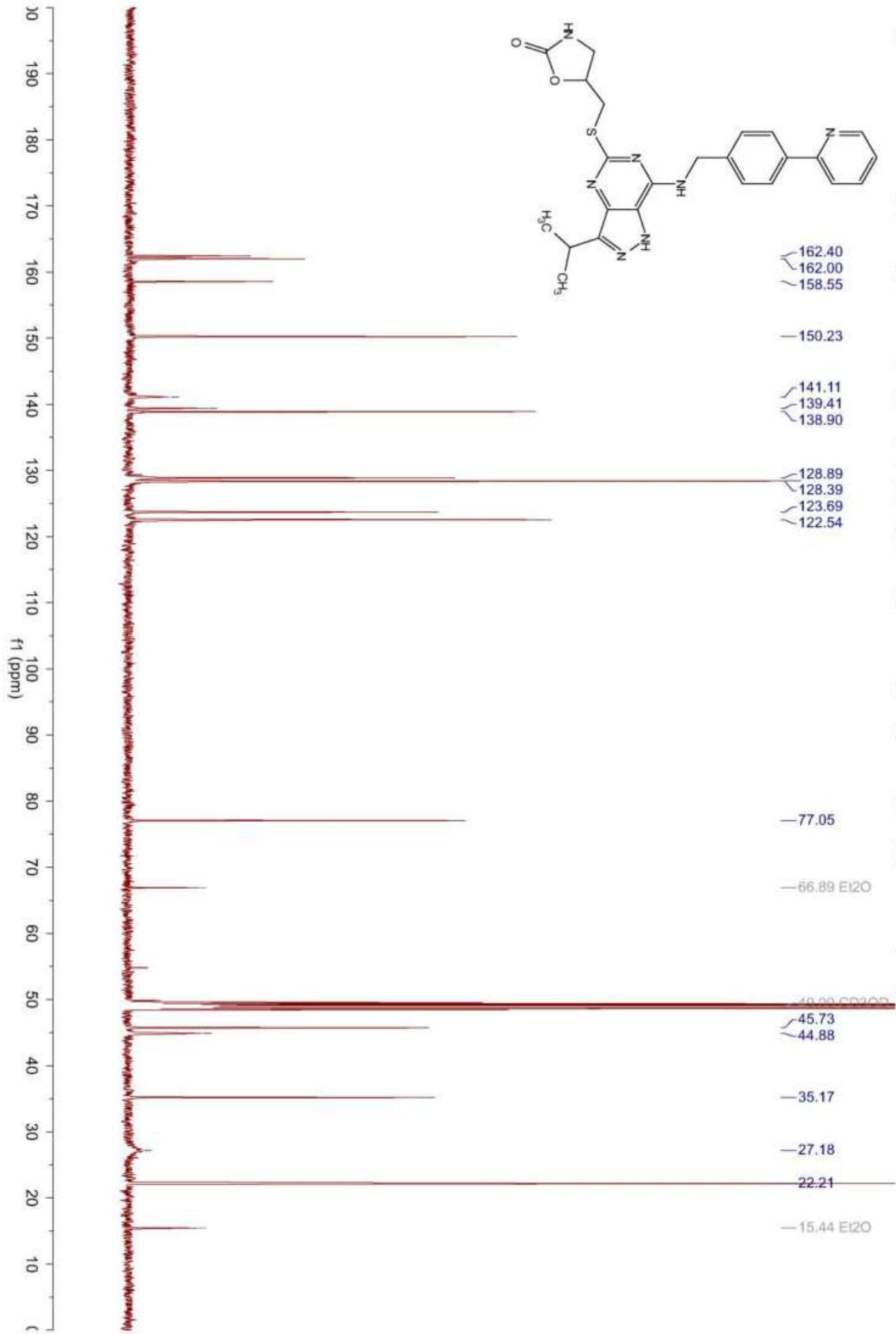
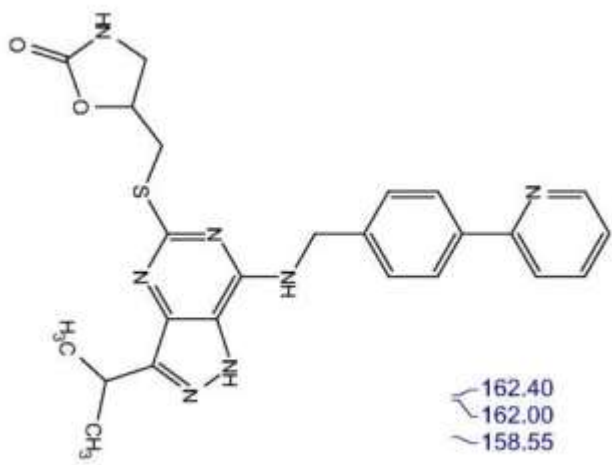
5-(2-Amino-2-methyl-1-propyl)thio-3-isopropyl-7-[4-(2-pyridyl)benzyl]amino-1(2)-H-pyrazolo[4,3-d]pyrimidine (4.24)



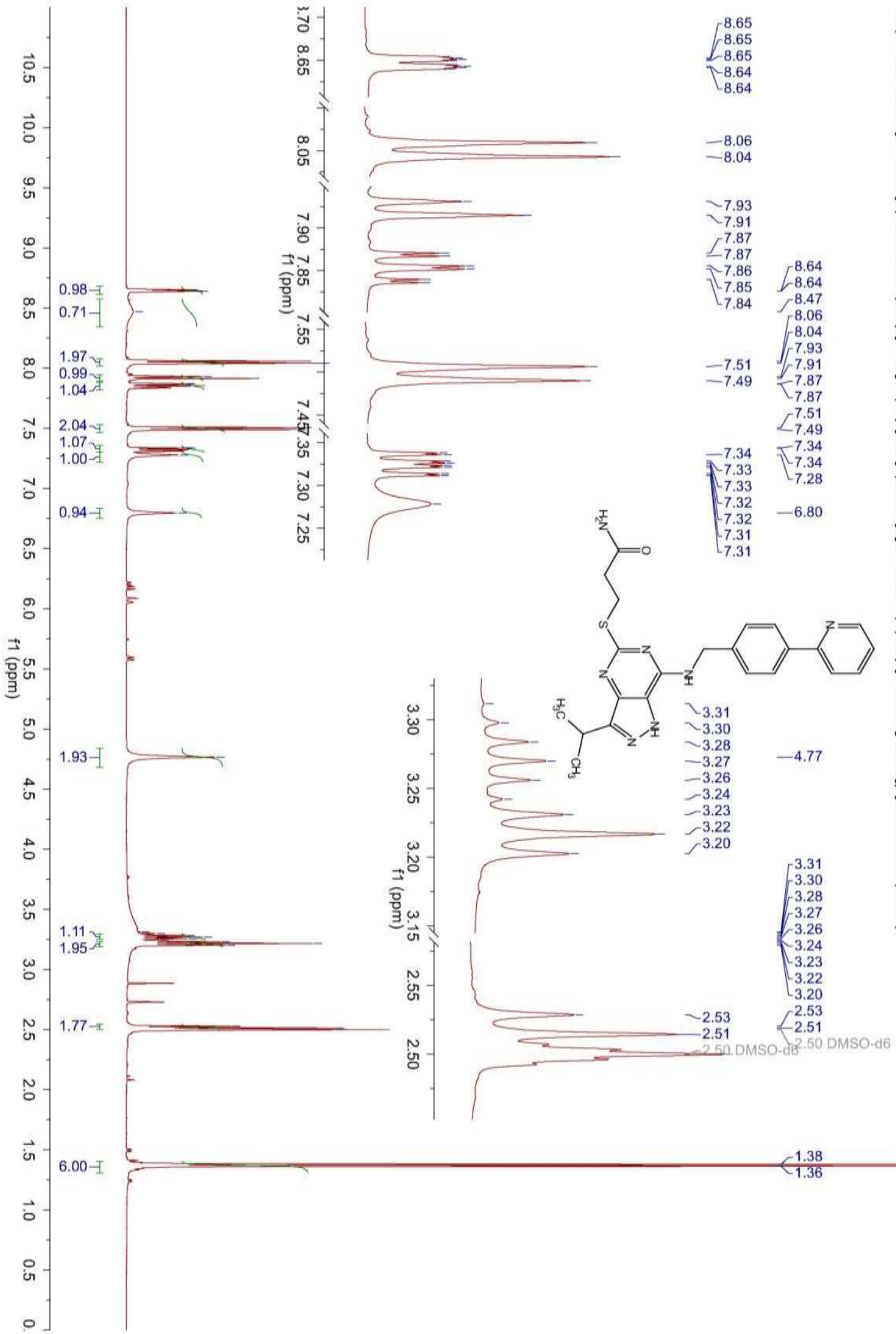
5-[(Oxazolidin-2-on-5-yl)methyl]thio-3-isopropyl-7-[4-(2-pyridyl)benzyl]amino-1(2H)-pyrazolo[4,3-d]pyrimidine (4.25)



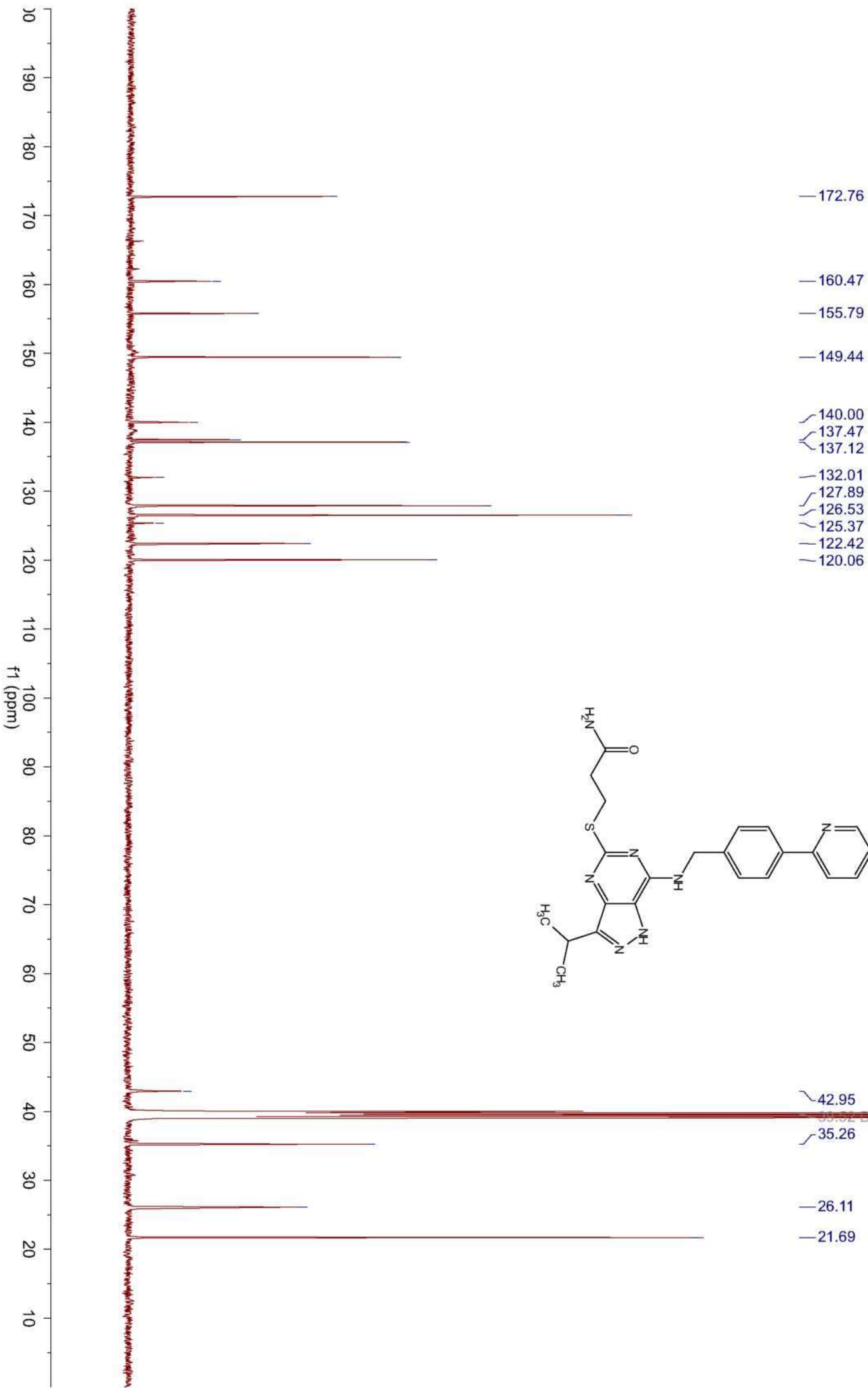
5-[(Oxazolidin-2-on-5-yl)methyl]methylthio-3-isopropyl-7-[4-(2-pyridyl)benzyl]amino-1(2H)-pyrazolo[4,3-d]pyrimidine (4.25)



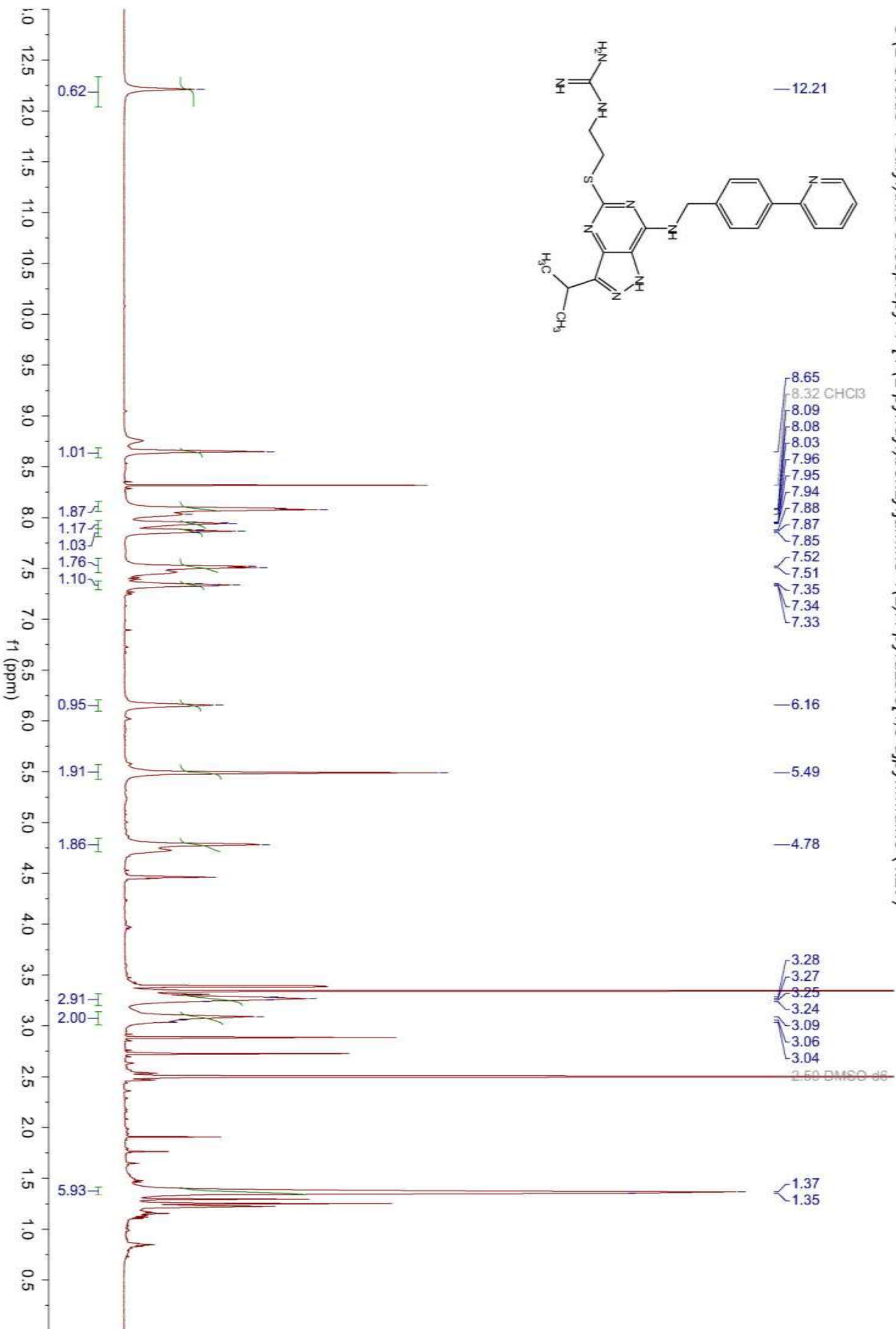
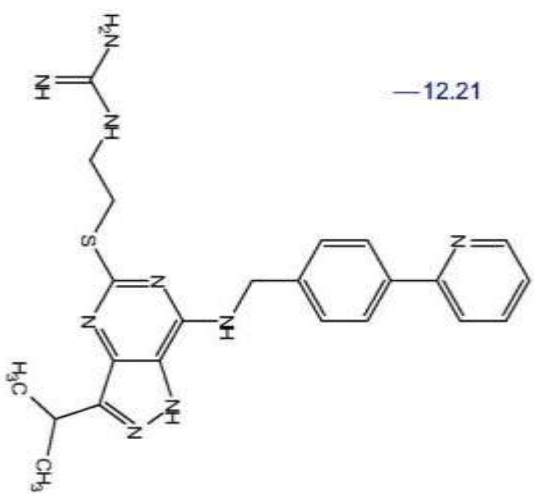
5-(2-Carbamoyl-1-ethyl)thio-3-isopropyl-7-[4-(2-pyridyl)benzyl]amino-1(2H)-pyrazolo[4,3-d]pyrimidine (4.26)



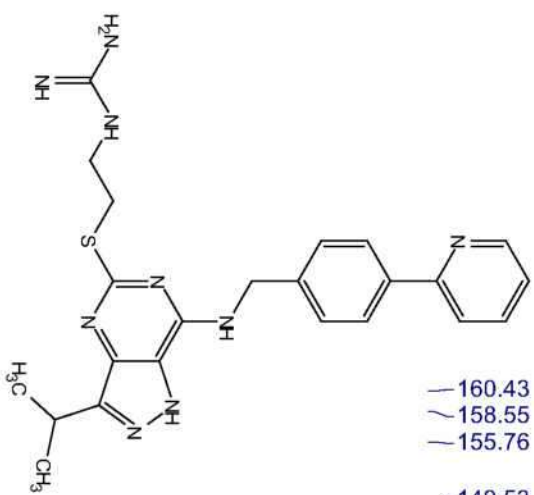
5-(2-Carbamoyl-1-ethyl)thio-3-isopropyl-7-[4-(2-pyridyl)benzylamino-1(2H)-pyrazolo[4,3-d]pyrimidine (4.26)



5-(2-Ureido-1-ethyl)thio-3-isopropyl-7-[4-(2-pyridyl)benzyl]amino-1(2H)-pyrazolo[4,3-d]pyrimidine (4.27)



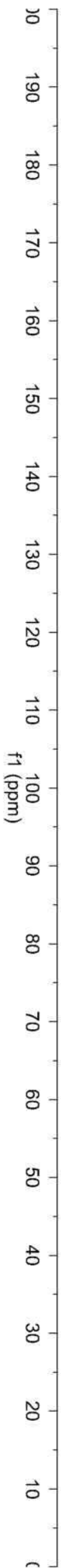
5-(2-Ureido-1-ethyl)thio-3-isopropyl-7-[4-(2-pyridyl)benzyl]amino-1(2)H-pyrazolo[4,3-d]pyrimidine (4.27)



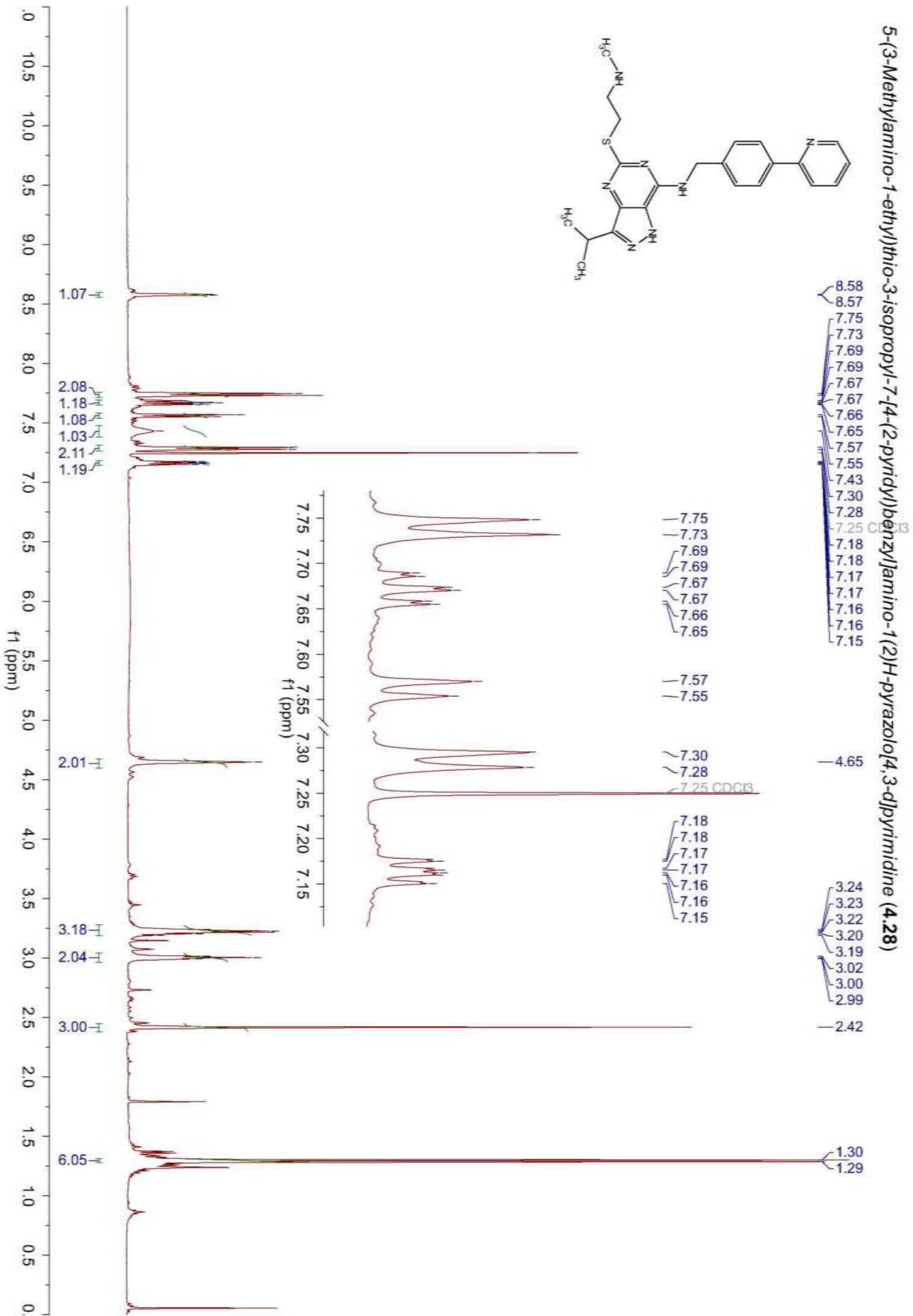
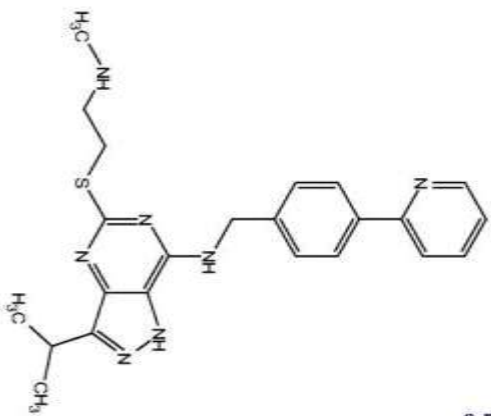
- 160.43
- 158.55
- 155.76
- 149.53
- 148.84
- 139.68
- 137.24
- 128.11
- 126.68
- 122.58
- 120.15

- 79.20
- 62.81

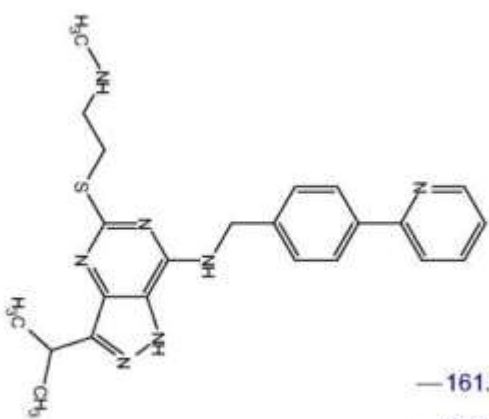
- 43.21
- 39.52 DMSO-d6
- 35.80
- 31.09
- 26.37
- 21.72



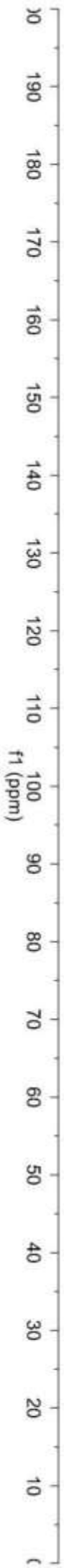
5-(3-Methylamino-1-ethyl)thio-3-isopropyl-7-[4-(2-pyridyl)benzylamino-1(2)H-pyrazolo[4,3-d]pyrimidine (4.28)



5-(3-Methylamino-1-ethyl)thio-3-isopropyl-7-[4-(2-pyridyl)benzyl]amino-1(2H)-pyrazolo[4,3-d]pyrimidine (4.28)

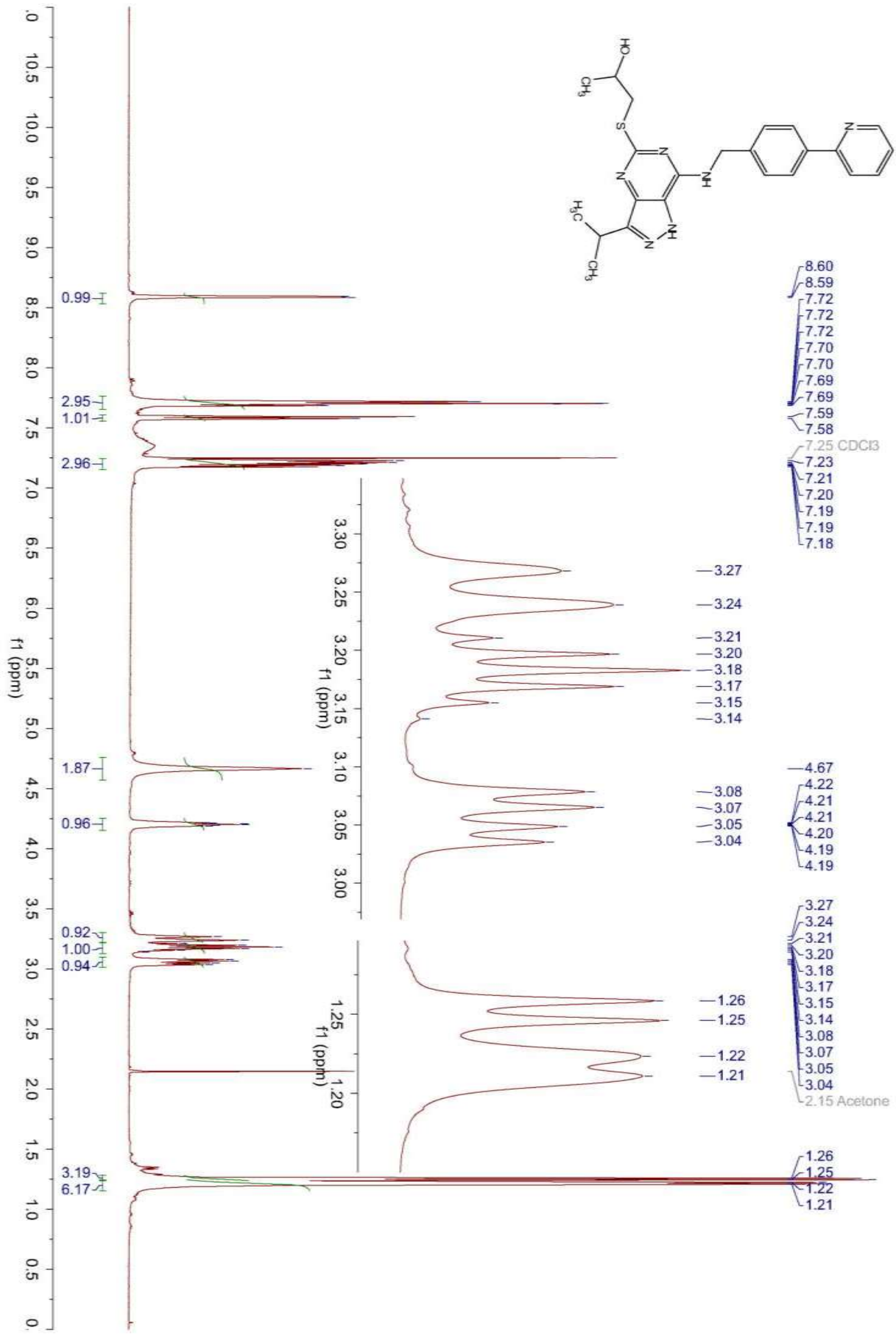
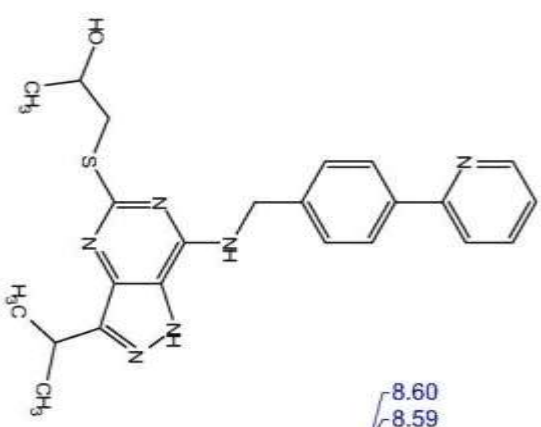


- 161.25
- 156.97
- 150.49
- 149.39
- 139.07
- 138.67
- 138.18
- 137.02
- 128.03
- 127.82
- 127.03
- 122.22
- 120.76

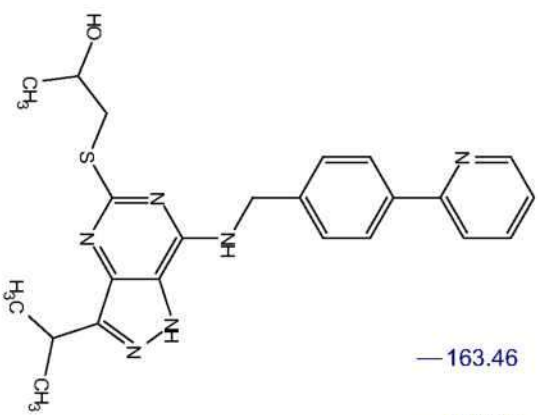


- 50.74
- 44.02
- 34.71
- 29.68
- 29.48
- 26.22
- 21.74
- 21.50

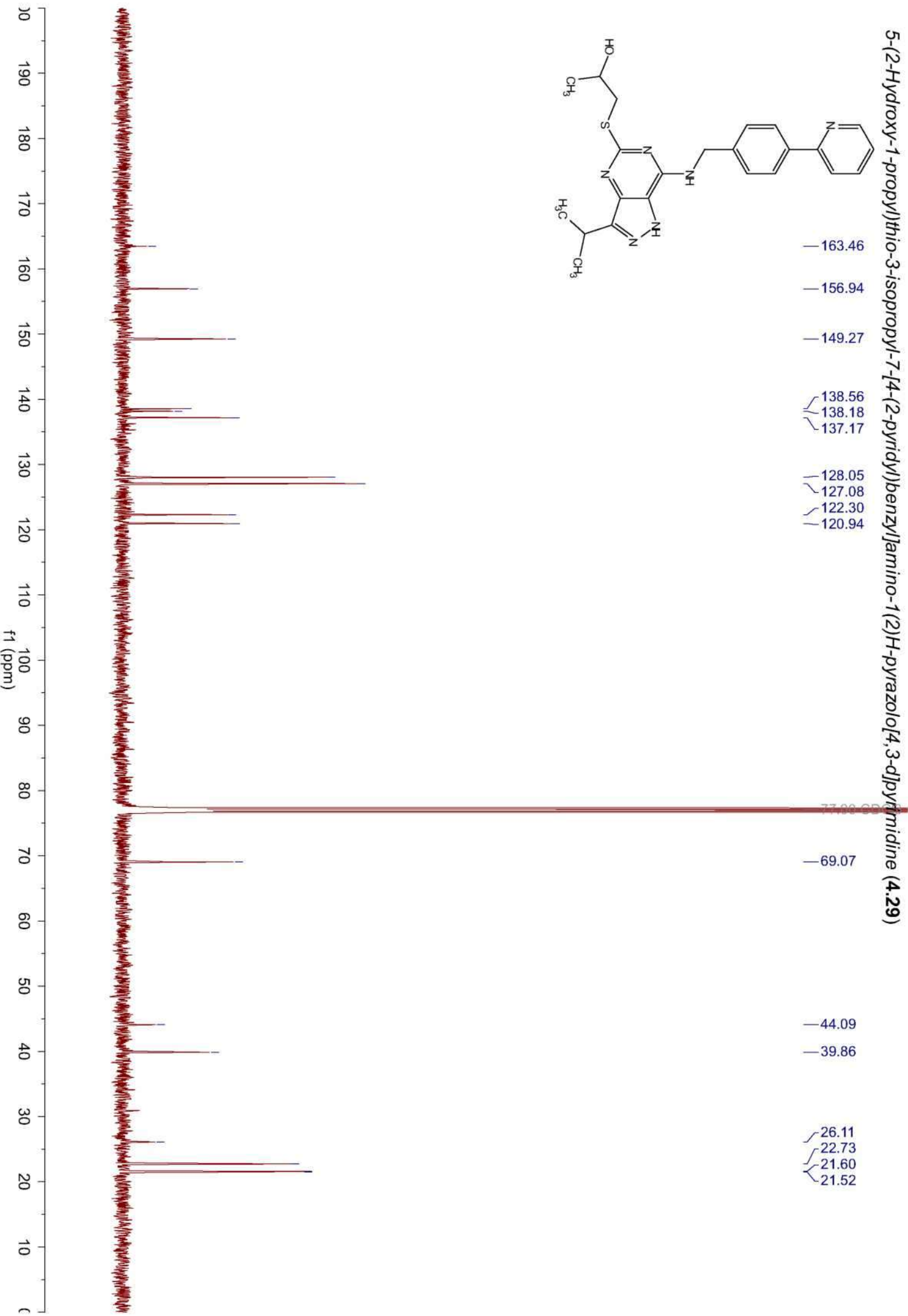
5-(2-Hydroxy-1-propyl)thio-3-isopropyl-7-[4-(2-pyridyl)benzyl]amino-1(2H)-pyrazolo[4,3-d]pyrimidine (4.29)



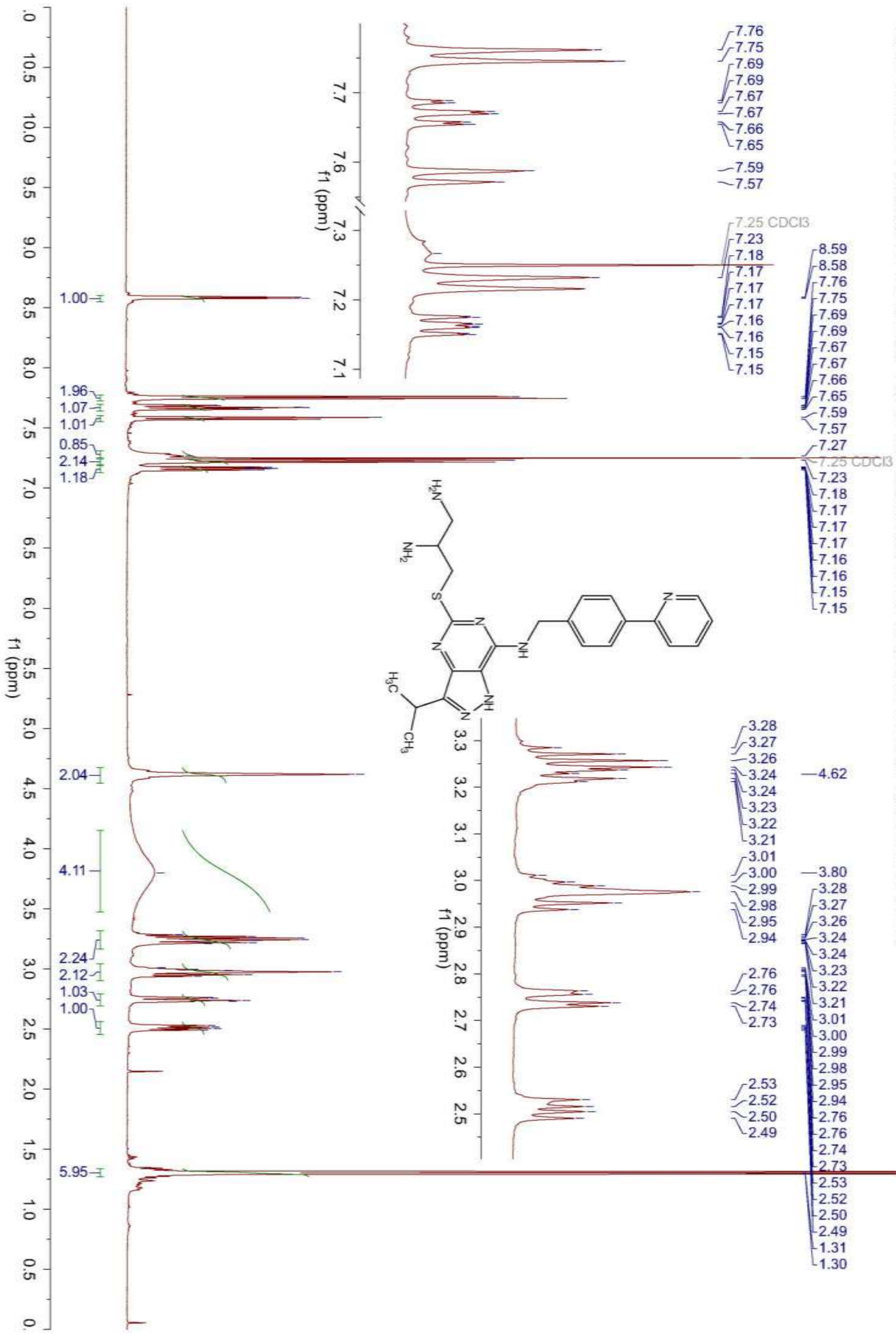
5-(2-Hydroxy-1-propyl)thio-3-isopropyl-7-[4-(2-pyridyl)benzyl]amino-1(2H)-pyrazolo[4,3-d]pyrimidine (4.29)



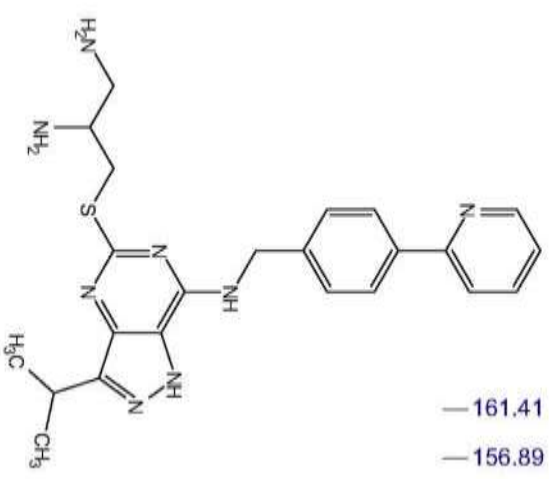
- 163.46
- 156.94
- 149.27
- 138.56
- 138.18
- 137.17
- 128.05
- 127.08
- 122.30
- 120.94



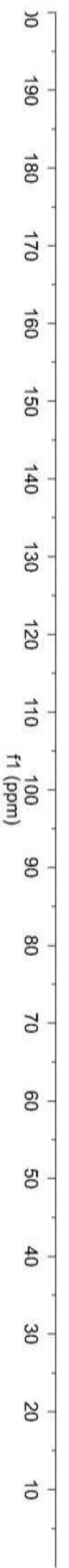
5-(2,3-Diamino-1-propyl)thio-3-isopropyl-7-[4-(2-pyridyl)benzyl]amino-1(2H)-pyrazolo[4,3-d]pyrimidine (4.30)



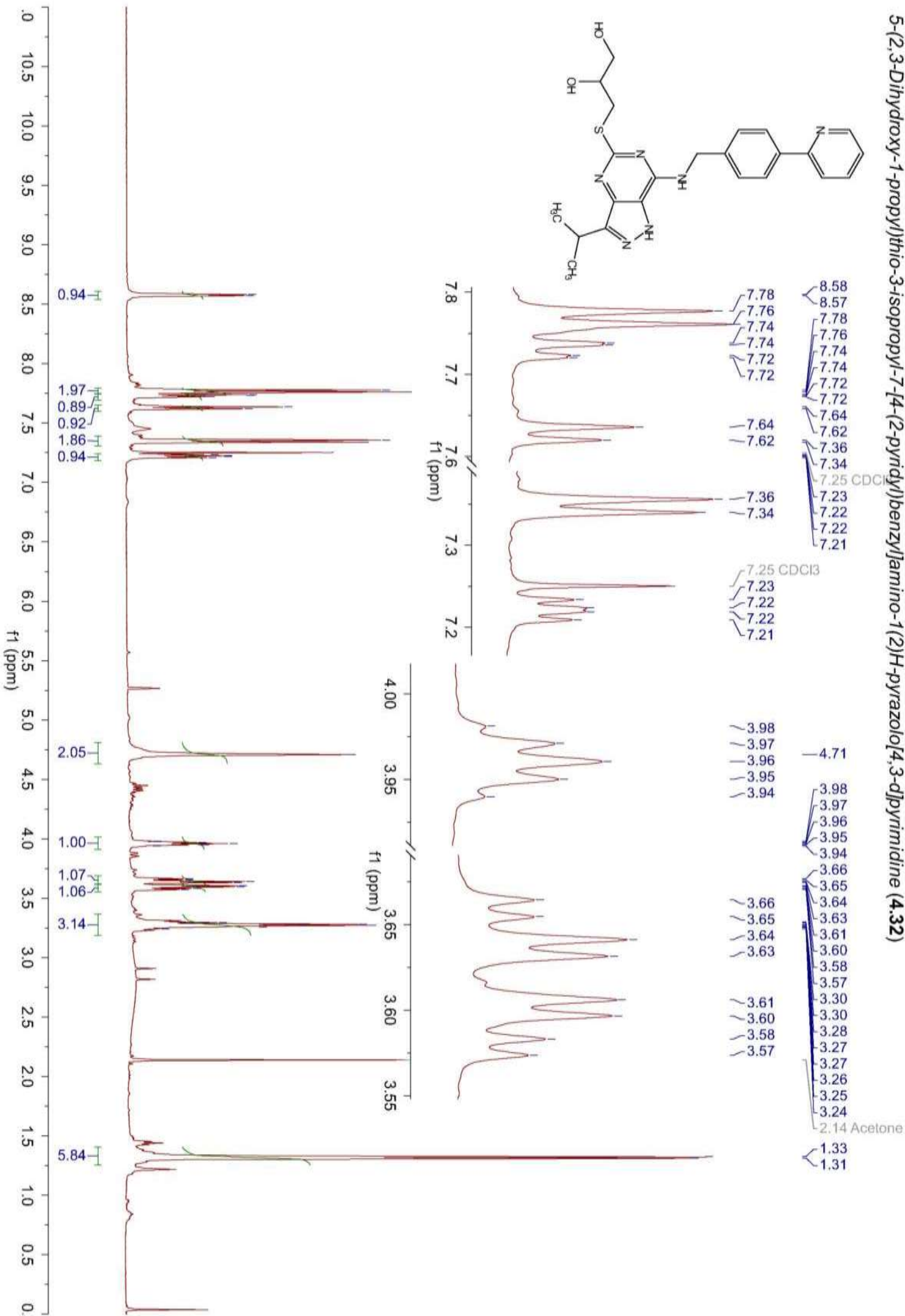
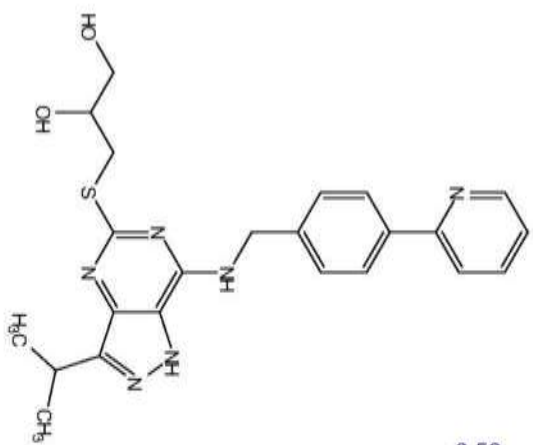
5-(2,3-Diamino-1-propyl)thio-3-isopropyl-7-[4-(2-pyridyl)benzyl]amino-1(2)H-pyrazolo[4,3-d]pyrimidine (4.30)



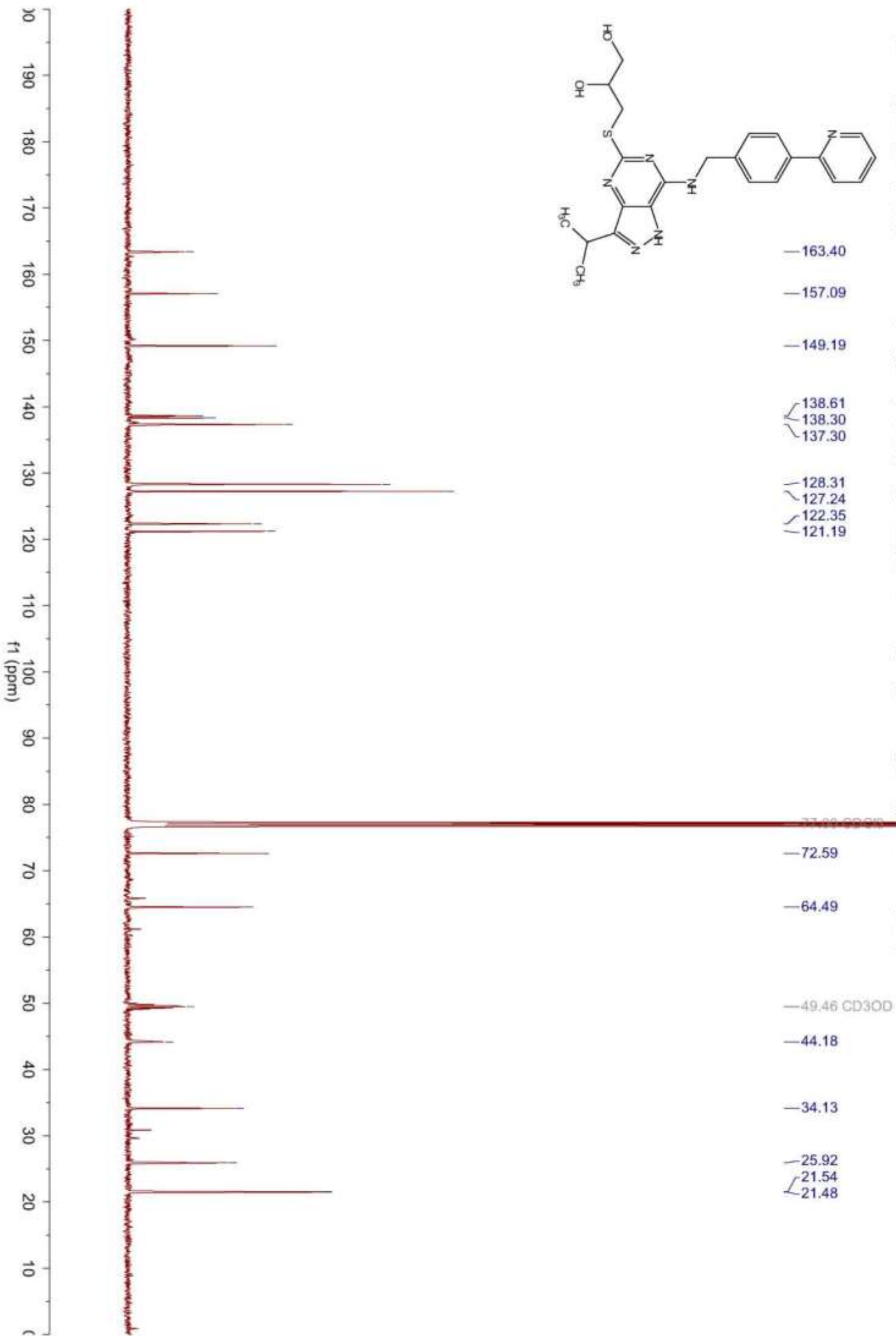
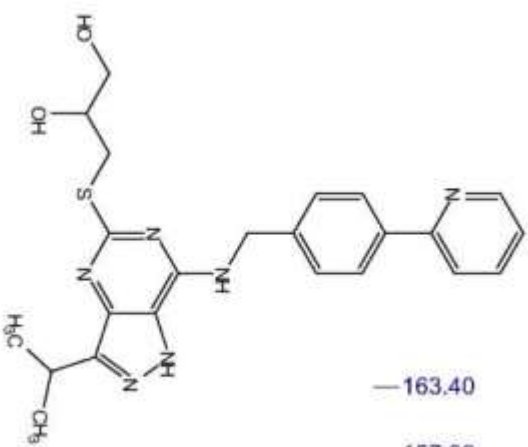
- 161.41
- 156.89
- 150.88
- 149.44
- 146.59
- 139.07
- 138.92
- 138.28
- 137.01
- 127.88
- 127.10
- 124.80
- 122.26
- 120.74



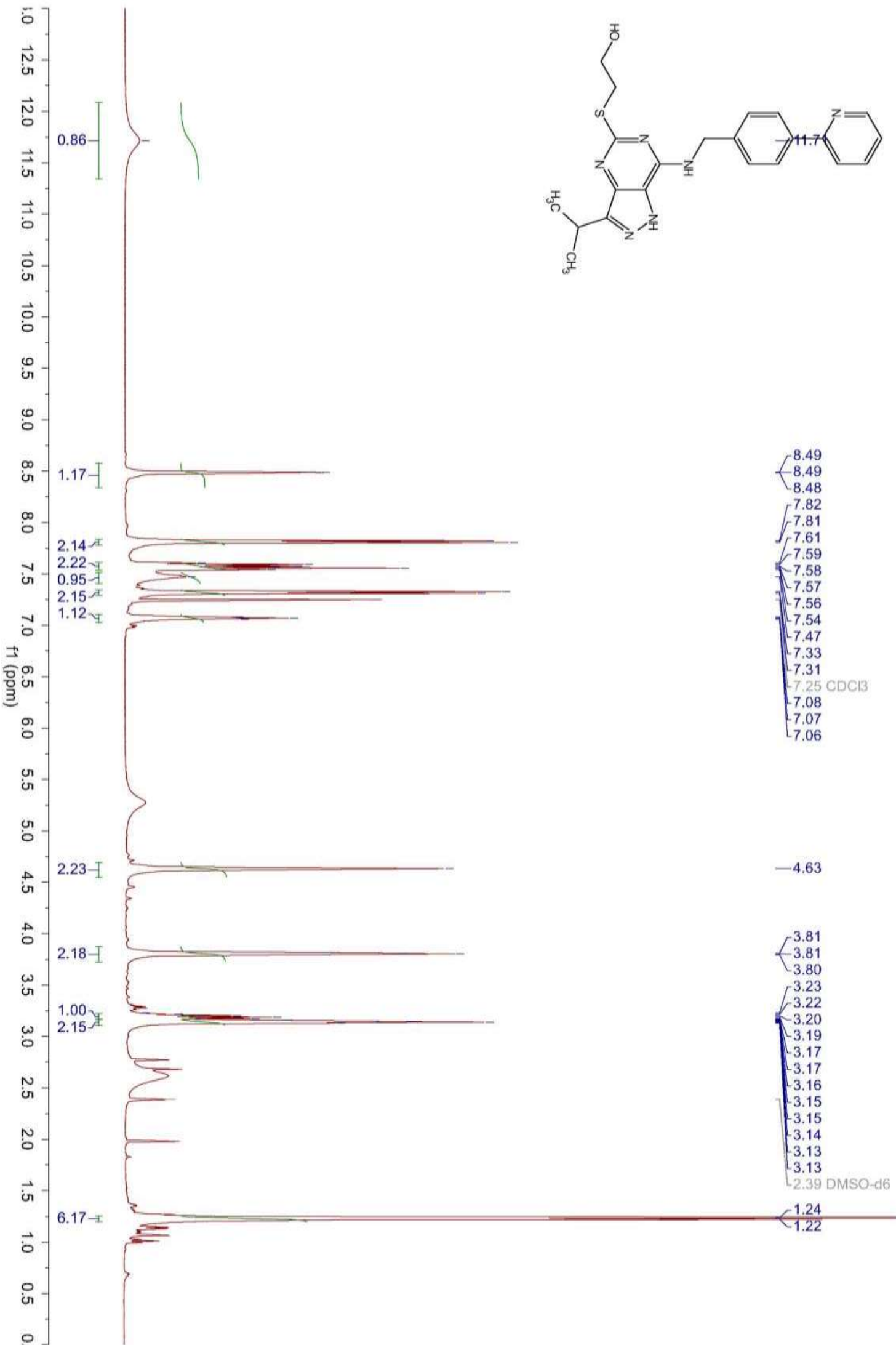
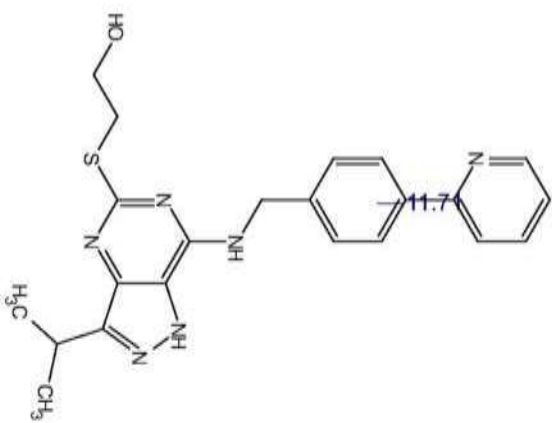
5-(2,3-Dihydroxy-1-propyl)thio-3-isopropyl-7-[4-(2-pyridyl)benzyl]amino-1(2H)-pyrazolo[4,3-d]pyrimidine (4.32)



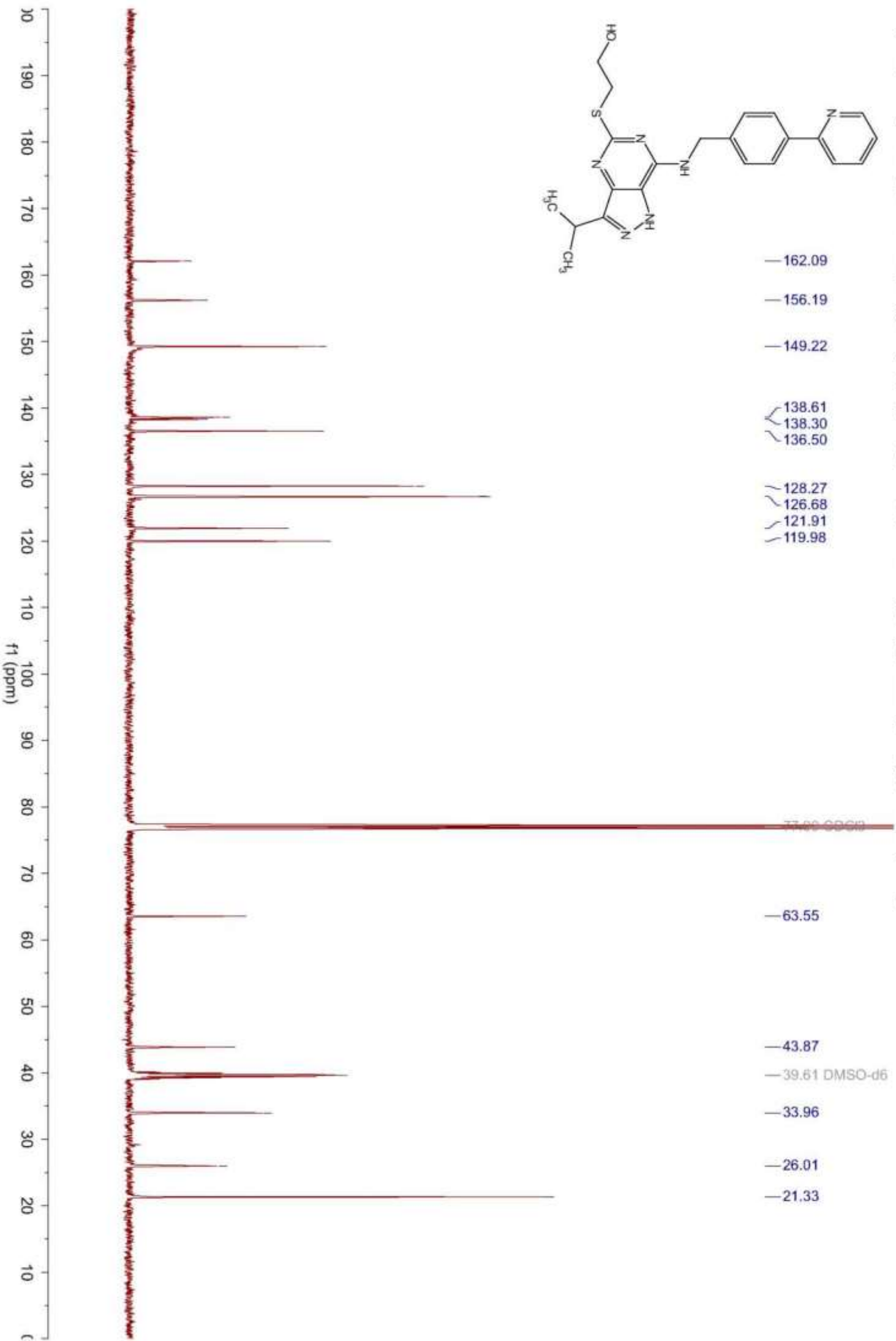
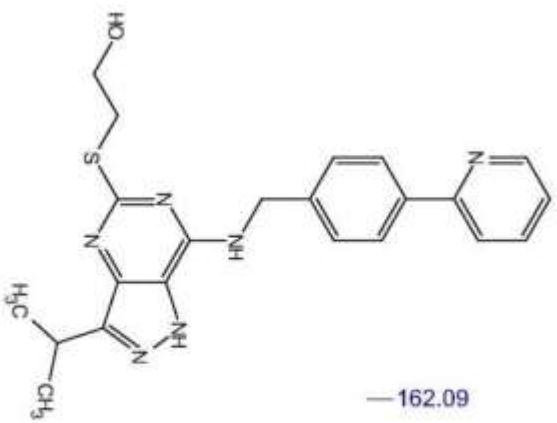
5-(2,3-Dihydroxy-1-propyl)thio-3-isopropyl-7-[4-(2-pyridyl)benzyl]amino-1(2H)-pyrazolo[4,3-d]pyrimidine (4.32)



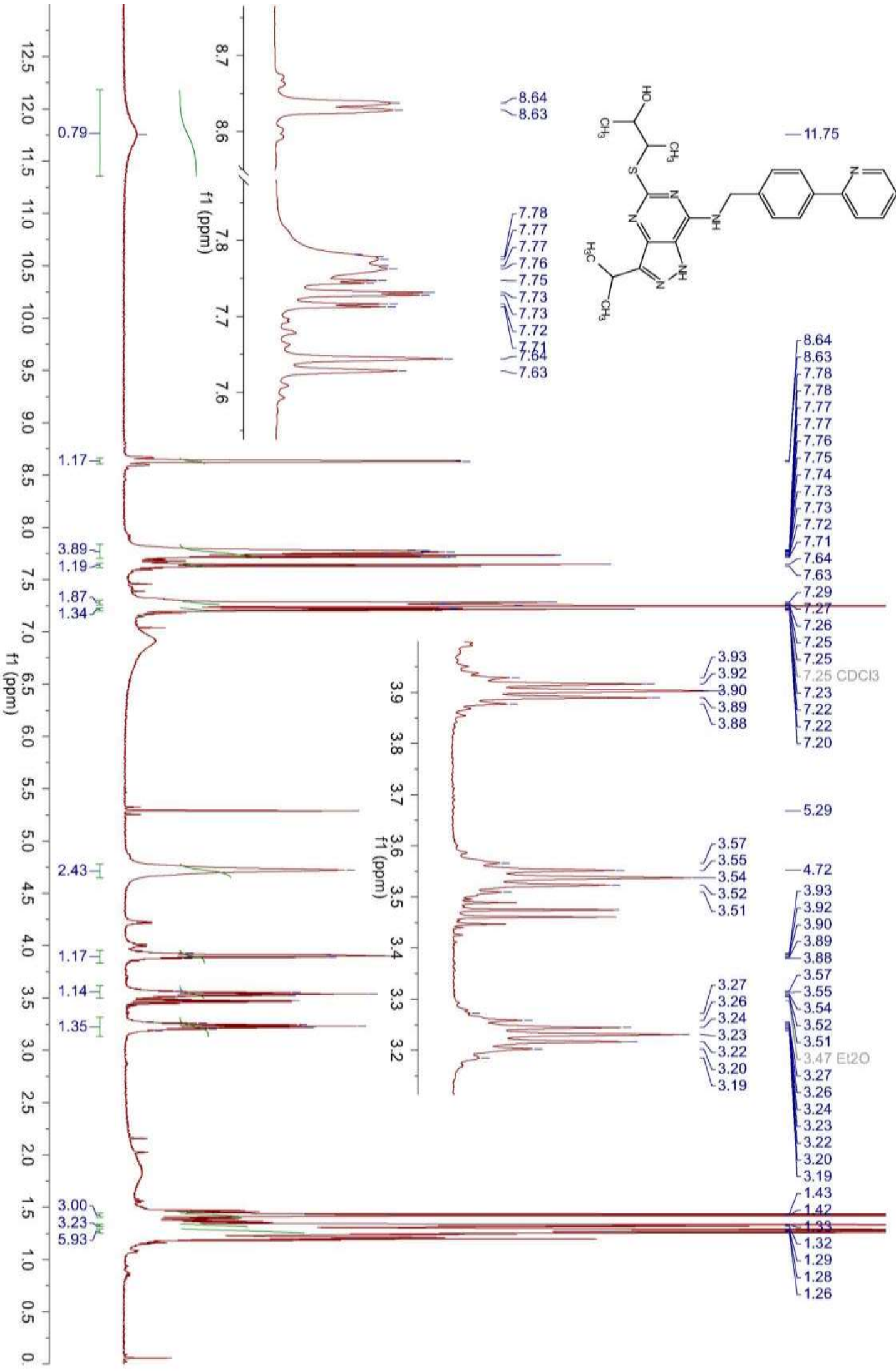
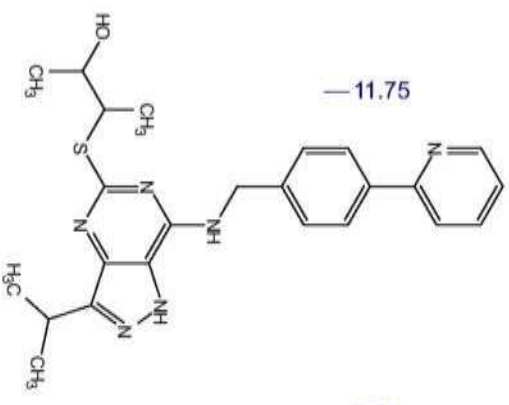
5-(2-Hydroxy-1-ethyl)thio-3-isopropyl-7-[4-(2-pyridyl)benzyl]amino-1-(2)H-pyrazolo[4,3-d]pyrimidin (4.33)



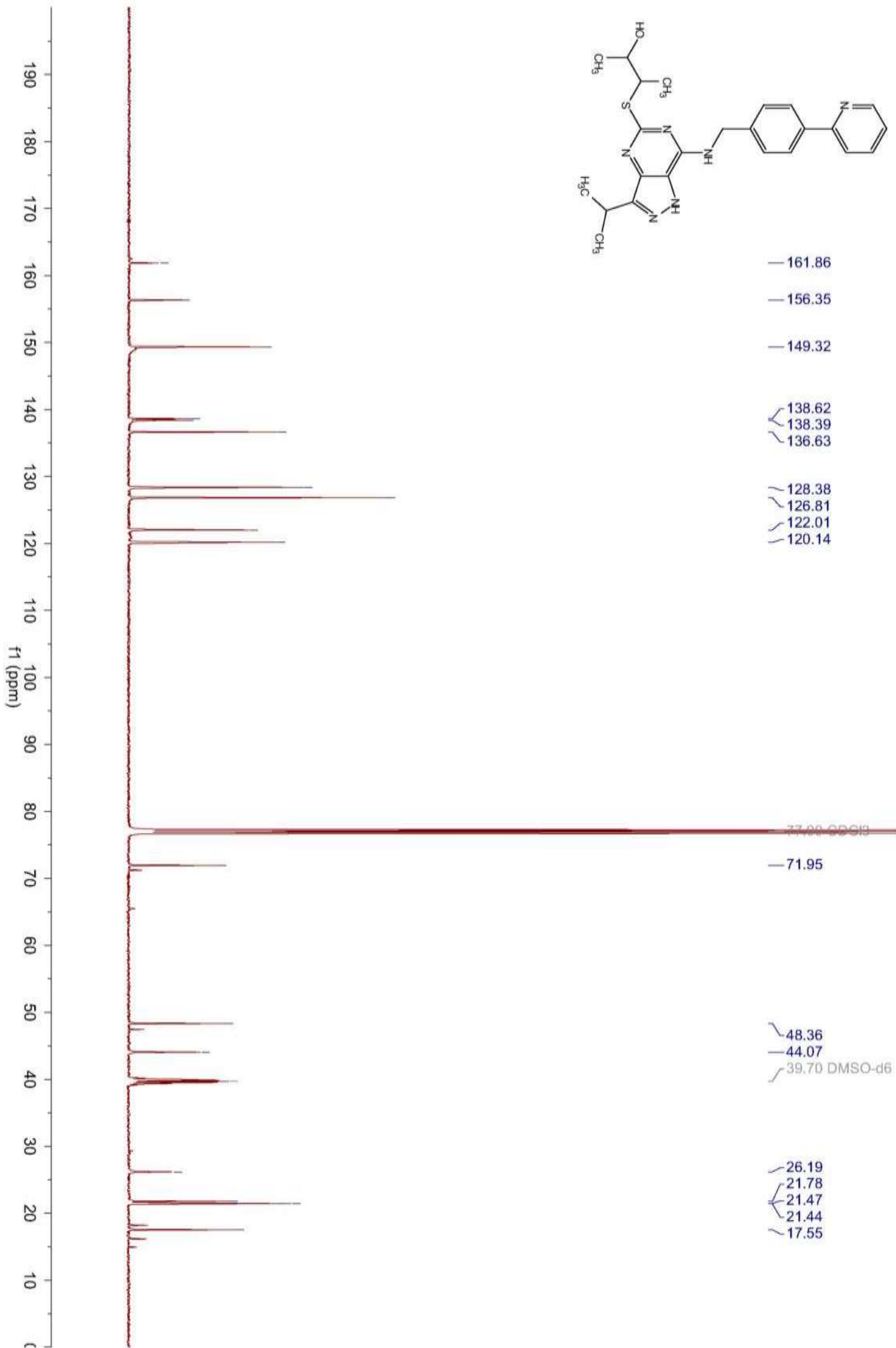
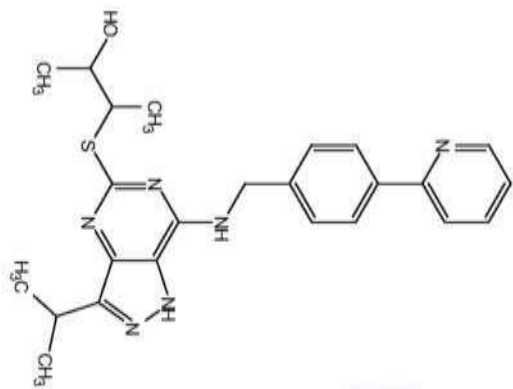
5-(2-Hydroxy-1-ethyl)thio-3-isopropyl-7-[4-(2-pyridyl)benzyl]amino-1(2H)-pyrazolo[4,3-d]pyrimidin (4.33)



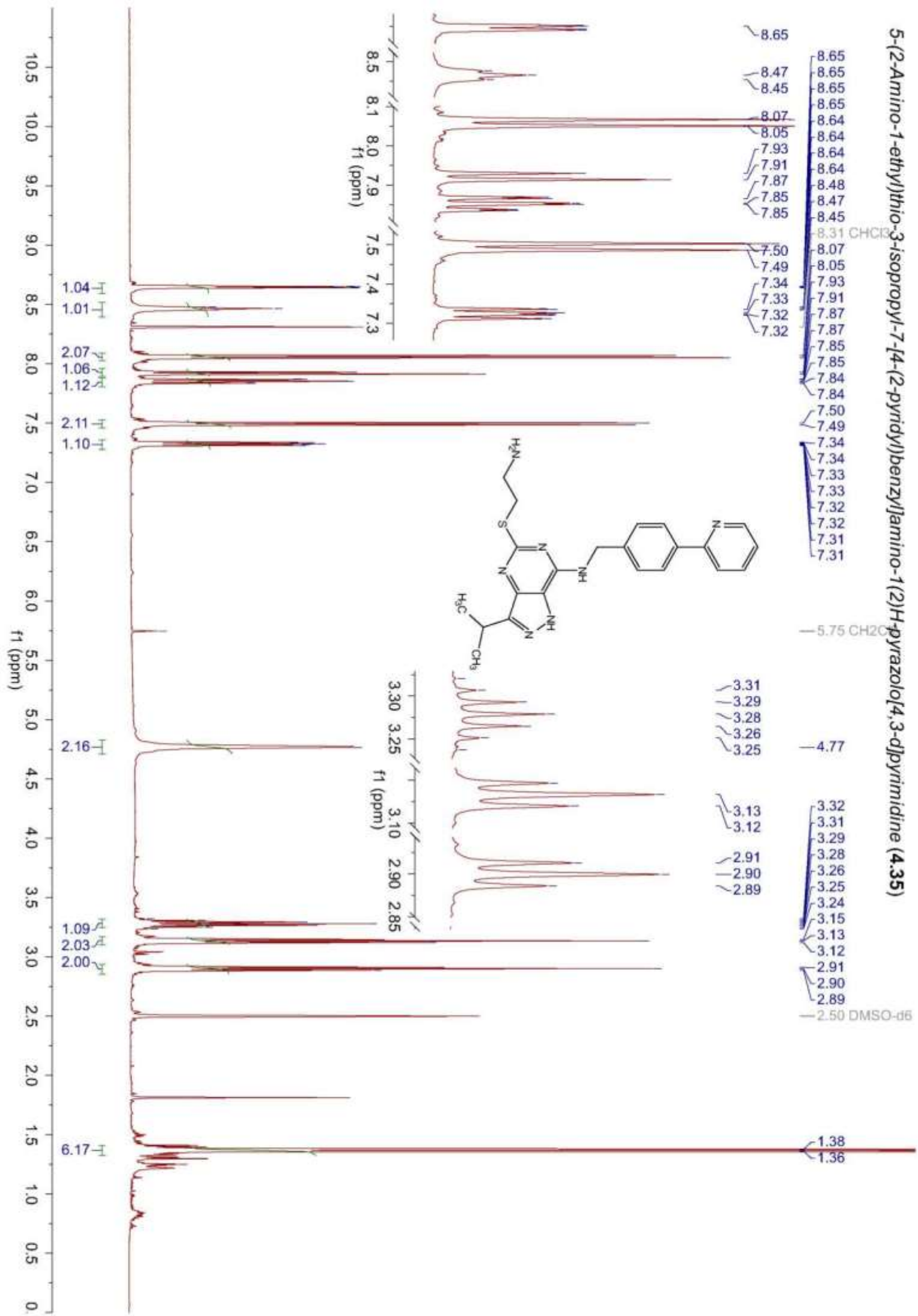
5-(3-Hydroxy-2-butyl)thio-3-isopropyl-7-[4-(2-pyridyl)benzylamino-1(2)H-pyrazolo[4,3-d]pyrimidine (4.34)



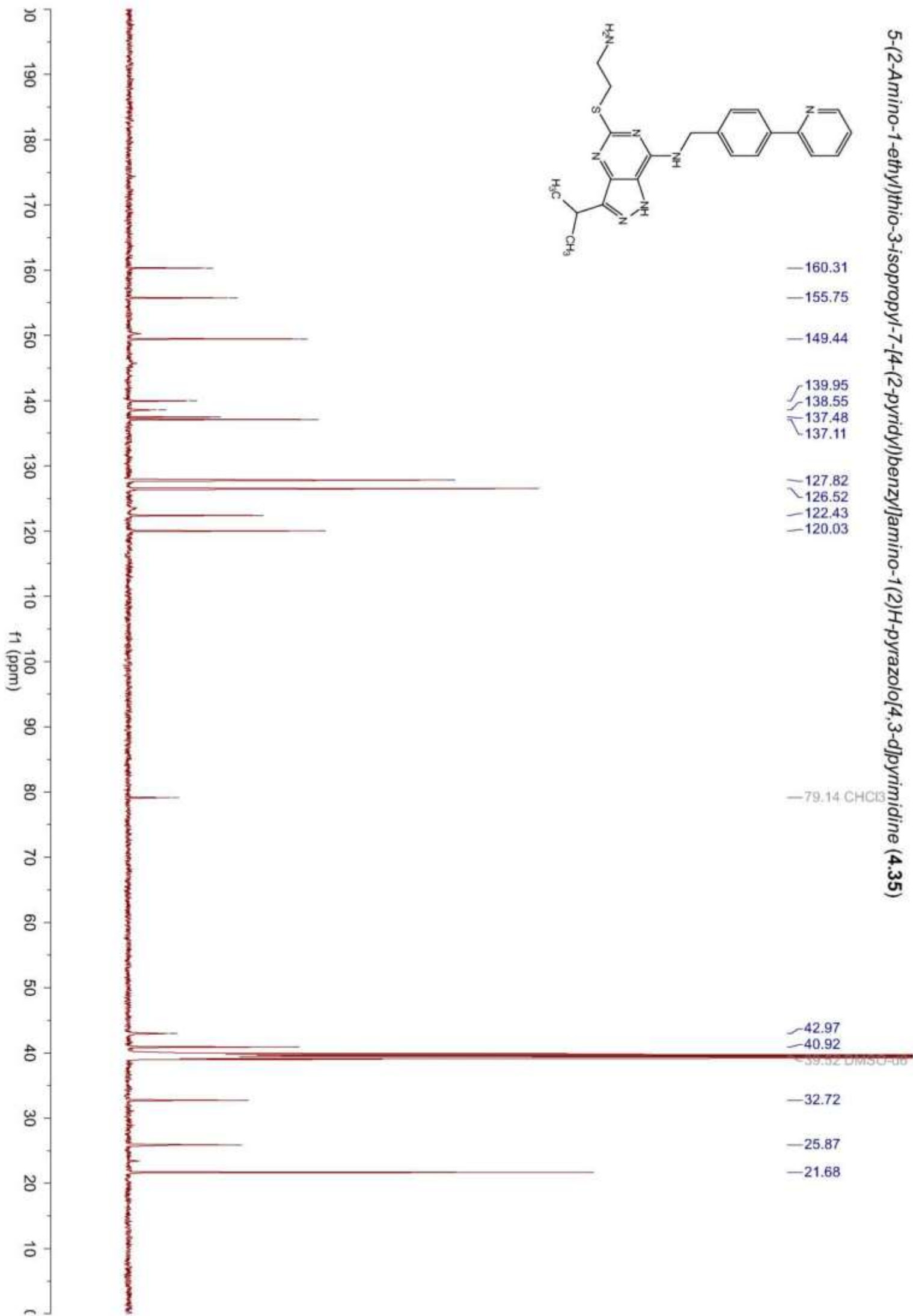
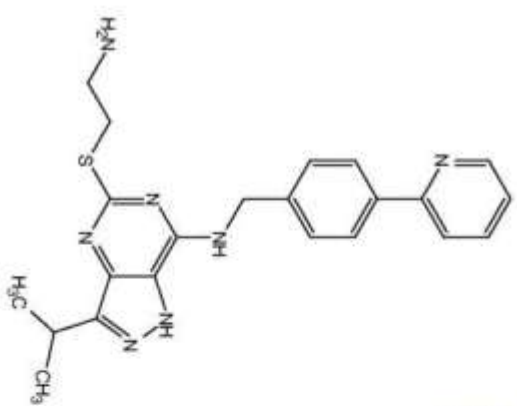
5-(3-Hydroxy-2-butyl)thio-3-isopropyl-7-[4-(2-pyridyl)benzyl]amino-1(2H)-pyrazolo[4,3-d]pyrimidine (4.34)



5-(2-Amino-1-ethyl)thio-3-isopropyl-7-[4-(2-pyridyl)benzyl]amino-1(2H)-pyrazolo[4,3-d]pyrimidine (4.35)



5-(2-Amino-1-ethyl)thio-3-isopropyl-7-[4-(2-pyridyl)benzyl]amino-1(2)H-pyrazolo[4,3-d]pyrimidine (4.35)



## 9. References

- (1)Vymetalova, L.; Havlicek, L.; Sturc, A.; Skraskova, Z.; Jorda, R.; Pospisil, T.; Strnad, M.; Krystof, V. 5-Substituted 3-isopropyl-7-[4-(2-pyridyl)benzyl]amino-1(2)H-pyrazolo[4,3-d]pyrimidines with anti-proliferative activity as potent and selective inhibitors of cyclin-dependent kinases. *Eur. J. Med. Chem.* **2016**, *110*, 291-301.
- (2)Nekardova, M.; Vymetalova, L.; Khirsariya, P.; Kovacova, S.; Hylsova, M.; Jorda, R.; Krystof, V.; Fanfrlik, J.; Hobza, P.; Paruch, K. Structural basis of the interaction of cyclin-dependent kinase 2 with roscovitine and its analogues having bioisosteric central heterocycles. *Chemphyschem.* **2017**, *18*, 785-795.
- (3)Bettayeb, K.; Oumata, N.; Echaliier, A.; Ferandin, Y.; Endicott, J. A.; Galons, H.; Meijer, L. CR8, a potent and selective, roscovitine-derived inhibitor of cyclin-dependent kinases. *Oncogene* **2008**, *27*, 5797-5807.
- (4)Fanfrlik, J.; Bronowska, A. K.; Rezac, J.; Prenosil, O.; Konvalinka, J.; Hobza, P. A reliable docking/scoring scheme based on the semiempirical quantum mechanical PM6-DH2 method accurately covering dispersion and H-bonding: HIV-1 protease with 22 ligands. *J Phys. Chem B* **2010**, *114*, 12666-12678.
- (5)Stewart, J. J. Optimization of parameters for semiempirical methods V: modification of NDDO approximations and application to 70 elements. *J Mol. Model.* **2007**, *13*, 1173-1213.
- (6)Klamt, A.; Schüürmann, G. COSMO: a new approach to dielectric screening in solvents with explicit expressions for the screening energy and its gradient. *J. Chem. Soc. , Perkin Trans. 2* **1993**, *0*, 799-805.
- (7)Schiebel, J.; Gaspari, R.; Wulsdorf, T.; Ngo, K.; Sohn, C.; Schrader, T. E.; Cavalli, A.; Ostermann, A.; Heine, A.; Klebe, G. Intriguing role of water in protein-ligand binding studied by neutron crystallography on trypsin complexes. *Nat. Commun.* **2018**, *9*, 3559.
- (8)Schrodinger, LLC. [Version 1.3r1 in]. 2010. The PyMOL Molecular Graphics System.
- (9)Diederichs, K.; Karplus, P. A. Improved R-factors for diffraction data analysis in macromolecular crystallography. *Nat. Struct. Biol.* **1997**, *4*, 269-275.
- (10) The CCP4 suite: programs for protein crystallography. *Acta Crystallogr. D. Biol. Crystallogr.* **1994**, *50*, 760-763.
- (11)Brunger, A. T. Free R value: a novel statistical quantity for assessing the accuracy of crystal structures. *Nature* **1992**, *355*, 472-475.
- (12)Chen, V. B.; Arendall, W. B., III; Headd, J. J.; Keedy, D. A.; Immormino, R. M.; Kapral, G. J.; Murray, L. W.; Richardson, J. S.; Richardson, D. C. MolProbity: all-atom structure validation for macromolecular crystallography. *Acta Crystallogr. D. Biol. Crystallogr.* **2010**, *66*, 12-21.